

University of St Andrews



Full metadata for this thesis is available in
St Andrews Research Repository
at:

<http://research-repository.st-andrews.ac.uk/>

This thesis is protected by original copyright

The Study of Molecular Fragmentations
by Semi-empirical Molecular Orbital Calculations

A Thesis

presented for the degree of

MASTER OF SCIENCE

in the Faculty of Science of the

University of St. Andrews

by

James R. Bews

August 1985

University of St. Andrews



Th
A 349

DECLARATION

I declare that this thesis is my own composition, that the work of which it is a record has been carried out by me, and that it has not been submitted in any previous application for a Higher Degree.

This thesis describes results of research carried out in the Department of Chemistry, United College of St. Salvator and St. Leonard, University of St. Andrews under the supervision of Dr. C. Glidewell since 1st. October 1977.

James R. Bews

CERTIFICATE

I hereby certify that James R. Bews has spent seven terms of research work under my supervision, has fulfilled the conditions of the Resolution of the University Court, 1974 No. 2, and is qualified to submit the accompanying thesis in application for the degree of Master of Science.

August 1985

C. Glidewell
Director of Research

ACKNOWLEDGEMENTS

I would like to thank Dr. C. Glidewell for his help and encouragement during the course of this work, and Dr. T.M. Shepherd and Dr. C.A. Vincent for encouraging me to put pen to paper.

I am indebted to Professor Lord Tedder and Professor Wyatt for providing the opportunity to carry out the research leading to this thesis.

Thanks are also due to all the staff of the Computing Laboratory, University of St. Andrews, without whose help and cooperation this work would have been impossible.

ABSTRACT

The semi-empirical molecular orbital programs MINDO/3, MNDO, UMNDO, CINPRO, CNINDO/2-3R, and CINMIN have been implemented on the VAX 11/780 computers, along with a job control procedure.

The molecular plotting program, PLUTO, and electron spin resonance spectrum simulation program for simulating exchange broadened spectra, XESR, have also been implemented.

Semi-empirical molecular calculations have been performed to study, at the MINDO/3 level of approximation, the first-row triatomic hydrides and their ions.

The mass spectral fragmentations of formic acid, formamide, ethyl acetate, and carbon tetrachloride have been studied in the MINDO/3 approximation.

The mass spectral fragmentation of boron trichloride, diboron tetrachloride, and tetraboron tetrachloride have been studied in the MNDO approximation.

CONTENTS

Declaration	i
Certificate	ii
Acknowledgements	iii
Abstract	iv
Contents	v
Chapter 1: Introduction	1
Chapter 2: Semi-empirical calculations	4
2.1 Huckel theory	6
2.2 Complete neglect of differential overlap	6
2.3 Intermediate neglect of differential overlap	9
2.4 Modified intermediate neglect of differential overlap	11
2.5 Partial neglect of diatomic differential overlap	13
2.6 Neglect of diatomic differential overlap	14
References	16
Chapter 3: Computational methods	18
3.1 Batch systems - overview	18
3.1.1 Job control	18
3.1.2 MINDO/3	25
3.1.3 MNDO	28
3.1.4 UMND0	29
3.1.5 Other semi-empirical systems implemented	31

3.2 Interactive systems	32
3.2.1 Molecule plotting	32
References	36

Chapter 4: MINDO/3 study of first-row triatomic

hydrides and their ions	38
Orbital energies	39
Heats of formation	45
Molecular structures at equilibrium	45
Six-electron species	46
Ionisation energies	48
Tables	49
References	68

Chapter 5: Molecular fragmentation of formic acid

Introduction	70
Molecular structures	71
Fragmentations	77
Appearance potentials	81
Tables	83
References	91

Chapter 6: Molecular fragmentation of formamide	92
Introduction	93
The formamide parent molecule	93
The formamide cation	94
Isomerization reactions of the formamide cation	96
Decomposition products of the formamide cation	97
Fragmentation of the formamide cation	102
Tables	105
References	117
Chapter 7: Molecular fragmentation of ethyl acetate	118
Introduction	118
The ethyl acetate parent molecule	119
The ethyl acetate molecular ion	119
Fragment ions	121
Neutral fragments	124
Rearrangement ions	125
Miscellaneous fragments	127
Molecular fragmentations	127
Ionisation energies, proton affinities and bond dissociation energies	129
Tables	130
References	141

Chapter 8: Molecular fragmentation of carbon tetrachloride	142
Introduction	142
Molecular energies	143
Molecular structures	144
Molecular fragmentations	147
The absence of $(\text{CCl}_4)^+$ from the mass spectrum	153
Ionisation energies, appearance potentials	
and bond energies	154
Tables	155
References	161
 Chapter 9: Mass spectral fragmentation of boron halides	 163
Introduction	163
Molecular structures	164
M and M^+	164
Fragment ions	166
Neutral fragments	169
Rearranged fragments	170
Electronic structures	171
Jahn-Teller effect	172
Mass spectral fragmentation	174
Molecular energies	174
Appearance potentials	177
Bond dissociation energies and bond energy terms	178
Symmetry constraints on fragmentation	179
Tables	181
References	189

Appendix A: Publications	191
Appendix B: ESR spectrum simulation	194
References	201

CHAPTER 1

INTRODUCTION

Molecular orbital (MO) calculations may be performed either at the ab initio level, or using semi-empirical approximations. The former techniques, although generally regarded by theoretical chemists as being the more reliable requires very large computer resources, both in terms of processing time and storage requirements, especially if sufficiently large basis sets are used to make calculations accurate. Semi-empirical calculations are very much more efficient in computer resources, allowing reasonably large molecules to be studied. A description of these semi-empirical methods is described in chapter 2. The implementation of the various semi-empirical methods used in this work is given in chapter 3, along with the molecular plotting program, PLUTO, which was used to generate the diagrams of the molecules and ions studied.

Chapter 4 describes the results of calculations performed at the MINDO/3 level of approximation on the first-row triatomic hydrides HMH, and their ions. The orbital energies, vertical and adiabatic ionisation energies, heats of formation, and optimised geometries are reported, and the variation of heat of formation and bond length as a function of HMH angle is reported for each species.

Chapters 5 to 9 describe mass spectral fragmentation processes studied by semi-empirical calculations. The fragmentations examined in chapters 5 to 8 were calculated at the MINDO/3 level of approximation, and the fragmentations studied in chapter 9 were calculated in the MNDO approximation.

Chapter 5 examines the fragmentation of formic acid, calculations having been performed on formic acid, its molecular ion, all the cations reported in its mass spectrum, and all the corresponding neutral fragments. The results of the calculations have been used to examine the fragmentation processes, both with respect to energy and the symmetries of the parent and daughter ions.

Chapter 6 gives the results of a similar series of calculations on formamide and its fragmentation products. The structures and energies of the transition states in the rearrangement and decomposition of formamide molecular cations is also reported.

Chapter 7 reports the similar studies of the fragmentation of ethyl acetate and the possible rearrangement ions formed during its fragmentation.

Chapter 8 gives the results of calculations on the mass spectral fragmentation of carbon tetrachloride. Reaction energy profiles are also reported for the reactions $(\text{CCl}_4)^+ \rightarrow (\text{CCl}_3)^+ + \text{Cl}$ and $(\text{CCl}_3)^+ \rightarrow (\text{CCl}_2)^+ + \text{Cl}$.

Chapter 9 describes the results of calculations on the mass spectral fragmentations of boron trichloride, diboron tetrachloride, and tetraboron tetrachloride.

Appendix A lists the publications arising from personal involvement in semi-empirical molecular calculations.

Appendix B describes a program implemented on the VAX computers at St. Andrews for the simulation of exchange broadened electron spin resonance (ESR) spectra. This program was not used in this work but the considerable modifications made to the original version of the program require documentation.

CHAPTER 2

SEMI-EMPIRICAL CALCULATIONS

The general hierarchy of available molecular orbital (MO) calculations is depicted in Figure 2.1. This shows the two approaches to MO calculations; ab initio calculations and semi-empirical calculations.

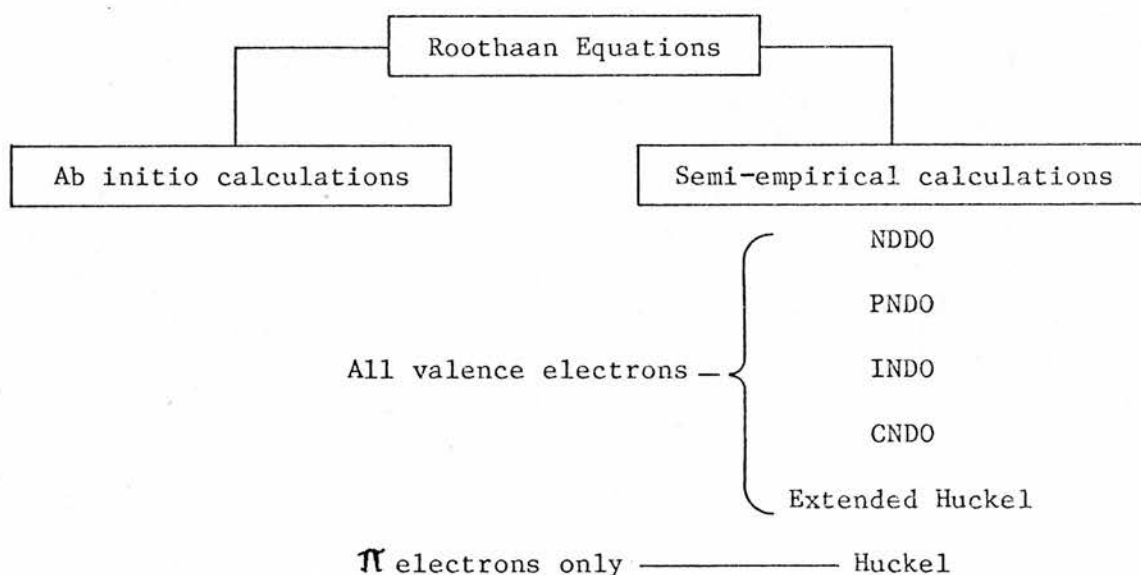


Figure 2.1

Roothaan [1] and Hall [2] independently formulated mathematical equations to represent the molecular orbital theory of Hund, Lennard-Jones and Mulliken [3] and the self consistent field method of Hartree [4] and Fock [5].

The ab initio methods are based on accurate evaluation using a chosen basis set of atomic orbitals with the calculation of all

the resulting integrals. This method is very costly in terms of computer time and storage requirements, especially if large basis sets are used. The Hartree-Fock technique used also neglects coulomb-correlation, the tendency of electron pairs to synchronise their motion. Although the neglect of this energy may be considered to be consistent within a series of similar molecules or ions it does mean that comparisons of energies obtained may only be applicable to related species.

Semi-empirical calculations employ techniques whereby the integrals need not be calculated precisely. These methods may for example involve the estimation of some integrals from known spectroscopic data, the use of simple functions known to simulate the integrals, or the neglect of integrals known to make a small contribution to the energy. The parameterisation thus performed, using known physical properties of many chemical species, has the advantage that effects such as the coulomb-correlation error in *ab initio* techniques are compensated by the parameterisation, giving reliable energies and other molecular properties from these calculations.

The various levels depicted in Figure 2.1 show the various levels of sophistication of the semi-empirical methods. These levels are mainly related to the consideration given to the overlapping of atomic orbitals (differential overlap).

2.1 Huckel Theory

Huckel theory [6] is the simplest approach in the hierarchy of Figure 2.1. This technique only considers π electrons and is therefore not of general use although it has been modified by Hoffmann [7] and Wolfsberg and Helmholtz [8] to give the Extended Huckel Theory by the inclusion of overlap to extend to σ bonding.

All the semi-empirical methods neglect the inner electrons of an atom, considering them to be part of the core of the atom. Extended Huckel Theory is the first of the methods which considers all the valence electrons.

2.2 Complete Neglect of Differential Overlap.

CNDO [9] is the least sophisticated of the neglect of differential overlap methods. Its initial parameterisation was in the method CNDO/1 [10]. These methods ignore the difference between orbital types and so the repulsion between electrons of orbitals k and m of atom A may be represented as

$$\Gamma_{km} = \langle S_A S_A | S_A S_A \rangle = \Gamma_{AA} \dots \dots (1)$$

The orbitals are regarded as being spherically symmetrical and so the two centre repulsion between electrons in an orbital k of atom A and l of atom B is regarded as being equal to the theoretical electron repulsion integral between Slater s orbitals:

$$\Gamma_{k1} = \langle kk | 11 \rangle = \langle S_A S_A | S_B S_B \rangle = \Gamma_{AB} \dots (2)$$

and the attraction of an electron in orbital k of atom A by the core of B is

$$V_{kk}^B = Z_B^* \langle S_A S_A | B \rangle = V_A^B \dots (3)$$

where Z^* is the effective core charge.

The total electron density is defined on atom A as

$$P_{AA} = \sum_k P_{kk} \dots (4)$$

The ZDO (zero differential overlap) approximation assumes that the probability of finding an electron in a given volume of space common to two orbitals is zero unless these are in fact the same orbital. Here, it was found that the Fock matrix elements can be represented by

$$F_{kk} = U_{kk}^A + (P_{AA} - 0.5P_{kk}) \Gamma_{AA} + \sum_{B \neq A} (P_{BB} \Gamma_{AB} - V_A^B) \dots (5)$$

$$F_{k1} = H_{k1} - 0.5P_{k1} \Gamma_{AB} \dots (6)$$

The total energy obtained in the CNDO approximation is

$$E_T = \sum_A E_A + \sum_{A < B} E_{AB} \dots (7)$$

where using the ZDO approximation

$$E_A = \sum_k^A P_{kk} U_{kk}^A + 0.5 \sum_{km}^A (P_{kk} P_{mm} - 0.5P_{km}^2) \Gamma_{AA} \dots (8)$$

and

$$E_{AB} = \sum_{k1}^{AB} (2P_{k1} \beta_{k1} - \frac{1}{2} P_{k1}^2 \Gamma_{AB} + \frac{Z^* Z^*}{\Gamma_{AB}} - P_{AA} V_A^B - P_{BB} V_B^A + P_{AA} P_{BB} \Gamma_{AB}) \dots (9)$$

These expressions involve one-centre terms U_{kk}^A which are obtained by comparing experimental and calculated ionization potentials:

$$U_{kk}^A = -IP_k^A - (Z^*-1)\Gamma_{AA} \dots\dots (10)$$

The H terms are proportional to the overlap between Slater-Zener atomic orbitals k and l:

$$H_{kl} = S_{kl}\beta_{kl} = S_{kl}(\beta_A^O + \beta_B^O) \dots\dots (11)$$

where β_A^O and β_B^O are parameterised by comparison with ab initio calculations on simple molecules containing atoms A and B.

The two electron terms Γ_{AA} and Γ_{AB} are calculated theoretically assuming Slater s orbitals.

This method was relatively successful as the first approximation but problems were found with the results for heats of formation and molecular geometries.

Because of these problems Pople and Segal modified CNDO to give a version CNDO/2 [11].

The first modification was to the U_{kk}^A term (eqn 10). Instead of being compared only with the ionization potential this has been changed to include reference to electron affinity:

$$U_{kk}^A = -0.5(IP_k + EA_k) - (Z^*-0.5)\Gamma_{AA} \dots\dots (12)$$

The second modification was to give the two-centre core-electron interaction (eqn 3) the same value as the corresponding two-centre electron - electron interaction:

$$V_A^B = Z^* \Gamma_{AB} \dots\dots (13)$$

These changes improved molecular geometries and dipole moments found by CNDO although poor results for heats of formation were still found.

2.3 Intermediate Neglect of Differential Overlap.

INDO [12] was developed by Pople to reduce the level of approximation caused by the omission of one-centre exchange integrals.

The one-centre two electron interactions were calculated in terms of Slater-Condon parameters:

$$\langle ss | pp \rangle = \langle ss | p_x p_x \rangle = F^0 = \Gamma_{AA} \dots\dots (14)$$

$$\langle p_x p_x | p_x p_x \rangle = F^0 + (4/25)F^2 \dots\dots (15)$$

$$\langle p_x p_x | p_y p_y \rangle = F^0 - (2/25)F^2 \dots\dots (16)$$

$$\langle sp_x | sp_x \rangle = (1/3)G' \dots\dots (17)$$

$$\langle p_x p_y | p_x p_y \rangle = (3/25)F^2 \dots\dots (18)$$

where F^0 , being equivalent to Γ_{AA} , was calculated as in CNDO from Slater s orbitals. G' and F^2 , are Slater-Condon parameters found from atomic spectra.

Because of the inclusion of one-centre terms the U_{kk}^A terms were modified:

$$\text{Hydrogen: } U_{SS}^H = -0.5(IP+EA) - 0.5\Gamma_{AA} \dots (19)$$

Boron to Fluorine:

$$U_{SS}^A = -0.5(IP_S+EA_S) - (Z^*-0.5)\Gamma_{AA} + \frac{1}{6}(Z^*-\frac{3}{2})G' \dots (20)$$

$$U_{PP}^A = -0.5(IP_P+EA_P) - (Z^*-0.5)\Gamma_{AA} + \frac{1}{3}G' + \frac{2}{25}(Z^*-\frac{5}{2})F^2 \dots (21)$$

This alteration in the level of approximation then gave the ability to perform unrestricted Hartree-Fock calculations on open shell systems because each set of electrons is treated separately. P_{kk} (eqn 4) is therefore redefined as

$$P_{kk}^\alpha + P_{kk}^\beta = P_{kk} \dots (22)$$

where P_{kk}^α and P_{kk}^β are the separate occupancies of atomic orbital k by alpha and beta electrons. The Fock matrix elements (eqns 5,6) were therefore redefined as

$$F_{kk}^u = U_{kk}^A (P_{kk} - P_{kk}^u) \langle kk | 11 \rangle + \sum_{m \neq k}^A (P_{mm} \langle kk | mm \rangle - P_{mm}^u \langle km | km \rangle) + \sum_{B \neq A} (P_{BB} \Gamma_{AB} - V_A^B) \dots (23)$$

and

$$F_{km}^u = (2P_{km} - P_{km}^u) \langle km | km \rangle - P_{km}^u \langle kk | mm \rangle \dots (24)$$

where k and m are on atom A and u is α or β .

$$F_{k1}^u = H_{k1} - P_{k1}^u \Gamma_{AB} \dots (25)$$

INDO gives improved results generally and is found to be most useful for the calculation of spin densities.

2.4 Modified Intermediate Neglect of Differential Overlap.

MINDO [13-16] is a modified form of INDO which has been developed through three forms MINDO/1 [13], MINDO/2 [14,15] and MINDO/3 [16]. It is an extension of INDO to include some aspects of PNDO [17].

As MINDO/3 is the most recent version of MINDO this is the form which will be described.

MINDO uses the two-centre repulsion integrals Γ_{k1} of PNDO (eqn 32). The electron repulsion integral was calculated by the Ohno-Klopman approximation [18,19]:

$$\Gamma_{AB} = [r_{AB}^2 + 0.25(1/r_{AA} + 1/\Gamma_{BB})^2]^{-0.5} \dots (26)$$

The resonance integral was defined as

$$H_{k1} = \beta_{AB} S_{k1} (IP_k + IP_1) \dots (27)$$

where β_{AB} is a parameter referring to an atom pair.

Core repulsion was developed from a method used in PNDO (eqn 34):

$$CR_{AB} = Z_A^* Z_B^* [\Gamma_{AB} + (1/r_{AB} - \Gamma_{AB}) e^{-\alpha \Gamma_{AB}}] \dots (28)$$

where α_{AB} is again a parameter for referring to an atom pair.

The parameterisation technique was also used for the k and l orbital exponents instead of the Slater-Zener values (eqn 11) and for the one-centre integrals. The latter parameterisation was performed by the method of Oleari [20] by fitting to known valence state energies.

These modifications also allowed the extension of INDO calculations to the third row of the periodic table, with the restriction that calculations may only be performed for atom-pairs for which parameters have been found.

MINDO also has a geometry optimisation technique based on the Davidson-Fletcher-Powell method [21]. The geometrical variables are differentiated by finite difference and the geometry is optimised to give a minimum on the potential energy surface.

Because of the parameterisation of MINDO it has been necessary to treat unpaired electrons as half an electron pair. This does not allow the extraction of spin density information as in INDO but other results for open-shell systems are generally acceptable.

In order to perform calculations on biradicals or biradical-like species MINDO also has the facility for performing

configuration interaction (CI) calculations [22].

2.5 Partial Neglect of Diatomic Differential Overlap.

PNDDO, commonly abbreviated to PNDO [17], treats the two-centre core-electron interaction and electron-electron repulsion differently depending on the orbital nature. This results in the inclusion of all one-centre differential overlap to give

$$F_{kk}^u = U_{kk}^A - \sum_B v_{kk}^B + P_{kk}^v A_A^- + \sum_{m \neq k}^A (P_{mm}^v A_{AA}^- + P_{mm}^u A_A^+) + \sum_{ln}^{BB} P_{ln} \langle kk | 11 \rangle \dots \dots (29)$$

$$F_{km}^u = - \sum_{B \neq A} v_{kk}^B + P_{km}^u A_A^+ + \sum_{B \neq A}^{BB} (\sum_{ln} P_{ln} \langle km | 1n \rangle) \dots \dots (30)$$

$$F_{k1} = H_{k1} + \sum_{mn}^{AB} P_{mn} \langle km | 1n \rangle \dots \dots (31)$$

where u or v is α or β respectively.

U_{kk}^A was obtained by the comparison of calculated and observed values for various atomic configurations. A_A^+ and A_B^- represent the repulsion of electrons of the same and opposite spins respectively. These were found in a similar manner to that of U_{kk}^A .

The two-centre repulsion integrals were evaluated using the expression

$$\Gamma_{AB}^{k1} = [r_{AB}^2 + \frac{1}{4} (\frac{T}{A_A} + \frac{T}{A_B})]^{-0.5} \dots \dots (32)$$

which was derived empirically and where

$$T_{uv} = 1$$

unless v is a p-sigma orbital when

$$T_{uv} = \exp\{-r_{AB}/2[1/A_A^- + 1/A_B^-]\} \dots (33)$$

The core repulsion was also derived empirically as

$$CR_{AB} = SE_{AB} + (Z_A^* Z_B^*/r_{AB} - SE_{AB})e^{-\alpha_{AB} r_{AB}} \dots (34)$$

where α_{AB} is an empirical parameter and SE_{AB} is the total two-centre electron repulsion:

$$SE_{AB} = \sum_{kl} N_k N_l \Gamma_{AB}^{kl} \dots (35)$$

N_i is the occupancy of the i^{th} orbital.

PNDO was parameterised for carbon and hydrogen. Its use has lapsed with the use of some of its approximations in MINDO and with the development of NDDO methods.

2.6 Neglect of Diatomic Differential Overlap.

NDDO was originally postulated by Pople and co-workers [9] and was first used by Sustmann et al [23] for closed-shell systems. This was later developed by Dewar and Thiel to give MNDO [24]. This method includes all two-centre integrals of the form $\langle km|ln \rangle$ and all two-centre Coulomb integrals were assumed to be independent of the orbital type. The Fock matrix elements were thus found to be

$$F_{kk} = U_{kk}^A + \sum_B V_{kk}^B + \sum_m P_{mm}^A [\langle kk | mm \rangle - \frac{1}{2} \langle km | km \rangle] + \sum_{Bln} P_{ln}^B \langle kk | ln \rangle \dots (36)$$

$$F_{km} = V_{km}^B + \frac{1}{2} P_{km}^A [3 \langle km | km \rangle - \langle kk | mm \rangle] + \sum_{Bln} P_{ln}^B \langle km | ln \rangle \dots (37)$$

$$F_{kl} = H_{kl} - \frac{1}{2} \sum_{mn} P_{mn}^{AB} \langle km | ln \rangle \dots (38)$$

These terms in the Fock matrix were fitted empirically rather than being determined analytically to compensate for errors introduced by the level of approximation.

The MNDO method includes the Davidson-Fletcher-Powell geometry optimisation used in MINDO/3 and the facility for Configuration Interaction. A later version [25] also has the facility for performing Unrestricted Hartree Fock calculations.

References

- [1] C.C.J. Roothaan, Rev. Mod. Phys., 23(1951), 69
- [2] G.G. Hall, Proc. Roy. Soc., A205(1951), 541
- [3] P-O. Lowdin and B. Pullman, "Molecular Orbitals in Chemistry and Biology", New York:Academic, 1954
- [4] D.R. Hartree, Proc. Camb. Phil. Soc. Math. Phys. Sci., 24(1928), 89 and 111
- [5] V. Fock, Z. Phys., 61(1930), 126
- [6] E. Huckel, Z. Phys., 70(1931),204; Int. Conf. Phys., Physical Soc., 2(1935), 9
- [7] R. Hoffmann, J. Chem. Phys., 39(1963), 1397
- [8] M. Wolfsberg and L. Helmholz, J. Chem. Phys., 20(1952), 837
- [9] J.A. Pople, D.P. Santry and G.A. Segal, J. Chem. Phys., 43(1965), S129
- [10] J.A. Pople and G.A. Segal, J. Chem. Phys., 43(1965), S136
- [11] J.A. Pople and G.A. Segal, J. Chem. Phys.,44(1966), 3289
- [12] J.A. Pople, D.L. Beveridge and P.A. Dobosh, J. Chem. Phys., 47(1967), 2026
- [13] N.C. Baird and M.J.S. Dewar, J. Am. Chem. Soc., 50(1969), 1262

- [14] M.J.S. Dewar and E. Haselbach, *J. Am. Chem. Soc.*, 92(1970), 590
- [15] N. Bodor, M.J.S. Dewar and D.H. Lo, *J. Am. Chem. Soc.*, 94(1972), 5303
- [16] R.C. Bingham, M.J.S. Dewar and D.H. Lo, *J. Am. Chem. Soc.*, 97(1975), 1285
- [17] M.J.S. Dewar and G. Klopman, *J. Am. Chem. Soc.*, 89(1967), 3089
- [18] K. Ohno, *Theor. Chem. Acta*, 2(1964), 219
- [19] G. Klopman, *J. Am. Chem. Soc.*, 86(1964), 4550
- [20] L. Oleari, L. DiSipio and G. DeMichelis, *Mol. Phys.*, 10(1966), 97
- [21] W.C. Davidson, *Comput. J.*, 10(1968), 406; R. Fletcher, *ibid.* 8(1965), 33; R. Fletcher and M.J.D. Powell, *ibid.*, 6(1963), 163
- [22] R.C. Bingham and M.J.S. Dewar, *J. Am. Chem. Soc.*, 94(1972), 9107
- [23] R. Sustmann, J.E. Williams, M.J.S. Dewar, L.C. Allen and P.v.R. Schleyer, *J. Am. Chem. Soc.*, 91(1969), 5350
- [24] M.J.S. Dewar and W. Thiel, *J. Am. Chem. Soc.*, 99(1977), 4899
- [25] M.J.S. Dewar, J. Stewart, W. Thiel and P. Weiner, *QCPE Bulletin* 1(1981), 428

CHAPTER 3

COMPUTATIONAL METHODS

This chapter describes the implementation of the computer programs used in this work. These programs fall into two categories: those requiring large amounts of computer resources are performed as batch jobs, while less demanding programs are capable of interactive processing.

3.1 Batch Systems - Overview

Batch processing is a technique whereby work is submitted to the computer to be processed when the computer's operating system allocates the time, memory and filespace required for the computation.

Commands must be given to the computer system to allocate the resources and files required. This is commonly referred to as "JOB CONTROL" and is the interface between the computer user and the program(s) with which calculations are to be performed.

3.1.1 Job Control

The initial work in this thesis was performed using the program MINDO/3 [1] mounted on the St. Andrews University IBM 360/44 computer and later on a Honeywell 66/80 computer at

Aberdeen University. These computers required the user to know how to manipulate the command structure to specify the required resources. Latterly all the batch programs described in this work were implemented on the twin VAX 11/780 computers at St. Andrews University. Because of the powerful Job Control Language [2] available on this computer system it was decided to write a command structure to ease the use of these programs for those with limited computer experience. This technique also allowed the existence of input files to be checked while submission was being carried out.

Four batch queues are available on the St. Andrews University VAX. These are FAST\$BATCH, SYS\$BATCH, SLOW\$BATCH and LONG\$BATCH with upper limits on computation times of 1 minute, 10 minutes, 1 hour and 3 hours respectively.

These queues allow any user to submit only one job to the computer at a given time. The job submission procedure described below permits the generation of a chain of command files, only the first of which is automatically submitted to the required batch queue. Each command file thus created, except the last, contains an instruction to submit the next command file to the batch queue for batch processing.

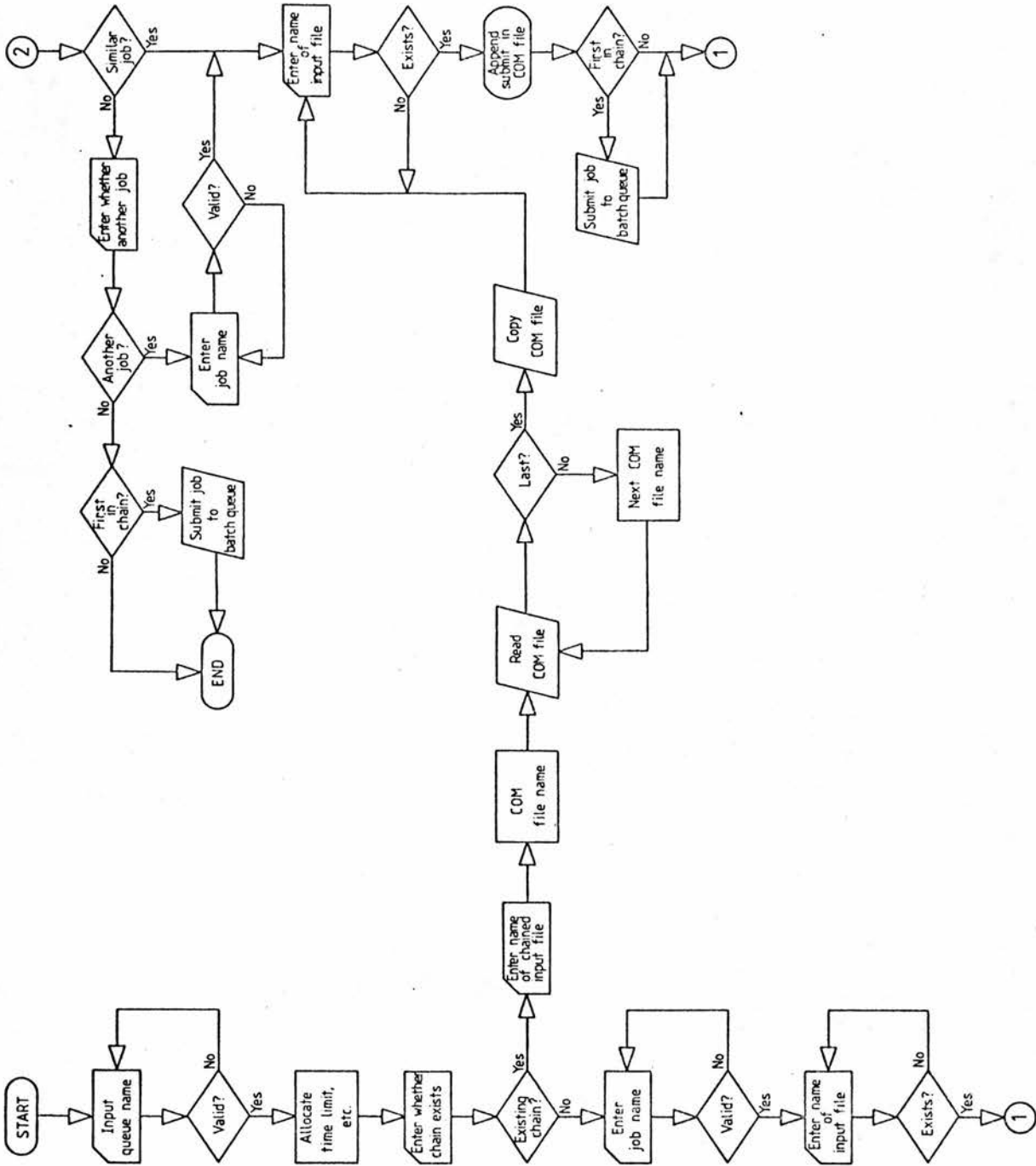
A flow diagram of the operation of this chaining command contained in the file [CHSJB.JCL]QUEUE.COM is given in figure 3.1. This file is accessible to all users of the St. Andrews VAX

system by the command

@[CHSJB.JCL]QUEUE

permitting them to submit jobs to the series of programs described in the first section of this chapter.

In operation, the QUEUE command asks to which batch queue the job(s) are to be submitted. The opportunity is then given to add the job(s) about to be submitted to an existing job chain. Input of the job name is then requested, which may be CNINDO, MINDO, MNDO, UMND0, etc. If this name does not match any of the programmed options the QUEUE command assumes that this is a special job for which a command procedure is available and checks to see if such a command file is present. The name of the input data file is then requested and the existence of the named file is checked. If the job name is MINDO or (U)MNDO the name of a restart file is requested. This may be given a name automatically by pressing the <RETURN> key in response to the question. In this case the file type is stripped from the file name and the file type .RST is allocated. The output option is then input which defaults to being output to the job .LOG file. If so desired the output may be directed to a named file which defaults to filename.LIS. The QUEUE command then asks if more of the named jobs are to be run and if so it prompts again for an input data file name. If no more of the jobs already specified are to be run the opportunity is given to add jobs of a different type to the job chain.



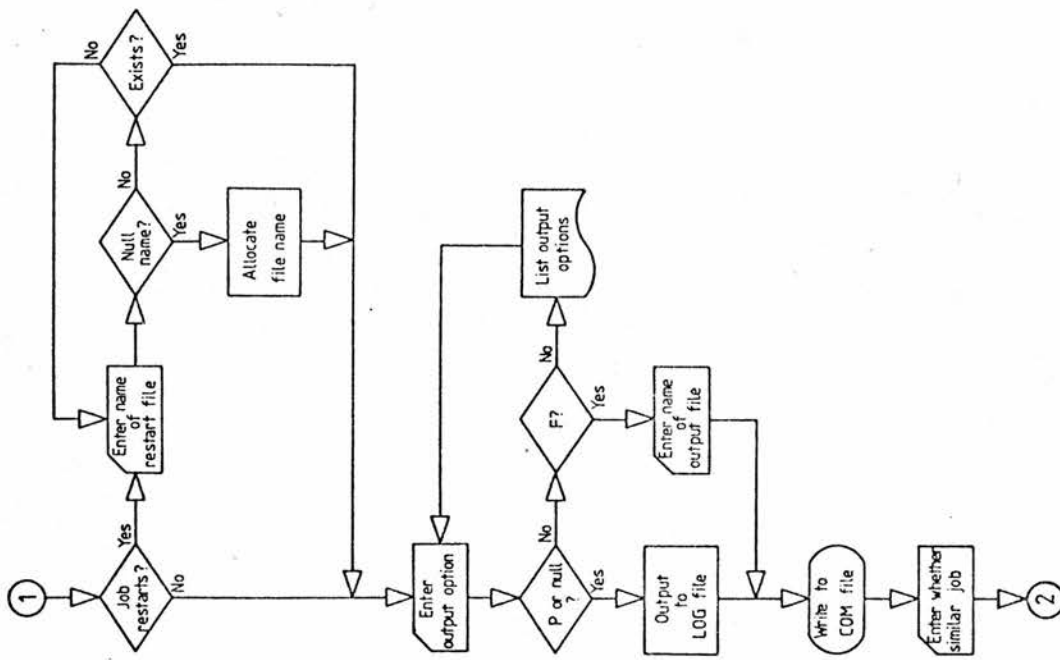


Figure 3.1 [CHSJB.JCL]QUEUE.COM Flow Diagram.

The actual running of the individual programs is further controlled by a command file [CHSJB.JCL]RUNQCPE.COM. This file is accessed when the job submitted becomes current, i.e. when it reaches to top of the queue on the computer's operating system. File allocation and parameter passing is performed by this command file using local modifications to the programs described later. These modifications allow the time limit of the batch queue to be passed automatically to the program in use rather than this information having to be explicitly given in the data input as is usual in these programs. File names passed to the program via the command file also allow any temporary files, or files being created by the program, to have the same file name as the input data file but with file types indicating the use to which they are put. A flow diagram describing the operation of this command file is given in figure 3.2.

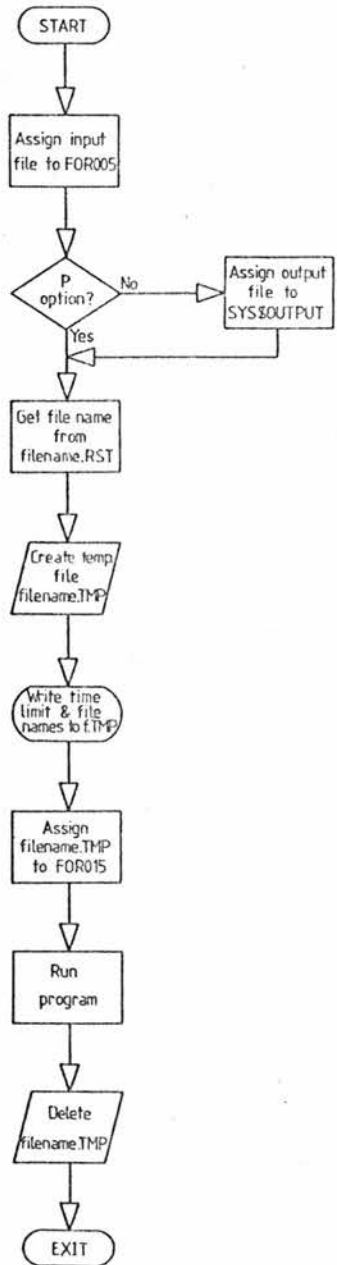


Figure 3.2 [CHSJB.JCL]RUNQCPE.COM Flow Diagram

3.1.2 MINDO/3

The program MINDO/3 [1] was initially implemented on the St. Andrews University IBM 360/44 computer and then on the Honeywell 66/80 computer at Aberdeen University. Latterly it was mounted on the twin DEC VAX 11/780 computers at St. Andrews University.

Modifications performed on the original program were performed initially to enable the correct functioning of the program and later amendments were made to ease the input and output of data and to give compatibility with the command techniques used in the previous section.

It was found when the tape containing MINDO/3 from QCPE was read into the local computers that all occurrences of the character ":" had been translated as "0". As this led to considerable confusion in the output produced all the output format statements had therefore to be examined and corrected.

The values of ETA, a value representing the precision of the arithmetic used, and THETA, the reciprocal of the highest number which can be represented on the computer, were found by reference to the manuals pertaining to the computer used. For the VAX 11/780 the value of ETA was 1×10^{-16} and THETA was 1.7×10^{-38} .

Timing information for the correct operation of MINDO/3 which provides times in units of 0.01 seconds was inserted in the subroutines TUSED and SECOND by calling the system subroutine

ACTIM. Although MINDO/3 will function with a dummy subroutine as supplied by QCPE this does not allow the program to operate its safety system. This extremely useful facility compares the time used for its latest cycle of calculations with the time which is still available. Should insufficient time remain to perform another cycle with a reasonable safety margin the program will store the data for the latest point of the calculation to a file which allows the calculation to be resubmitted and restarted from that point.

Problems were found when calculations involving configuration interaction were performed. This problem was traced to subroutine DBLCI. It was found that the version of MINDO/3 supplied assumed that array dimensioning could be performed automatically. The subroutine was changed as follows:

```
DIMENSION VECT (50, 1), EIGNVL (1)
```

was changed to

```
DIMENSION VECT (50,30), EIGNVL (50)
```

It was also found that the call of the subroutine GIVENS by DBLCI referred to an obsolete version and thus:

```
CALL GIVENS (2,2,2, EMAT, DUMSPC, EDBL, VECDBL)
```

was changed to

```
CALL GIVENS (2,2,2, EMAT, DUMSPC, EDBL, VECDBL, 3).
```

Modification was made to most of the input formats which specified the inclusion of spaces by increasing the width of existing data fields. This allows easier formation of data files because each field for numeric data can be terminated by a comma. Thus data preparation on a visual display unit (terminal) only requires the number of items on a line, i.e. a card image, to be counted rather than the number of spaces.

Output of calculation results was modified so that heats of formation were output in kJ mol^{-1} as well as kcal mol^{-1} .

A section was also added to the program which read on Fortran unit 15 the time available for the computation, the name of the restart file, and the filename for use in the creation of other files.

The restart file is called filename.RST and other files were named within the program as filename.TM1 for temporary workspace, filename.BOM for the bond order matrix and filename.GEO for geometry output. These files were opened and closed by commands added to the program which allowed the various uses of files for transferring data as specified within the MINDO/3 data specification. Thus filename.BOM could be used to write and read bond order data and filename.GEO is the equivalent of the output of a punched deck of cards. The file filename.GEO was found to be especially useful for the transfer of optimised geometries from MINDO/3 to INDO [3] programs which did not have the facilities

for geometry optimisations but can be used for the calculation of spin densities.

Input requirements for MINDO/3 are documented by comments in the source program [CHSJB.MINDO]MINDO.FOR. Specification of MINDO/3 to the QUEUE command is by the response MINDO to the prompt for the job name.

3.1.3 MNDO

MNDO [4] was implemented on the VAX 11/780 computers in a similar manner to MINDO/3 to allow use via the job submission procedures previously described.

The program obtained from QCPE was not parameterised for beryllium and these parameters were added from the work of Dewar and Rzepa [5] and from Dewar and Lo's treatment [6] of the work of Oleari et al [7].

Input specifications are given by comments in the source program [CHSJB.MNDO]MNDO.FOR and MNDO is the job name recognised by the QUEUE command.

3.1.4 UMNDO

The program UMNDO [8] was obtained prior to its release by QCPE from Dr. J.J.P. Stewart of Strathclyde University. This program was modified to suit the local job submission procedure so that file name and time limit information is passed to the program. Modifications to the program specified by QCPE [9] were also implemented to correct problems in the treatment of Configuration Interaction.

The value for NATORB(16), the number of atomic orbitals on sulphur, in subroutine START1 was found to be 9 in the program and was changed to 4.

In its original form this program required dummy geometry values and optimisation flags for the first three atoms to satisfy the free format method of input. This was modified to expect only required values and to allow the end of the input data file to terminate input.

The original program echoed all input to an output file on Fortran unit FOR007. These output statements were all removed and this output file, which was assigned the name filename.GEO, was used in conjunction with a facility to output optimised geometries as in the other programs previously described.

Fortran unit 12 was used in the original version to contain a resume of the results. This was assigned filename.OUT and was

extended to include all error messages generated by the program, enabling convenient examination of output from a computer terminal. These .OUT files were also found to be a convenient method of following intermediate points in a long optimisation requiring several restarts.

In order to test complex geometries a geometry test option was added. This facility terminates the program after evaluation of the input geometry and calculation of interatomic separations. The subroutine VECPRN was also modified so that the interatomic separations were output via unit 12 to the .OUT file so that these may be examined prior to job submission for optimisation.

Input and output of the P-matrix was changed from the original form which used printer files to reading and writing using the restart file which is an unformatted file and uses file space more efficiently.

Eigenvectors have been changed to be automatically printed with the facility for suppressing them if not required.

As a result of performing large calculations it was also found necessary to increase the array dimensions of DIELRE, the two-centre overlap integrals from 40000 to 90000.

This program, having all the facilities of MNDO plus the easier input of options and the ability to perform Unrestricted

Hartree Fock calculations, has superseded the use of MNDO.

The various options are input by keyword specification in a free format. One keyword available is HELP which prints the instructions for the use of UMNDO. Thus an input file containing only the word HELP will output the instructions for future use of the UMNDO program.

3.1.5 Other Semi-empirical Systems Implemented

During the studies carried out for this work several other computation methods were implemented. These included several programs for CNDO/INDO calculations. CINPRO [10] and CNINDO/2-3R [11] both perform INDO calculations of elements up to fluorine and CNDO calculations up to chlorine and bromine respectively. CINPRO also has the facility for spin projection calculations. CINMIN [12] is capable of geometry optimisation. All these programs had severe restrictions in their method of geometry input, being either coordinate input or an unusual version of Z-matrix input. The geometry input subroutines used in the previously described programs were modified and added to the three programs described here. This allowed compatibility with other techniques being used and enabled the easy use of optimised geometries output from MINDO/3 and (U)MNDO programs as input for CNINDO studies.

Of these three programs CNINDO/2-3R studies were

discontinued because they were not regarded as being sufficiently accurate. CINPRO remains in use as a method of spin density calculation following MINDO/3 or (U)MNDO geometry optimisation. CINMIN was also discarded as a useful tool because of its low efficiency for geometry optimisation. This was found to be approximately an order of magnitude slower than MINDO/3 optimisation with no benefits to make the method worth the increased computation time.

Although not used in this work these programs, as with the other programs previously described, remain generally available for any user of the St. Andrews VAX 11/780 computers.

3.2 Interactive Systems

The computer was also used for processes which could be performed directly from the terminal. Other than trivial calculations the facilities available were used for graphical processes, especially for molecule plotting. Interactive use allowed direct control of programs with immediate data modification to readily obtain the desired results.

3.2.1 Molecule Plotting

The program PLUTO [13] was obtained from Mr. John Low of Dundee University. This program contained all the computational techniques necessary for the plotting of chemical species with subroutines used to provide a link to local plotting procedures.

GHOST-80 [14] the locally supported suite of graphical output subroutines was interfaced to PLUTO to provide the required functions:

CALL PAPER(1) - Open the route to the plotting device

CALL PSPACE - Define the physical plotting area used

CALL MAP - Define the relationship between internal dimensions and the plotting area

CALL POSITN - Move to the specified plotting position

CALL JOIN - Join the given point to the previous point

CALL PLOTNC - Plot a "+" at the specified point

CALL GRNPEN - Specify a green pen for two colour stereoscopic views

CALL REDPEN - Specify the red pen for the other representation of the stereoscopic view

CALL TYPECS - Print specified text at the current plotting position

CALL PICSAV - Save the current picture in the specified file

CALL FRAME - End the current picture

CALL GREND - End all graphical output

Initial implementation of PLUTO did not use the PICSAV facility. The original program as received had to be linked to two different versions of the GHOST subroutine library, one to interface with the video plotting devices, and the other version to interface to the hard copy plotter, the Tektronix T4662. This necessitated the maintenance of two large execution modules on

the VAX and required PLUTO to be run twice, the first time on the video graphics terminal to chose the ideal viewpoint of the molecule being plotted, and the second time to produce the final copy on the T4662 plotter. Because of the file space required and the waste of computer time the program was modified so that after the presentation of the picture produced on the video graphics terminal the opportunity is given to save the picture in a named file. This file may subsequently be processed by the VAX system command

T4662

to produce the hard copy output on the plotter. Use of these gridfiles ensures that an efficient system is used to reproduce the picture originally shown on the video screen rather than performing the original calculation again.

The default picture sizes were set to be 180x180 mm for normal plots and 2x180x180 mm for monochromatic stereoscopic plots. Maximum size was set at 250x250 mm, this being the maximum size available on the Tektronix T4662 plotter.

Originally PLUTO performed a CALL FRAME at the end of the first of the stereoscopic pairs. This had the effect of erasing the first plot on the video graphics screen and so a test was introduced to detect this condition and the CALL FRAME was only performed when plotting of a complete picture was completed.

PLUTO reads input via Fortran logical unit 1 and so before running PLUTO the VAX command

```
ASSIGN <filename.type> FOR001
```

has to be performed.

Output from PLUTO is given to the screen by default, with the facility for specifying an output channel via the command

```
ECHO n
```

where n is a Fortran logical unit number which has to be assigned in an analagous manner to that above:

```
ASSIGN <ofilename.type> FOR00n
```

where n usually is given the value 9. The program was also modified so that if the command

```
ECHO 0
```

is given the majority of the output is suppressed.

Instructions for the operation of PLUTO on the VAX system are contained in the file [CHSJB.MANUAL]PLUTO.MEM, and a copy of the data used as an example in this manual is contained in the file [CHSJB.PLOT]PLUTEST.DAT. Use of PLUTO is by the command

```
RUN [CHSJB.PLOT]PLUTO
```

on the St. Andrews VAX-B computer (SAVB).

References

- [1] R.C. Bingham, M.J.S. Dewar and D.H. Lo, J. Am. Chem. Soc., 97(1975), 1285; QCPE 309
- [2] "VAX/VMS Command Language User's Guide", Digital Equipment Corporation, Massachusetts, 1982
- [3] J.A. Pople and D.L. Beveridge, "Approximate Molecular Orbital Theory", McGraw-Hill, New York, 1970
- [4] M.J.S. Dewar and W. Thiel, J. Am. Chem. Soc., 99(1977), 4899; QCPE 353
- [5] M.J.S. Dewar and H.S. Rzepa, J. Am. Chem. Soc., 94(1972), 5296
- [7] L.Oleari, L. DiSipio and G. DeMichelis, Mol. Phys., 10(1966), 97
- [8] M.J.S. Dewar, J.J.P. Stewart, W. Thiel and P. Weiner, QCPE Bulletin, 1(1981), 428; QCPE 428
- [9] J.J.P. Stewart, QCPE Bulletin, 2(1982), 58
- [10] D.A. Brewer, B.H. Lengsfeld and J.C. Schug, QCPE Newsletter, 56(1977), 10
- [11] H.L. Hase and A. Schweig, Chim. Acta, 31(1973), 215; QCPE Newsletter, 46(1974), 261
- [12] A. Arbor, M. Fraser and D.M. Hayes, QCPE 389 (1980)

- [13] S. Motherwell, Crystallographic Data Centre, University Chemical Laboratory, Cambridge; W.B. Clegg, Department of Inorganic Chemistry, The University, Newcastle upon Tyne
- [14] W.A.J. Prior, and R.J. Sutherland, "GHOST-80", Culham Laboratory; M. Bain, "GHOST-80 User Manual", Computing Laboratory, University of St. Andrews

CHAPTER 4

MINDO/3 STUDY OF FIRST-ROW TRIATOMIC HYDRIDES AND THEIR IONS

The first semi-empirical calculations performed in this work comprised the study of the first-row triatomic hydrides, and of their cations and anions.

Walsh [1] first attempted the explanation of the structures of small molecules in molecular orbital terms, and these were followed by the Extended Huckel calculations of Gimarc [2] for the neutral series NH_n ($n=2,3,4$). Some ab initio calculations have been performed for some of the triatomic hydrides [3-5] but these have tended to be inconsistent [6].

As many of the MINDO/3 parameters have been found empirically it was considered that the study of this series of hydrides and their ions would be a fair indication of the reliability of this semi-empirical method.

The calculations were performed using the version of MINDO/3 described in chapters 2 and 3 on the series MH_2 ($M=B,C,N,O,F$) in their neutral, anionic and cationic forms. Both singlet and triplet calculations were performed on BH_2^- , CH_2 , and NH_2^+ .

A further series of calculations was also carried out with the angle $\angle HMH$ fixed from 75° to 180° in 15° increments,

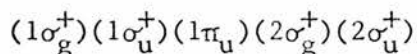
optimising the M-H distances at each point. These calculations were performed using the "reaction coordinate" facility of MINDO/3 which allows the variation of one of the geometrical parameters over a specified range of values, optimisation of the remaining parameters being performed at each of these values.

The results of these calculations are given in tables 4.1-4.18.

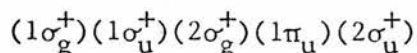
Orbital Energies

The variation of orbital energy as a function of H-O-H angle is depicted in figure 4.1.

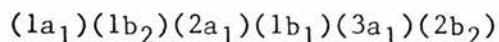
In the linear configuration all the species studied, except the singlet states of BH_2^- , CH_2 and NH_2^+ and the boron species BH_2^+ and BH_2 were found to adopt the order of molecular orbitals:



The boron species BH_2^+ and BH_2 adopted the order



Reduction of the H-M-H angle from 180° caused, by descent of symmetry, the order:



since the degeneracy of π_u is broken on bending to $a_1 + b_1$. This orbital ordering is maintained for most species between H-M-H angles of 180° and 75° . The orbitals $2b_2$ and $3a_1$ cross at low angles in CH_2^+ and NH_2^+ and the orbitals $2a_1$ and $1b_2$ cross at low H-M-H angle in H_2F^+ , H_2F and H_2O^- .

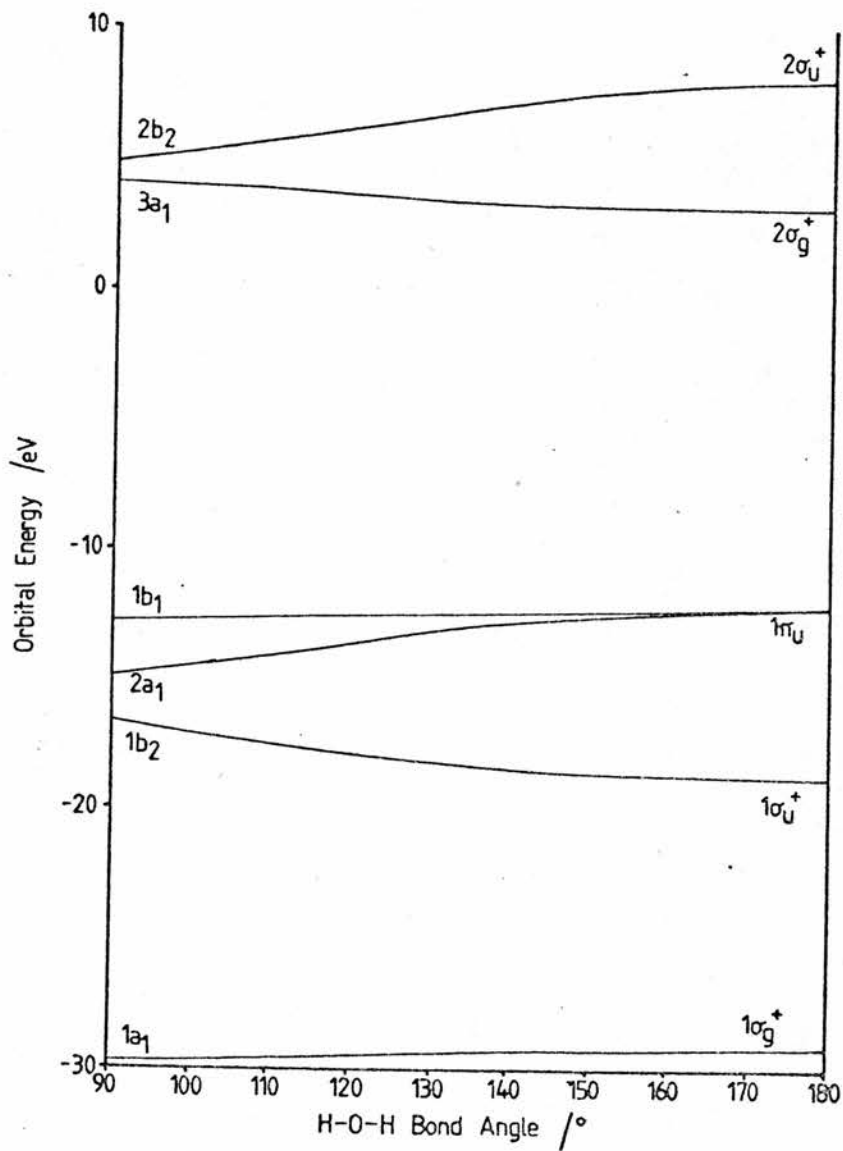


Figure 4.1 Orbital energies as a function of H-O-H angle in H_2O

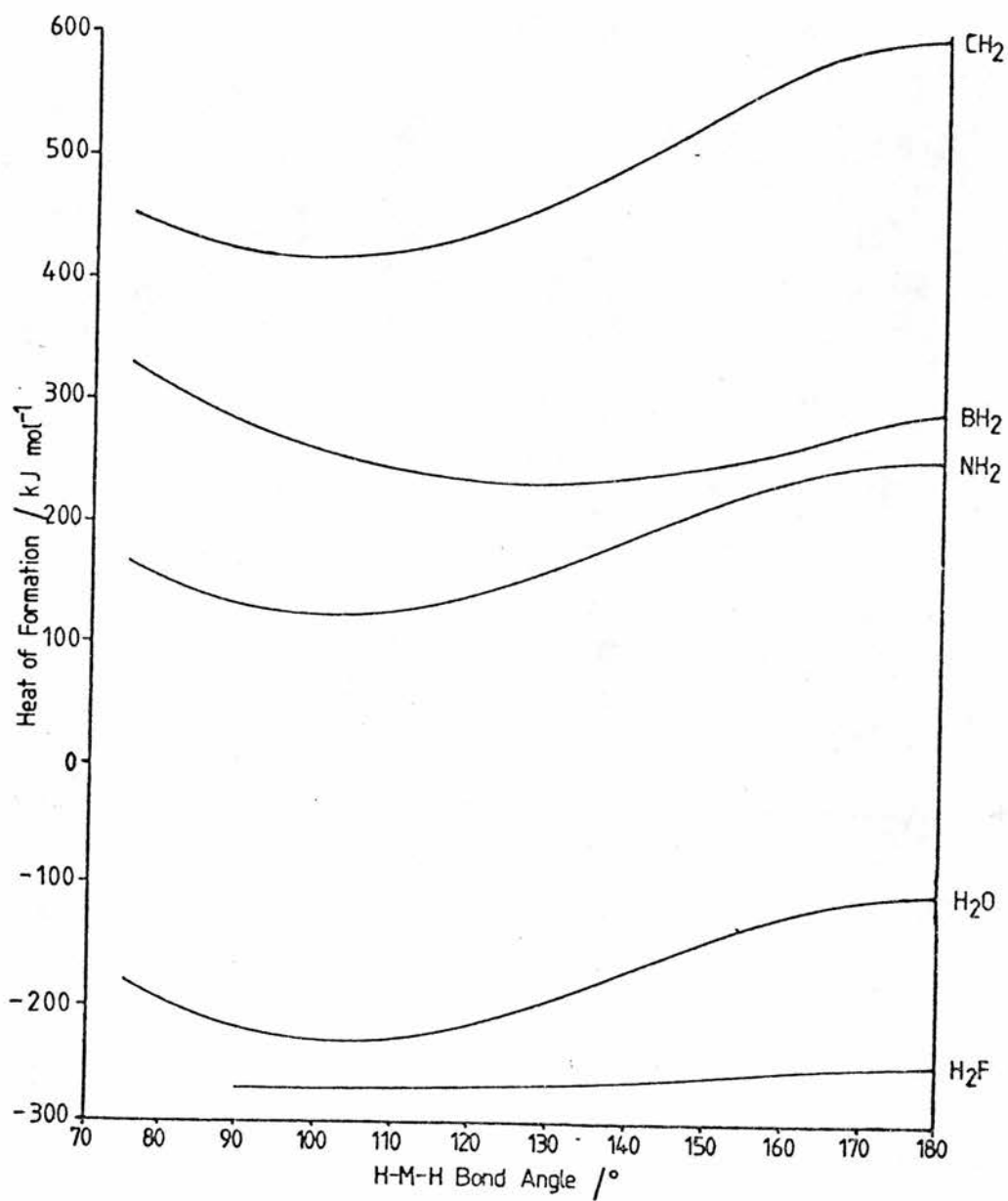


Figure 4.2 Heat of formation of neutral MH_2 as a function of H-M-H angle

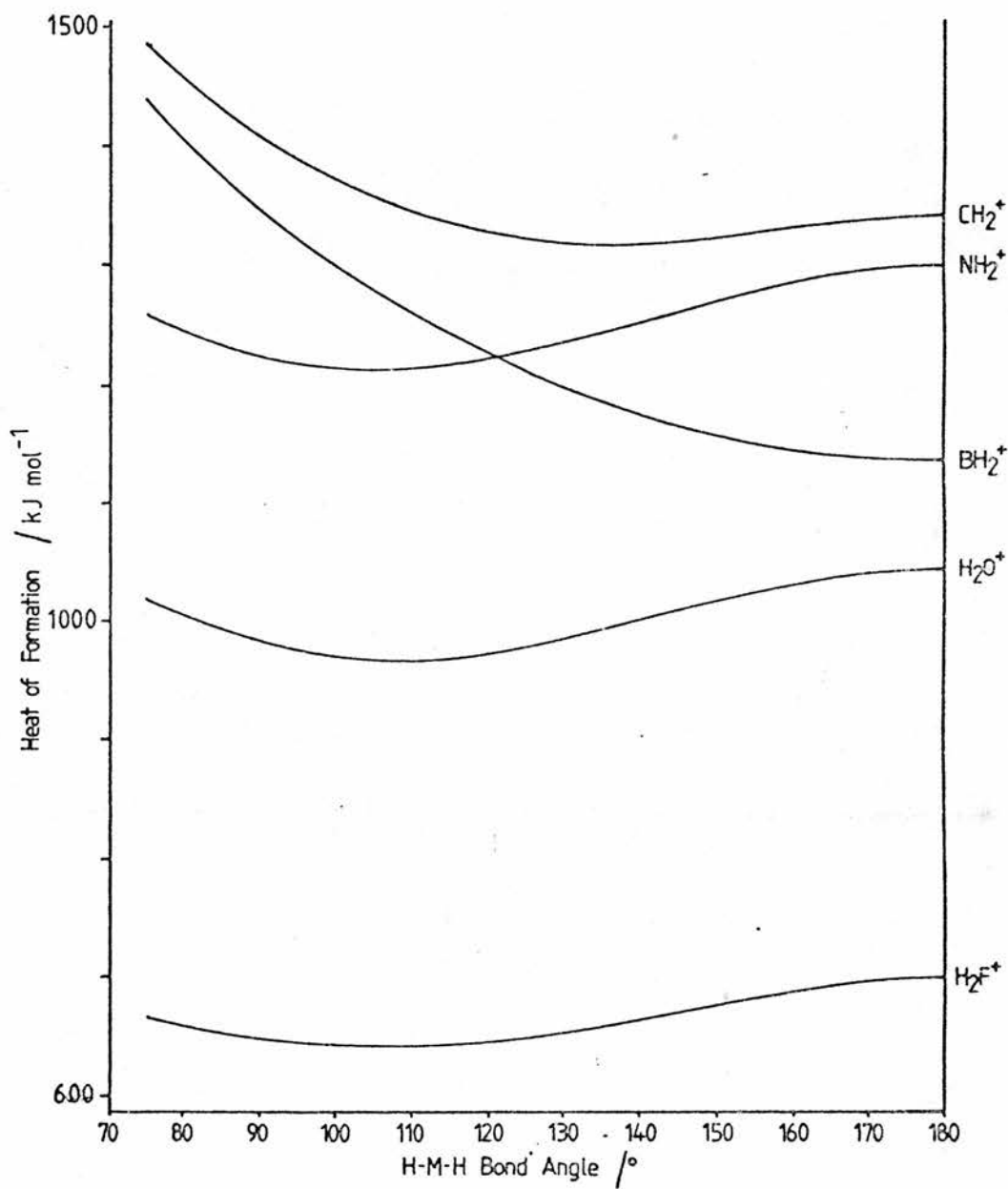


Figure 4.3 Heat of formation of cationic $(MH_2)^+$ as a function of H-M-H angle

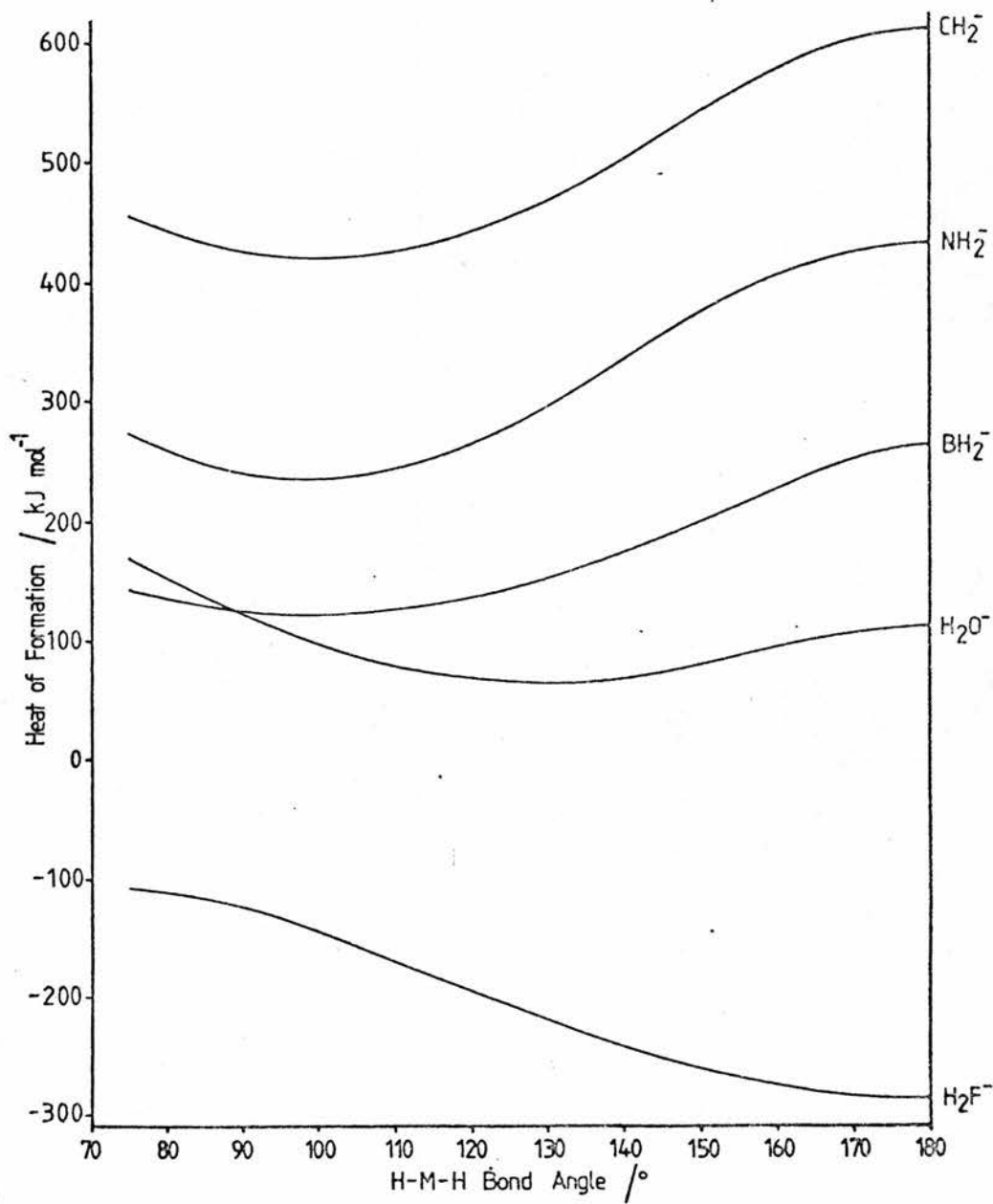


Figure 4.4 Heat of formation of anionic $(\text{MH}_2)^-$ as a function of H-M-H angle

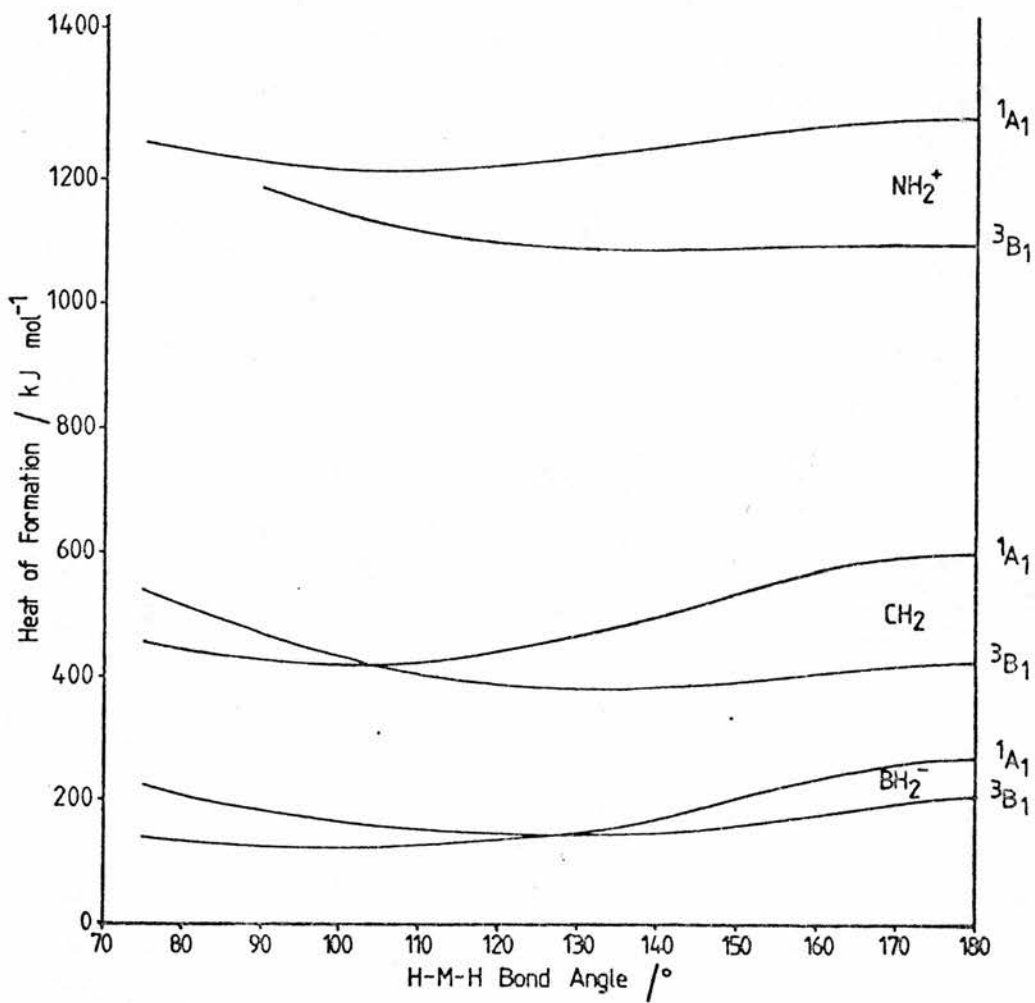


Figure 4.5 Heat of formation of singlet and triplet NH_2^+ , CH_2 , and BH_2^- as a function of H-M-H angle

Heats of Formation

Figures 4.2-4.4 show the variation of heat of formation as a function of H-M-H angle for $(MH_2)^+$, MH_2 and $(MH_2)^-$. The variation of heat of formation of singlet and triplet forms of NH_2^+ , CH_2 and BH_2^- are shown in figure 4.5. The values calculated for heat of formation may be compared with the experimental values [7]: BH_2 201kJ mol^{-1} ; $CH_2(^3B_1)$ $397\pm 20\text{kJ mol}^{-1}$; NH_2 168.6kJ mol^{-1} and H_2O -241.8kJ mol^{-1} .

Molecular Structures at Equilibrium

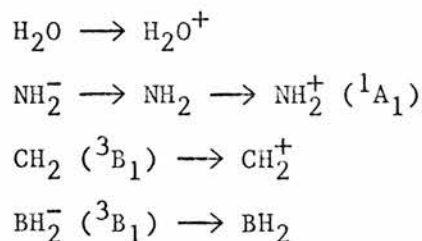
The geometry of each species at minimum energy as given in tables 4.1-4.18 may be compared with some experimental values in table 4.19.

Comparison may also be made with ab initio calculations for the species: NH_2^+ (3B_1) ($\langle HNH \rangle = 140^\circ$) [3], NH_2^+ (1A_1) ($\langle HNH \rangle = 120^\circ$) [3], H_2O^+ ($\langle HOH \rangle = 112.5^\circ$) [4], and H_2F^+ ($\langle HFH \rangle = 116^\circ$) [5].

For each M in the series studied, the $d(H-H)$ value for the species with the minimum $\langle HMH \rangle$ may be considered to be the sum of the non-bonded radii for hydrogen atoms: $H_B = 0.97\text{\AA}$ (Exptal = 1.07\AA), $H_C = 0.86\text{\AA}$ (Exptal = 0.87\AA), $H_N = 0.81\text{\AA}$ (Exptal = 0.80\AA), $H_O = 0.75\text{\AA}$ (Exptal = 0.76\AA) and $H_F = 0.77\text{\AA}$.

Walsh [1] and Gimarc [2] suggest that species with four or

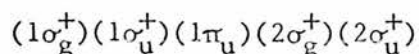
ten valence-shell electrons will have linear ground states, and that species with between five and nine will have non-linear ground states with $\langle \text{HMH} \rangle$ close to 100° for six, seven and eight electrons and wider angles for species with five or nine valence-shell electrons. The data in tables 4.1-4.18 support this generalisation. Support is also given to their deduction [1,2] that on ionisation by removal of a non-bonding electron from $1b_1$ there will be little geometrical change, as for the ionisations:



Six-electron Species

Great interest has been shown experimentally [9-11] and theoretically [6,13] in CH_2 , but little in the analogous six-electron species BH_2^- and NH_2^+ . The results shown here agree with previous MINDO/3 calculations [13].

As was generally found for the species studied here, the linear triplets assumed the order of molecular orbitals

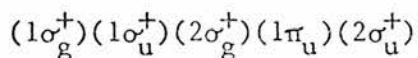


in which the two components for $1\pi_u$ are each singly occupied with identical energies (c.f. tables 4.4, 4.7 and 4.10). When the

singlet species CH_2 and NH_2^+ were constrained to be linear, where one component of $1\pi_u$ was doubly occupied, the doubly occupied orbital was found to be much more tightly bound, but the mean of the two orbital energies ($2a_1$ and $1b_1$) was exactly that of the corresponding triplet.

It may also be noted that the energies of the four remaining orbitals $1\sigma_g^+$, $1\sigma_u^+$, $2\sigma_g^+$ and $2\sigma_u^+$ are identical for the singlet and triplet forms of CH_2 (tables 4.6 and 4.7) and NH_2^+ (tables 4.9 and 4.10).

The linear configuration of BH_2^- (1A_1) adopted the orbital ordering



which readily accommodates a singlet configuration. The triplet form was found to be the only boron species studied in which $1\pi_u$ was found to be tighter bound than $2\sigma_g^+$.

The optimised geometries for the triplet forms of CH_2 and NH_2^- were found to be 36.36 and 129.0 kJ mol^{-1} respectively more stable than their singlet forms. For BH_2^- the singlet was found to be more stable by 22.72 kJ mol^{-1} than the triplet. The variation of ΔH_f^\ominus with $\langle \text{HMH} \rangle$ for the singlets and triplets of the six-electron species is shown in figure 4.5.

Ionisation Energies

Valence-shell vertical ionisation energies were calculated for H₂O as 12.76, 14.36, 17.28 and 29.61 eV. The first three may be compared with the observed He-I photoelectron spectral values of 12.61, 13.89 and 17.20 eV [14]. Tables 4.1-4.18 include the calculated values of the first ionisation energies. Vertical ionisation energies were calculated, using Koopman's theorem, from the binding energies of the HOMO. Adiabatic energies were calculated from the energies at equilibrium of the parent species and its ionised daughter. The adiabatic energies may be compared reasonably with the experimental data [17]: BH₂, 8.12 eV; CH₂ (³B₁), 11.82 eV; NH₂, 11.4 eV (probably to NH₂⁺ (¹A₁)); and H₂O, 12.61 eV. It was found that even with feebly bound species such as H₂F⁻ and unbound species such as NH₂⁻ which are diamagnetic the adiabatic ionisation energy was always calculated to be lower than the vertical ionisation energy. In paramagnetic species it was found that the vertical ionisation energy was always seriously underestimated; this is a consequence of the 'half-electron' method used by MINDO/3 in the RHF treatment of doublet and triplet states: for such states only the calculated adiabatic energies are of significance.

$\langle \text{HMH} \hat{O} \Delta \text{H}_f^\ddagger / \text{kJ mol}^{-1} \rangle$	$d(\text{M-H})/\text{\AA}$	Orbital Energy/eV					
		1a ₁	1b ₂	2a ₁	1b ₁	3a ₁	2b ₂
180	1.185	-25.33	-19.88	-8.67	-8.43	-8.43	-5.15
165	1.186	-25.33	-19.85	-8.98	-8.43	-8.13	-5.18
150	1.187	-25.35	-19.76	-9.38	-8.43	-7.75	-5.26
135	1.191	-25.38	-19.61	-9.78	-8.44	-7.40	-5.40
120	1.196	-25.41	-19.39	-10.18	-8.44	-7.07	-5.59
105	1.203	-25.46	-19.09	-10.57	-8.46	-6.80	-5.81
90	1.212	-25.53	-18.69	-10.97	-8.48	-6.60	-6.04
75	1.223	-25.65	-18.17	-11.41	-8.53	-6.51	-6.26
180.0	1.185	-25.33	-19.88	-8.67	-8.43	-8.43	-5.15

Electron Population		First Ionisation Energy /eV		Dipole Moment/D	d(H-H)/\AA
M	H	Vertical	Adiabatic		
2.280	0.860	19.88	-	-	2.370

Table 4.1 BH₂⁺ (¹Σ_g⁺)

$\langle \text{HMH} \rangle / ^\circ$	$\Delta H_f^\circ / \text{kJ mol}^{-1}$	$d(\text{M-H}) / \text{\AA}$	Orbital Energy/eV						Dipole Moment/D	$d(\text{H-H}) / \text{\AA}$
			1a ₁	1b ₂	2a ₁	1b ₁	3a ₁	2b ₂		
180	294.4	1.226	-16.94	-12.07	-4.42	-0.31	-0.31	-0.31	2.63	
165	272.5	1.208	-16.93	-12.03	-4.56	-0.41	-0.41	-0.06	2.63	
150	248.9	1.198	-16.97	-11.93	-4.88	-0.47	0.32	0.32	2.58	
135	237.0	1.198	-17.01	-11.74	-5.24	-0.49	0.68	0.68	2.46	
120	237.8	1.198	-17.06	-11.48	-5.60	-0.51	1.02	1.02	2.32	
105	252.6	1.198	-17.14	-11.13	-5.95	-0.53	1.30	1.30	2.16	
90	283.2	1.202	-17.24	-10.66	-6.31	-0.55	1.50	1.50	2.00	
75	331.5	1.206	-17.40	-10.06	-6.71	-0.59	1.58	1.58	1.88	
130.156	235.8	1.198	-17.02	-11.67	-5.36	-0.50	0.79	0.79	2.42	

Electron Population		First Ionisation Energy /eV		Dipole Moment/D	$d(\text{H-H}) / \text{\AA}$
M	H	Vertical	Adiabatic		
2.820	1.090	5.36	9.34	0.321	2.174

Table 4.2 BH₂ (²A₁)

$\langle \text{HMH} \rangle / ^\circ$	$\Delta H_F^\ddagger / \text{kJ mol}^{-1}$	$d(\text{M-H}) / \text{\AA}$	Orbital Energy/eV						2b ₂
			1a ₁	1b ₂	2a ₁	1b ₁	3a ₁	2b ₁	
180	266.0	1.361	-8.86	-4.57	-0.55	7.23	7.23	7.23	9.66
165	242.0	1.339	-8.69	-4.43	-0.61	7.31	7.31	7.56	9.81
150	201.0	1.311	-8.59	-4.21	-0.75	7.37	7.37	8.02	9.94
135	163.6	1.292	-8.57	-3.95	-0.96	7.39	7.39	8.44	9.96
120	136.8	1.282	-8.60	-3.62	-1.20	7.40	7.40	8.82	9.91
105	123.5	1.277	-8.65	-3.20	-1.46	7.40	7.40	9.15	9.82
90	125.3	1.274	-8.72	-2.65	-1.74	7.40	7.40	9.39	9.74
75	142.2	1.271	-8.86	-2.05	-1.95	7.40	7.40	9.53	9.73
99.241	122.3	1.276	-8.67	-3.00	-1.57	7.40	7.40	9.25	9.79

Electron Population		First Ionisation Energy /eV	Dipole Moment/D	$d(\text{H-H}) / \text{\AA}$
M	H	Vertical	Adiabatic	
3.394	1.303	1.57	1.18	1.944

Table 4.3 BH₂⁻ (¹A₁)

	$\langle \text{HMH} \rangle / ^\circ$	$\Delta H_f^\ominus / \text{kJ mol}^{-1}$	$d(\text{M-H}) / \text{\AA}$	Orbital Energy/eV						Dipole Moment/D	$d(\text{H-H}) / \text{\AA}$
				1a ₁	1b ₂	2a ₁	1b ₁	3a ₁	2b ₂		
180	204.3	1.132	-8.62	-4.34	3.44	3.44	3.44	8.03	10.47		
165	184.6	1.161	-8.55	-4.28	3.40	3.40	3.60	7.96	10.39		
150	159.5	1.173	-8.57	-4.16	3.10	3.10	3.75	8.22	10.33		
135	146.6	1.176	-8.64	-3.98	2.75	2.75	3.79	8.57	10.23		
120	145.5	1.183	-8.69	-3.72	2.38	2.38	3.80	8.85	10.06		
105	157.3	1.187	-8.79	-3.37	2.04	2.04	3.80	9.12	9.90		
90	183.3	1.190	-8.92	-2.92	1.69	1.69	3.78	9.29	9.73		
75	223.7	1.190	-9.16	-2.33	1.32	1.32	3.73	9.34	9.64		
128.144	144.5	1.177	-8.66	-3.87	2.58	2.58	3.80	8.71	10.15		

Electron Population		First Ionisation Energy /eV		Dipole Moment/D	$d(\text{H-H}) / \text{\AA}$
M	H	Vertical	Adiabatic		
3.942	1.029	-3.80	0.95	-	2.117

Table 4.4 BH_2^- ($^3\text{B}_1$)

$\langle \text{HMH} \rangle^{\circ}$	$\Delta H_{\text{F}}^{\circ} / \text{kJ mol}^{-1}$	$d(\text{M-H}) / \text{\AA}$	Orbital Energy/eV					
			1a ₁	1b ₂	2a ₁	1b ₁	3a ₁	2b ₂
180	1341.3	1.086	-32.99	-23.17	-13.15	-9.16	-6.98	-3.76
165	1333.8	1.089	-33.01	-23.13	-13.30	-9.17	-6.89	-3.85
150	1321.7	1.091	-33.12	-23.04	-13.70	-9.20	-6.60	-4.04
135	1318.0	1.093	-33.22	-22.82	-14.20	-9.23	-6.21	-4.30
120	1329.2	1.097	-33.32	-22.47	-14.73	-9.24	-5.81	-4.60
105	1359.2	1.101	-33.41	-22.00	-15.25	-9.26	-5.46	-4.94
90	1410.9	1.111	-33.46	-21.36	-15.76	-9.26	-5.23	-5.31
75	1487.7	1.121	-33.54	-20.59	-16.26	-9.25	-5.12	-5.64
136.845	1317.9	1.093	-33.15	-22.81	-14.13	-9.21	-6.29	-4.28

Electron Population		First Ionisation Energy /eV	Dipole Moment/D	$d(\text{H-H}) / \text{\AA}$
M	H			
3.278	0.861	14.13	-	2.032

Table 4.5 CH₂⁺ (²A₁)

$\langle \text{HMH} \rangle^{\circ}$	$\Delta \text{H}_f^{\circ} / \text{kJ mol}^{-1}$	$d(\text{M-H}) / \text{\AA}$	Orbital Energy/eV						$d(\text{H-H}) / \text{\AA}$
			1a ₁	1b ₂	2a ₁	1b ₁	3a ₁	2b ₂	
180	598.4	1.064	-23.49	-14.26	-7.78	0.20	2.30	5.44	
165	581.1	1.072	-23.51	-14.21	-7.85	0.21	2.27	5.32	
150	534.0	1.094	-23.56	-14.07	-8.18	0.19	2.30	4.97	
135	480.2	1.108	-23.66	-13.83	-8.73	0.15	2.60	4.61	
120	440.0	1.115	-23.78	-13.46	-9.28	0.12	3.00	4.29	
105	420.7	1.120	-23.89	-12.94	-9.79	0.10	3.38	3.98	
90	425.3	1.127	-23.99	-12.27	-10.27	0.10	3.67	3.67	
75	456.1	1.137	-24.08	-11.41	-10.74	0.11	3.40	3.82	
100.177	419.4	1.122	-23.92	-12.75	-9.95	0.10	3.48	3.88	
Electron Population		First Ionisation Energy /eV		Dipole Moment/D					
M	H	Vertical	Adiabatic						
3.812	1.094	9.95	9.31	1.043	1.722				

Table 4.6 CH₂ (¹A₁)

	$\langle \text{HMH} \hat{O} \Delta \text{H}_f^\ominus \rangle / \text{kJ mol}^{-1}$	$d(\text{M-H}) / \text{\AA}$	Orbital Energy/eV					
			1a ₁	1b ₂	2a ₁	1b ₁	3a ₁	2b ₂
180	419.0	1.064	-23.49	-14.26	-3.79	-3.79	2.30	5.44
165	408.5	1.069	-23.50	-14.22	-3.93	-3.79	2.36	5.34
150	391.1	1.075	-23.57	-14.09	-4.32	-3.81	2.62	5.13
135	383.2	1.085	-23.60	-13.83	-4.83	-3.82	2.96	4.84
120	390.5	1.085	-23.74	-13.49	-5.36	-3.84	3.40	4.56
105	417.3	1.095	-23.79	-12.98	-5.89	-3.85	3.72	4.19
90	466.4	1.105	-23.86	-12.34	-6.40	-3.86	3.96	3.81
75	540.6	1.105	-24.08	-11.57	-6.88	-3.87	4.15	3.52
135.801	383.0	1.078	-23.67	-13.88	-4.80	-3.83	2.99	4.89

Electron Population		First Ionisation Energy /eV	Dipole Moment/D	$d(\text{H-H}) / \text{\AA}$
M	H			
4.146	0.927	3.83	0.896	1.998
		Vertical	Adiabatic	
		9.69		

Table 4.7 CH₂ (³B₁)

$\langle \text{HMH} \rangle / ^\circ$	$\Delta \text{H}_f^\ominus / \text{kJ mol}^{-1}$	$d(\text{M-H}) / \text{\AA}$	Orbital Energy/eV						$d(\text{H-H}) / \text{\AA}$
			1a ₁	1b ₂	2a ₁	1b ₁	3a ₁	2b ₂	
180	611.6	1.053	-13.89	-5.23	1.62	5.61	11.64	14.66	
165	595.4	1.063	-13.89	-5.19	1.58	5.63	11.55	14.52	
150	546.3	1.102	-13.88	-5.08	1.20	5.59	11.28	13.98	
135	486.4	1.129	-13.93	-4.87	0.53	5.51	11.46	13.49	
120	443.2	1.137	-14.03	-4.49	-0.02	5.47	11.89	13.19	
105	422.4	1.142	-14.13	-3.95	-0.52	5.46	12.29	12.89	
90	426.6	1.149	-14.23	-3.26	-0.99	5.46	12.59	12.60	
75	458.6	1.159	-14.32	-2.38	-1.45	5.46	12.31	12.77	
99.891	420.9	1.144	-14.16	-3.74	-0.69	5.46	12.41	12.79	
Electron Population		First Ionisation Energy /eV		Dipole Moment/D					
M	H	Vertical	Adiabatic						
4.628	1.186	-5.46	-0.39 (to ³ B ₁)						
			-0.02 (to ¹ A ₁)						
				-	1.751				

Table 4.8 CH₂⁻ (²B₁)

$\langle \text{HMH} \rangle / ^\circ$	$\Delta H_f^\ominus / \text{kJ mol}^{-1}$	$d(\text{M-H}) / \text{\AA}$	Orbital Energy/eV					
			1a ₁	1b ₂	2a ₁	1b ₁	3a ₁	2b ₂
180	1300.8	0.995	-34.09	-26.21	-20.15	-10.65	-6.90	-3.31
165	1292.7	0.999	-34.10	-26.15	-20.20	-10.67	-6.87	-3.41
150	1271.0	1.008	-34.14	-25.97	-20.37	-10.73	-6.78	-3.70
135	1243.4	1.019	-34.20	-25.69	-20.69	-10.83	-6.60	-4.11
120	1220.8	1.030	-34.30	-25.30	-21.13	-10.93	-6.34	-4.60
105	1212.7	1.039	-34.43	-24.77	-21.61	-11.00	-6.08	-5.10
90	1225.0	1.050	-34.54	-24.09	-22.07	-11.03	-5.89	-5.58
75	1260.2	1.065	-34.62	-23.24	-22.51	-11.01	-5.86	-6.00
106.016	1212.7	1.039	-34.42	-24.81	-21.57	-11.00	-6.09	-5.06

Electron Population		First Ionisation Energy /eV	Dipole Moment/D	$d(\text{H-H}) / \text{\AA}$
M	H			
4.368	0.816	-	-	1.659

Table 4.9 NH_2^+ ($^1\text{A}_1$)

	$\langle \text{HMH} \hat{O} \Delta \text{H}_f^e \rangle / \text{kJ mol}^{-1}$	$d(\text{M-H}) / \text{\AA}$	Orbital Energy/eV						2b ₂
			1a ₁	1b ₂	2a ₁	1b ₁	3a ₁		
180	1099.2	0.995	-34.09	-26.21	-15.40	-15.40	-15.40	-6.90	-3.31
165	1094.4	0.997	-34.10	-26.16	-15.52	-15.42	-15.42	-6.82	-3.41
150	1086.0	0.999	-34.19	-26.03	-15.86	-15.49	-15.49	-6.58	-3.64
135	1084.8	1.008	-34.22	-25.74	-16.33	-15.54	-15.54	-6.26	-4.01
120	1097.7	1.008	-34.41	-25.38	-16.88	-15.61	-15.61	-5.85	-4.40
105	1130.1	1.018	-34.46	-24.81	-17.42	-15.62	-15.62	-5.54	-4.88
90	1184.4	1.028	-34.54	-24.10	-17.95	-15.61	-15.61	-5.36	-5.31
140.573	1083.7	1.000	-34.28	-25.90	-16.15	-15.54	-15.54	-6.35	-3.84

Electron Population		First Ionisation Energy /eV	Dipole Moment/D	d(H-H)/\AA
M	H			
4.504	0.748	15.54	-	1.883

Table 4.10 NH_2^+ (${}^3\text{B}_1$)

$\langle \text{HMH} \rangle^{\circ}$	$\Delta H_f^{\circ} / \text{kJ mol}^{-1}$	$d(\text{M-H}) / \text{\AA}$	Orbital Energy/eV						Dipole Moment/D	$d(\text{H-H}) / \text{\AA}$
			1a ₁	1b ₂	2a ₁	1b ₁	3a ₁	2b ₂		
180	255.3	0.969	-24.12	-16.19	-9.26	-4.52	3.15	7.00		
165	244.9	0.974	-24.12	-16.13	-9.31	-4.54	3.14	6.88		
150	215.7	0.988	-24.12	-15.96	-9.50	-4.64	3.15	6.52		
135	176.5	1.006	-24.12	-15.69	-9.91	-4.79	3.25	5.99		
120	142.5	1.022	-24.18	-15.28	-10.46	-4.93	3.51	5.42		
105	126.3	1.034	-24.28	-14.72	-11.03	-5.03	3.82	4.89		
90	134.6	1.046	-24.40	-13.99	-11.57	-5.08	4.08	4.39		
75	171.0	1.061	-24.50	-13.08	-12.07	-5.08	3.93	4.18		
102.214	125.8	1.036	-24.31	-14.60	-11.14	-5.04	3.88	4.80		
Electron Population		First Ionisation Energy /eV		Dipole Moment/D		$d(\text{H-H}) / \text{\AA}$				
M	H	Vertical	Adiabatic							
5.092	0.954	5.04	9.93 (to ³ B ₁)							
			11.26 (to ¹ A ₁)					1.613		

Table 4.11 NH₂ (²B₁)

$\langle \text{HMH} \text{O} \rangle \Delta H_{\text{f}}^{\circ} / \text{kJ mol}^{-1}$	$d(\text{M-H}) / \text{\AA}$	Orbital Energy/eV					
		1a ₁	1b ₂	2a ₁	1b ₁	3a ₁	2b ₂
180	0.958	-13.89	-6.04	1.70	1.70	13.19	17.38
165	0.966	-13.87	-6.00	1.66	1.65	13.12	17.22
150	0.994	-13.77	-5.89	1.39	1.46	12.85	16.62
135	1.034	-13.62	-5.71	0.63	1.10	12.71	15.71
120	1.052	-13.68	-5.32	-0.12	0.91	13.05	15.10
105	1.062	-13.78	-4.74	-0.76	0.82	13.47	14.60
90	1.073	-13.91	-3.96	-1.33	0.77	13.80	14.13
75	1.087	-14.01	-3.00	-1.88	0.76	13.67	13.99
99.057	1.066	-13.83	-4.45	-0.99	0.80	13.61	14.41

Electron Population		First Ionisation Energy /eV	Dipole Moment/D	$d(\text{H-H}) / \text{\AA}$
M	H			
5.768	1.116	-0.80	-	1.622

Table 4.12 $\text{NH}_2^-(^1\text{A}_1)$

$\langle \text{HMH} \rangle^{\circ} \Delta H_f^{\circ} / \text{kJ mol}^{-1}$	$d(\text{M-H}) / \text{\AA}$	Orbital Energy/eV					
		1a ₁	1b ₂	2a ₁	1b ₁	3a ₁	2b ₂
180	0.949	-39.90	-29.61	-24.12	-18.78	-7.72	-3.21
165	0.951	-39.93	-29.56	-24.20	-18.81	-7.68	-3.32
150	0.956	-40.03	-29.41	-24.46	-18.90	-7.45	-3.65
135	0.963	-40.17	-29.17	-24.88	-19.02	-7.32	-4.12
120	0.969	-40.34	-28.81	-25.39	-19.13	-7.05	-4.68
105	0.976	-40.50	-28.31	-25.95	-19.21	-6.82	-5.27
90	0.985	-40.62	-27.66	-26.49	-19.25	-6.69	-5.85
75	0.999	-40.65	-27.01	-26.86	-19.21	-6.76	-6.38
108.419	0.975	-40.46	-28.43	-25.82	-19.20	-6.87	-5.13

Electron Population		First Ionisation Energy /eV		Dipole Moment/D	$d(\text{H-H}) / \text{\AA}$
M	H	Vertical	Adiabatic		
5.798	0.604	19.20	-	-	1.581

Table 4.13 H_2O^+ (${}^2\text{B}_1$)

$\langle \text{HMH} / \circ \Delta \text{H}_F^\circ / \text{kJ mol}^{-1}$	$d(\text{M-H}) / \text{\AA}$	Orbital Energy/eV					
		1a ₁	1b ₂	2a ₁	1b ₁	3a ₁	2b ₂
180	0.900	-29.16	-18.82	-12.24	-12.24	3.08	7.96
165	0.904	-29.18	-18.76	-12.32	-12.27	3.10	7.81
150	0.914	-29.23	-18.58	-12.59	-12.37	3.17	7.41
135	0.927	-29.23	-18.30	-13.06	-12.51	3.35	6.82
120	0.938	-29.45	-17.89	-13.67	-12.66	3.62	6.17
105	0.948	-29.59	-17.32	-14.31	-12.76	3.92	5.51
90	0.959	-29.71	-16.58	-14.94	-12.81	4.13	4.88
75	0.974	-29.76	-15.68	-15.54	-12.79	4.17	4.28
104.027	0.948	-29.61	-17.28	-14.36	-12.76	3.94	5.48

Electron Population		First Ionisation Energy /eV	Dipole Moment/D	$d(\text{H-H}) / \text{\AA}$
M	H			
6.506	0.747	12.37	2.108	1.495

Table 4.14 H₂O (¹A₁)

$\langle \text{HMH} \rangle^{\circ} \Delta H_{\text{F}}^{\circ} / \text{kJ mol}^{-1}$	$d(\text{M-H}) / \text{\AA}$	Orbital Energy/eV					
		1a ₁	1b ₂	2a ₁	1b ₁	3a ₁	2b ₂
180	1.023	-17.28	-8.42	-1.85	-1.85	6.16	15.83
165	1.028	-17.33	-8.39	-2.06	-1.94	6.24	15.65
150	1.038	-17.44	-8.26	-2.59	-2.13	6.51	15.22
135	1.045	-17.56	-7.97	-3.25	-2.28	6.70	14.78
120	1.051	-17.67	-7.50	-3.92	-2.35	7.49	14.36
105	1.059	-17.71	-6.82	-4.55	-2.37	7.95	13.91
90	1.069	-17.70	-5.95	-5.12	-2.32	8.32	13.49
75	1.087	-17.59	-4.90	-5.65	-2.19	8.47	13.08
133.487	1.046	-17.57	-7.93	-3.32	-2.29	7.01	14.73

Electron Population		First Ionisation Energy /eV	Dipole Moment/D	$d(\text{H-H}) / \text{\AA}$
M	H	Vertical	Adiabatic	
6.726	1.137	-7.01	-3.00	1.923

Table 4.15 $\text{H}_2\text{O}^- (^2\text{A}_1)$

	$\langle \text{HMH} \rangle / ^\circ$	$\Delta H_f^\ominus / \text{kJ mol}^{-1}$	$d(\text{M-H}) / \text{\AA}$	Orbital Energy/eV					
				1a ₁	1b ₂	2a ₁	1b ₁	3a ₁	2b ₂
180	699.1	0.946	-48.40	-27.76	-25.01	-25.01	-25.01	-9.60	-4.95
165	692.6	0.947	-48.50	-27.80	-25.15	-25.15	-25.10	-9.56	-5.08
150	676.6	0.950	-48.76	-27.90	-25.53	-25.53	-25.32	-9.47	-5.41
135	658.5	0.953	-49.06	-27.97	-26.05	-26.05	-25.59	-9.35	-5.85
120	645.1	0.955	-49.36	-27.95	-26.63	-26.63	-25.85	-9.25	-6.33
105	640.9	0.957	-49.62	-27.85	-27.24	-27.24	-26.06	-9.22	-6.81
90	648.1	0.960	-49.84	-27.67	-27.87	-27.87	-26.24	-9.31	-7.22
75	667.5	0.968	-50.01	-27.42	-28.53	-28.53	-26.37	-9.55	-7.53
106.713	640.9	0.957	-49.59	-27.87	-27.17	-27.17	-26.04	-9.22	-6.75

Electron Population		First Ionisation Energy /eV	Dipole Moment/D	$d(\text{H-H}) / \text{\AA}$
M	H			
7.132	0.434	26.04	-	1.535

Table 4.16 H₂F⁺ (¹A₁)

$\langle \text{HMH} \rangle / ^\circ$	$\Delta H_F^\circ / \text{kJ mol}^{-1}$	$d(\text{M-H}) / \text{\AA}$	Orbital Energy/eV					
			1a ₁	1b ₂	2a ₁	1b ₁	3a ₁	2b ₂
180	-242.7	0.955	-38.42	-18.15	-14.95	-14.95	-5.07	3.75
165	-245.8	0.953	-38.48	-18.15	-15.08	-15.01	-5.00	3.68
150	-253.1	0.952	-38.62	-18.12	-15.41	-15.12	-4.81	3.50
135	-259.9	0.950	-38.76	-18.00	-15.84	-15.23	-4.57	3.27
120	-263.4	0.949	-38.85	-17.75	-16.32	-15.29	-4.31	3.05
105	-263.6	0.948	-38.88	-17.36	-16.79	-15.28	-4.09	2.87
90	-263.3	0.948	-38.84	-16.86	-17.27	-15.21	-3.96	2.78
112.880	-263.8	0.948	-38.87	-17.58	-16.54	-15.30	-4.20	2.96

Electron Population		First Ionisation Energy /eV	Dipole Moment/D	$d(\text{H-H}) / \text{\AA}$
M	H			
7.220	0.890	9.28	0.716	1.581

Table 4.17 H₂F (²A₁)

	$\langle \text{HMH} \rangle^{\circ} \Delta H_{\text{f}}^{\ominus} / \text{kJ mol}^{-1}$	$d(\text{M-H}) / \text{\AA}$	Orbital Energy/eV					
			1a ₁	1b ₂	2a ₁	1b ₁	3a ₁	2b ₂
180	-286.1	1.000	-28.66	-8.86	-5.25	-5.25	-0.70	12.12
165	-279.6	1.000	-28.64	-8.79	-5.33	-5.23	-0.61	12.11
150	-260.5	0.999	-28.58	-8.56	-5.54	-5.16	-0.34	12.09
135	-230.8	0.998	-28.46	-8.18	-5.83	-5.05	-0.04	12.08
120	-194.0	0.997	-28.28	-7.64	-6.15	-4.87	0.46	12.10
105	-155.5	0.996	-28.02	-6.94	-6.45	-4.60	0.87	12.18
90	-123.4	0.998	-27.65	-6.73	-6.07	-4.24	1.23	12.36
75	-106.8	1.007	-27.16	-7.02	-5.08	-3.77	1.45	12.46
180.000	-286.1	1.000	-28.66	-8.86	-5.25	-5.25	-0.70	12.12

Electron Population		First Ionisation Energy /eV	Dipole Moment/D	$d(\text{H-H}) / \text{\AA}$
M	H			
7.176	1.412	0.70	-	2.000

Table 4.18 H₂F⁻ (¹Σ_g⁺)

Species	H-M-H /°	d(M-H) /Å	Reference
BH ₂	131	1.18	[8]
CH ₂ (¹ A ₁)	102.4	1.111	[9]
CH ₂ (³ B ₁)	136 ₋₈	1.078	[10,11]
NH ₂	103.4	1.024	[8]
H ₂ O	104.53	0.9571	[12]

Table 4.19 Experimental Molecular Structure

References

- [1] A.D. Walsh, J. Chem. Soc., (1953), 2260
- [2] B.M. Gimarc, J. Am. Chem. Soc., 93(1971), 593
- [3] S.Y. Chu, A.K.Q. Siu and E.F. Hayes, J. Am. Chem. Soc., 94(1972), 2969
- [4] W. Meyer, Int. J. Quantum Chem., 55(1971), 341
- [5] H. Lischka, Theor. Chim. Acta, 31(1973), 39
- [6] Review: C. Thomson, "Theoretical Chemistry", Chemical Society Specialist Periodical Reports, The Chemical Society, London, 2(1975), 83
- [7] JANAF Thermochemical Tables, Dow Chemical Co., Midland, Michigan (1965).
- [8] G. Herzberg, "Infra-red and Raman Spectra", D. Van Nostrand, Princeton, N.J. (1945).
- [9] G. Herzberg and J.W.C. Johns, Proc. Roy. Soc., A295(1966), 107.
- [10] G. Herzberg and J.W.C. Johns, J. Chem. Phys., 54(1971), 2276.
- [11] E. Wasserman, V.J. Kuck, R.S. Hutton and W.A. Yager, J. Am. Chem. Soc., 92(1970), 7491

- [12] W.S. Benedict, N. Gailer and E.K. Plyler, *J. Chem. Phys.*,
24(1956), 1139
- [13] M.J.S. Dewar, R.C. Haddon and P.K. Weiner, *J. Am. Chem.
Soc.*, 96(1974), 253
- [14] D.W. Turner, C. Baker, A.D. Baker and C.R. Brundle,
"Molecular Photoelectron Spectroscopy", Wiley, London
(1970).
- [15] V.I. Vedeneyev, L.V. Gurvich, V.N. Kandrát'yev, V.A.
Medvedev and Ye.L. Frankevich, "Bond Energies, Ionisation
Potentials, and Electron Affinities", Arnold, London (1966).

CHAPTER 5

MOLECULAR FRAGMENTATION OF FORMIC ACID

Formic acid has been previously studied by electron-impact mass spectroscopy [1], He(I) photoelectron spectroscopy [2] and charge-exchange mass spectroscopy [3]. MINDO/3 was used here for the theoretical study of formic acid and its fragmentation.

Calculations were performed using the version of MINDO/3 described in chapters 2 and 3. Energy optimisation was performed with respect to all geometrical variables, except when the "reaction coordinate" facility of MINDO/3 was used to vary a geometrical parameter. In these cases optimisation was performed on all geometrical variables except the one under study.

Two fundamental experimental data have been used in conjunction with the computed values: the dissociation energy of H_2 , 36116 cm^{-1} [5] i.e. $432.1 \text{ kJ mol}^{-1}$, and the ionisation energy of the hydrogen atom, $1312.1 \text{ kJ mol}^{-1}$ [6].

The energies of formic acid and its fragments are given in table 5.1, optimised geometries in table 5.2 and electron populations in table 5.3.

Introduction

The electron-impact mass spectrum of formic acid [1]

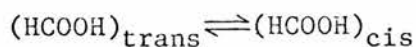
contains the major ions: $(\text{HCOOH})^+$, RI=57.1%; $(\text{HCO}_2)^+$, RI=45.9%; $(\text{CO}_2)^+$, RI=91.1%; $(\text{HCO})^+$, RI=100%; $(\text{CO})^+$, RI=83.3%; $(\text{H}_2\text{O})^+$, RI=26.3% and $(\text{HO})^+$, RI=7.9%. Formation of these ions may be described from fragmentation of the parent ion. However the parent ion may exist in a variety of excited electronic states with different geometries and energies.

Photoelectron spectroscopy shows five or six bands in the He(I) spectrum of formic acid [2], corresponding to the existence of five or six electronic states of the ion $(\text{HCOOH})^+$. It is likely that the fragmentation patterns of different electronic states will differ.

Charge-exchange mass spectroscopy has shown [3,4] that different fragment ions are observed with appearance potentials corresponding to the different ionisations.

Molecular Structures

The neutral formic acid molecule was calculated to be planar with the hydrogen atoms trans to one another as shown in figure 5.1A. An energy minimum was also found with cis planar configuration 14.0 kJ mol^{-1} higher than the trans form. This energy difference corresponds to an equilibrium constant



of 3.5×10^{-3} at 298 K.

The first six calculated vertical ionisation energies and the electronic states of the $(\text{HCOOH})^+$ ions are given in table 5.4 and are also depicted in figure 5.5. The ordering of these states agrees with the extensive ab initio calculations of Basch et al. [7] but the MINDO/3 calculations were found to be closer to the experimental values [2].

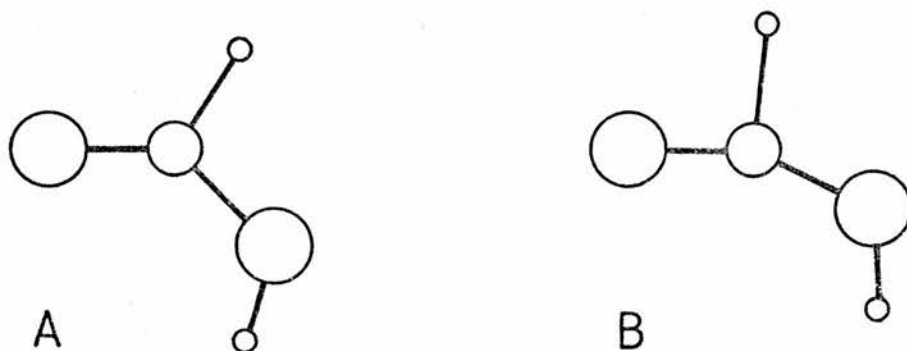
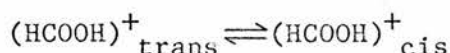


Figure 5.1 The equilibrium structure of (A) HCOOH and (B) $(\text{HCOOH})^+$

The first ionisation involves removal of a σ electron from a molecular orbital localised mainly on the two oxygen atoms: the geometry of the molecular cation, compared with that of the parent molecule, shows a decrease in $\langle \text{HCO}_1$ with a corresponding increase in the other two angles at carbon, and a decrease in the CO_1 distance as shown in figure 5.1B. Optimisation of the geometry of the first ion $\tilde{X}(^2A')$ gives a heat of formation 1019.2 kJ mol^{-1} higher than that of the parent ion. This corresponds to the adiabatic ionisation energy as shown in table 5.5 and figure 5.5. The adiabatic ionisation energies of the other $(\text{HCOOH})^+$ ions

could not be calculated by this version of MINDO/3.

Apart from the change in dihedral angle the geometry of the cis and trans forms of formic acid differed only slightly. A similar result was found for the two conformers of $(\text{HCOOH})^+$. The energy difference between the two conformers of the ion was 7.59 kJ mol^{-1} , corresponding to an equilibrium constant



of 4.7×10^{-2} .

Table 5.6 lists ΔH_f^\ominus of HCOOH and $(\text{HCOOH})^+$ as a function of dihedral angle. If the 90° conformation is assumed to have the maximum ΔH_f^\ominus it can be seen that the rotational barrier is ca. 31 kJ mol^{-1} for $(\text{HCOOH})_{\text{trans}}$ and ca. 24 kJ mol^{-1} for $(\text{HCOOH})^+_{\text{trans}}$.

The $(\text{M}-1)^+$ ion, HCO_2^+ , could be either C-protonated or O-protonated carbon dioxide. Geometry optimisations were performed from both forms which both converged to the same minimum, which is the O-protonated species with an almost linear OCO fragment as shown in figure 5.3D. In order to confirm these findings a "reaction coordinate" calculation was performed starting with the C-protonated form of HCO_2^+ , and with the C-H distance varied between 0.80 \AA and 2.20 \AA . The variation of ΔH_f^\ominus is shown in figure 5.2 and the resulting geometries at several points along the reaction coordinate are shown in figure 5.3. Figure 5.2 shows that there is only one minimum on the reaction coordinate, corresponding to the O-protonated form.

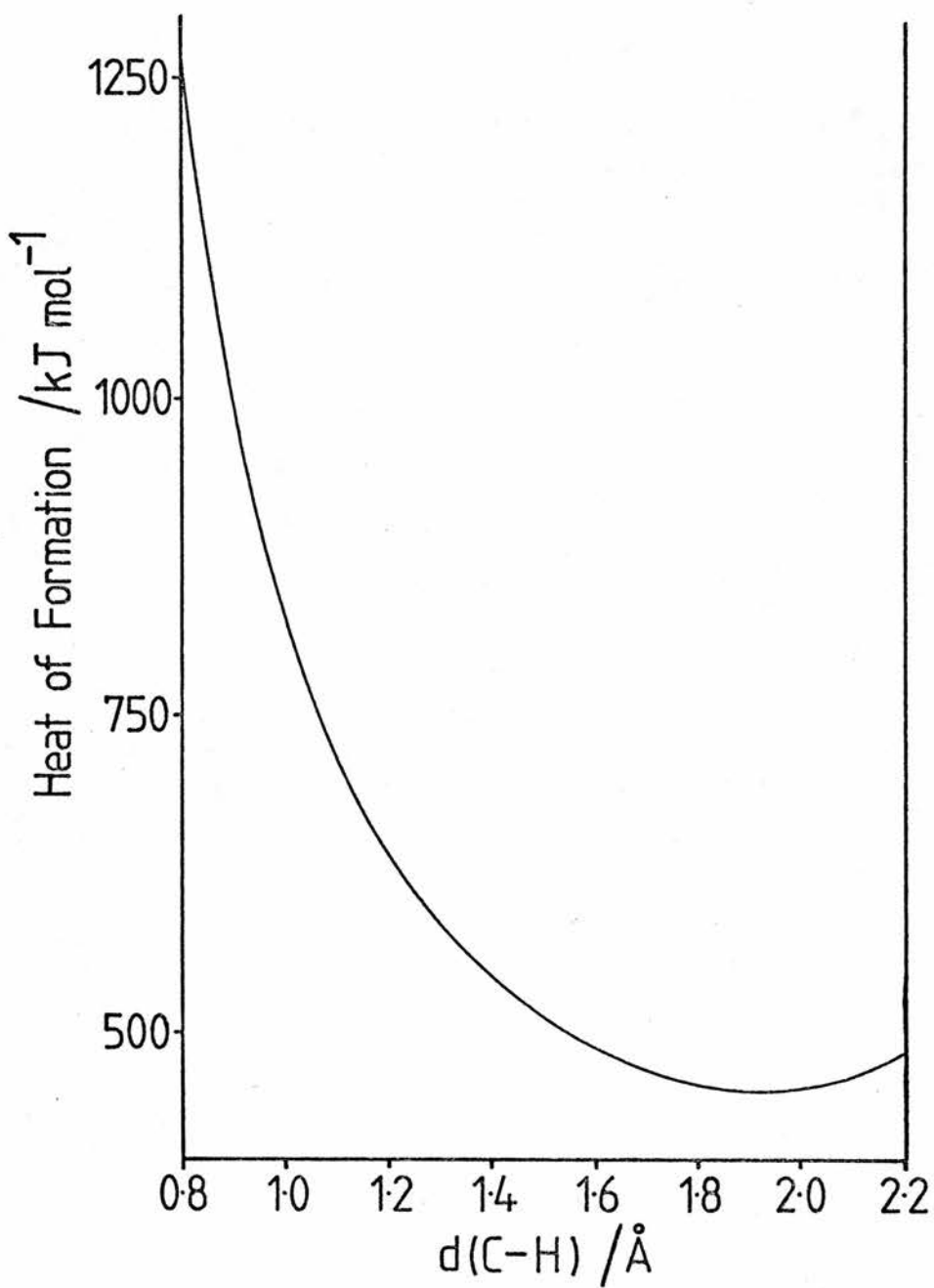


Figure 5.2 Variation of ΔH_f^\ominus with $d(\text{C-H})$ for $(\text{HCOO})^+$

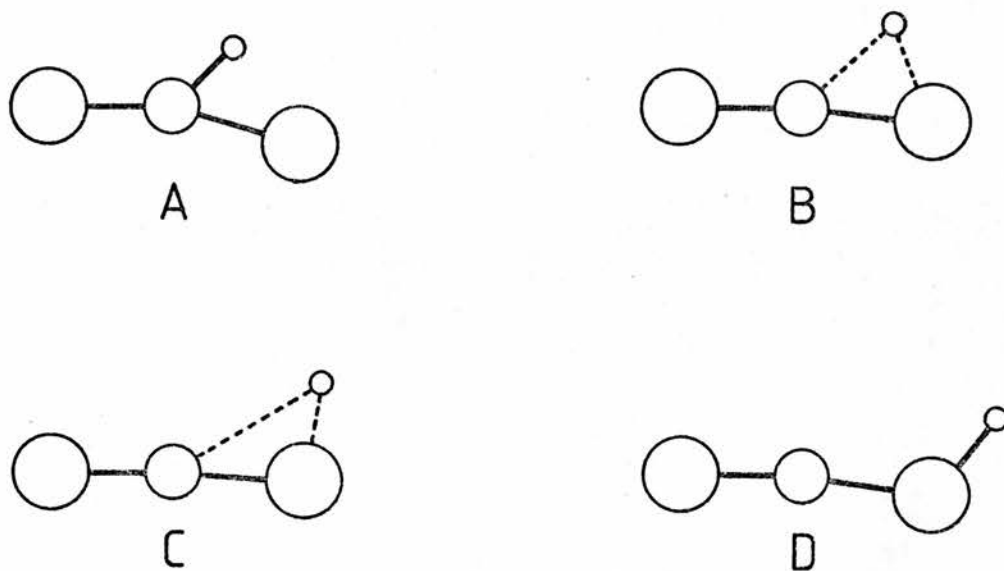


Figure 5.3 The structure of $(\text{HCOO})^+$ with different C-H distances

(A) 0.80\AA

(B) 1.20\AA

(C) 1.65\AA

(D) 1.926\AA

The doubly-protonated form of carbon dioxide, $(\text{HCOOH})^{2+}$, was also investigated. This was found to be non-planar with C_2 symmetry in which the OCO fragment was non-linear. The ΔH_f^\ominus and equilibrium geometry are contained in tables 5.1 and 5.2 respectively, and the geometry is depicted in figure 5.4.

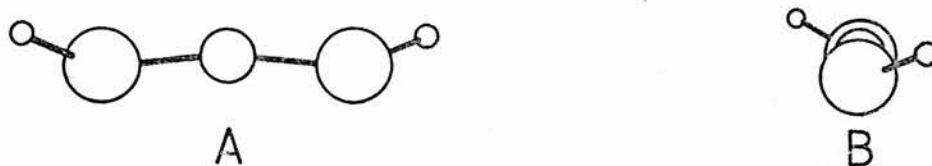


Figure 5.4 The structure of $(\text{HOCOH})^{2+}$ viewed (A) normal to the OCO plane and (B) along the O...O direction

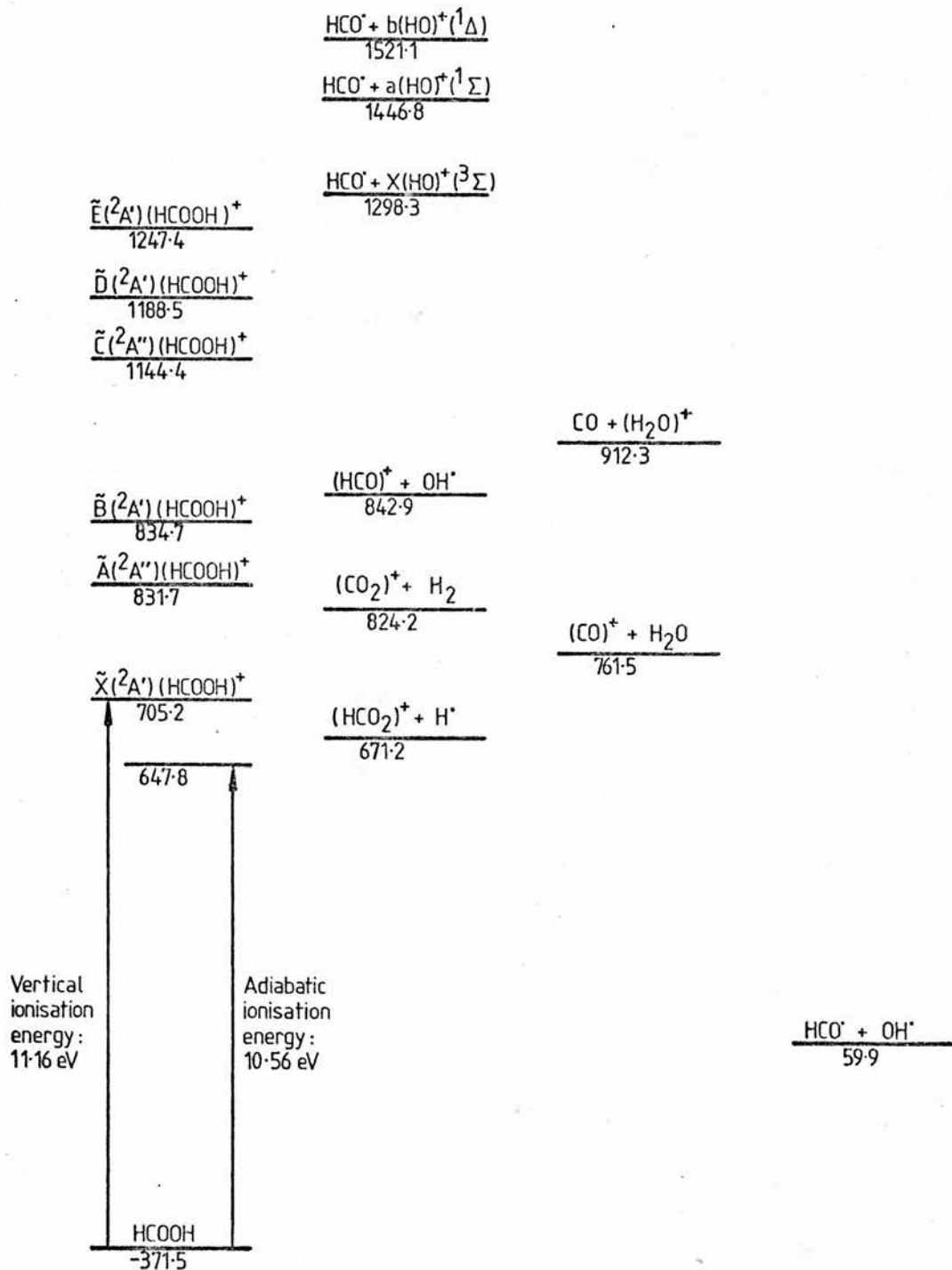


Figure 5.5 Energies of the states of $(\text{HCOOH})^+$ and their fragmentation products: ΔH_f^\ominus in kJ mol^{-1}

Fragmentations

The fragmentations of the formic acid cation may be written as



Figure 5.5 shows the energies of the pairs of fragment ions and their corresponding neutral fragments relating to the major peaks observed in the mass spectrum.

It can be seen from figure 5.5 that $[(\text{HCO}_2)^+ + \text{H}\cdot]$ is similar in energy to $\tilde{\text{X}}(^2\text{A}') (\text{HCOOH})^+$. $[(\text{HCO})^+ + \text{OH}\cdot]$ is similar in energy to $\tilde{\text{A}}(^2\text{A}'')$ and $\tilde{\text{B}}(^2\text{A}') (\text{HCOOH})^+$; $[(\text{CO})^+ + \text{H}_2\text{O}]$ is lower than $\tilde{\text{A}}(^2\text{A}'')$ and $\tilde{\text{B}}(^2\text{A}')$; and $[(\text{H}_2\text{O}^+ + \text{CO})]$ is below $\tilde{\text{C}}(^2\text{A}')$. It has been assumed that after ionisation has occurred, either in a photoelectron spectrum or in a charge-exchange mass spectrum, that no further significant increase in energy of the ion occurs. Thus the $\tilde{\text{X}}(^2\text{A}')$ state of $(\text{HCOOH})^+$ could only produce $[(\text{HCO}_2)^+ + \text{H}\cdot]$, and similarly the upper states could not give rise to fragments significantly higher in energy.

Constraint on the possible fragmentations also arises from the symmetries of the reacting ionic states and their putative fragments. The point-group symmetry classes of all the species studied are listed in tables 5.1 and 5.4. The correlation between $(\text{HCOOH})^+$ and its symmetry-allowed fragmentations is shown in figure 5.6. It may be deduced that $(\text{HCO}_2)^+$ must be produced from one of the $^2\text{A}'$ states of $(\text{HCOOH})^+$, namely $\tilde{\text{X}}$, $\tilde{\text{B}}$, $\tilde{\text{D}}$, or $\tilde{\text{E}}$. $(\text{HCO})^+$ must arise from one of the $^2\text{A}''$ states ($\tilde{\text{A}}$ or $\tilde{\text{C}}$), as must $(\text{CO}_2)^+$ and $(\text{H}_2\text{O})^+$.

REACTANTS

PRODUCTS

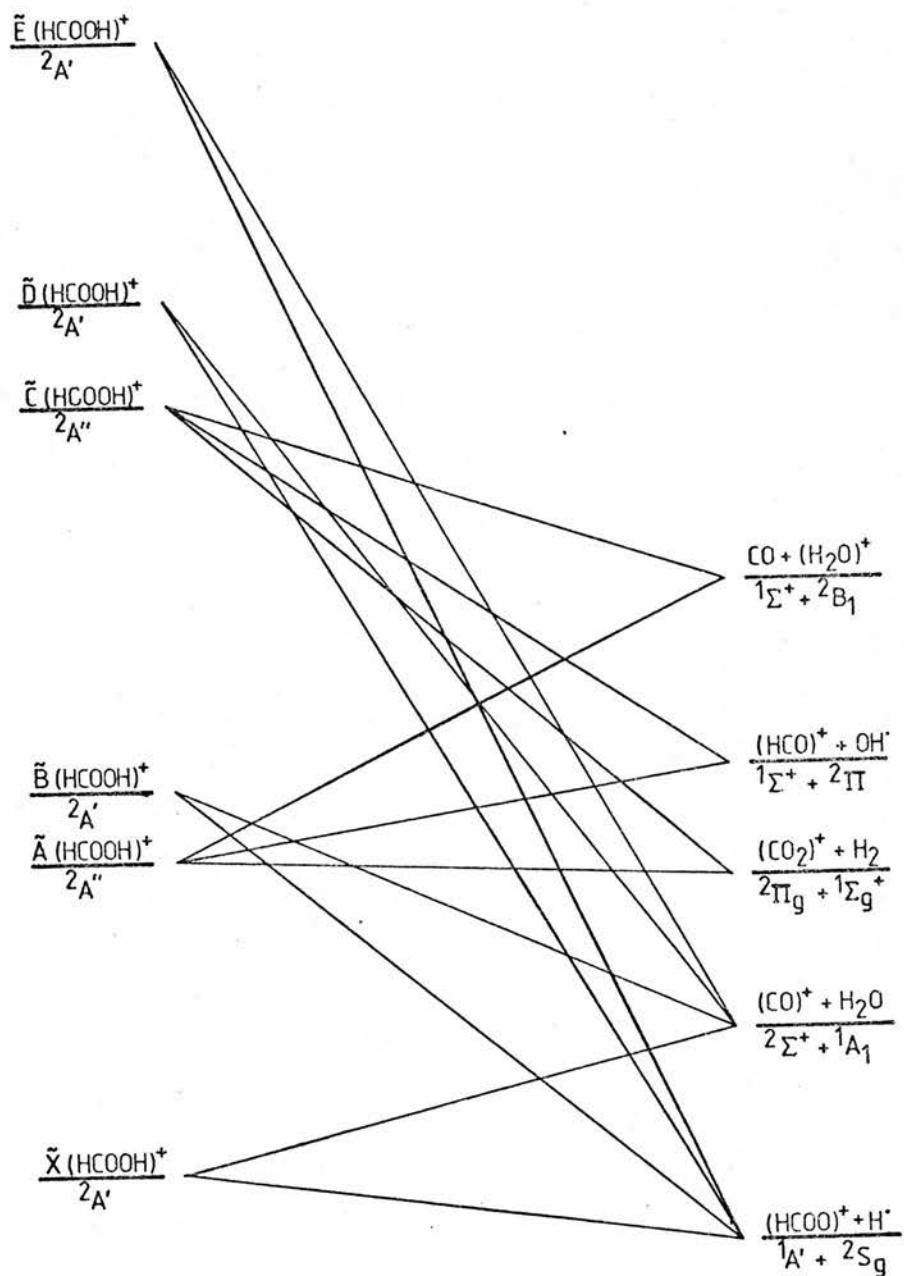
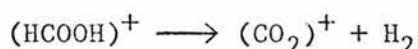


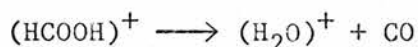
Figure 5.6 Symmetry correlation of the states of $(\text{HCOOH})^+$ and their fragmentation products

Although the ion $(\text{HCO}_2)^+$ can be formed from any of the $2A'$ states it is closest in energy to the $\tilde{X}(2A')$ ground state of $(\text{HCOOH})^+$ and its formation from this state has been confirmed by charge-exchange mass spectrometry [3,4] in which the onset of the $(\text{HCO}_2)^+$ ion occurs at an energy corresponding to the first ionisation of HCOOH to $\tilde{X}(2A')$ $(\text{HCOOH})^+$. This fragmentation was also studied by "reaction coordinate" calculation of energy as a function of $d(\text{C-H})$. The results of these calculations are depicted in figure 5.7, where the energy profile shows an activation energy of 75 kJ mol^{-1} . The geometry of the activated complex is shown in figure 5.8.

Both of the fragmentations



and



must occur from the $\tilde{C}(2A')$ state of $(\text{HCOOH})^+$. Formation as a concerted process from $\tilde{B}(2A')$ $(\text{HCOOH})^+_{\text{trans}}$ would be possible with respect to energy. However, although formation of $(\text{H}_2\text{O})^+$ is symmetry-allowed in a concerted reaction assuming a planar transition state, formation of $(\text{CO}_2)^+$ is symmetry-forbidden. Calculation of activation energies was not possible for these reactions because of the inability of MINDO/3 to deal with excited doublets.

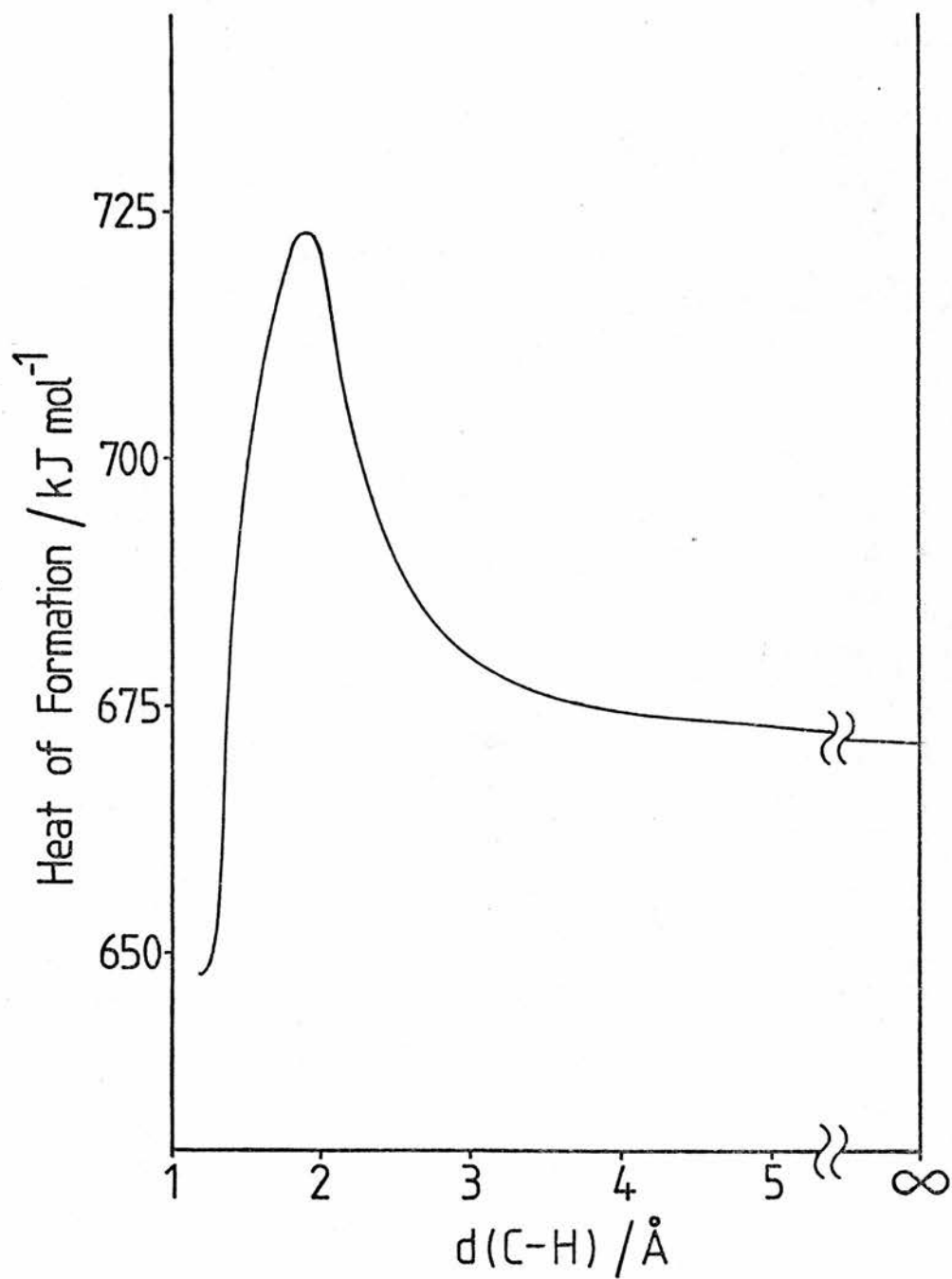
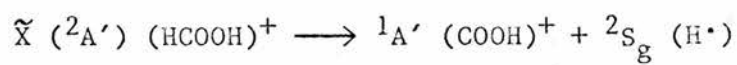


Figure 5.7 Energy profile for the reaction



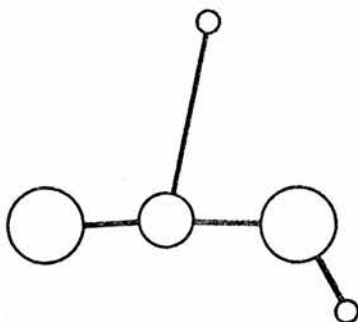
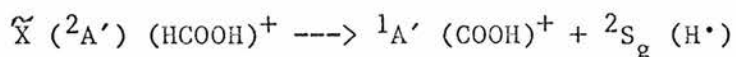


Figure 5.8 The structure of the transition state in the reaction



Appearance Potentials

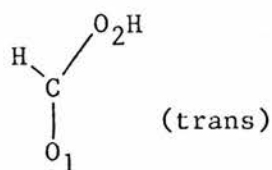
The appearance potentials of ions formed from HCOOH, calculated assuming that each ion is formed in its minimum-energy configuration, are shown in table 5.7. These were found to be in reasonable agreement with experimental values [10] except for $(\text{HCO}_2)^+$. Charge-exchange mass spectroscopy of HCOOH showed [3,4] that the ions $(\text{HCO}_2)^+$ and $(\text{HCO})^+$ had the same appearance potential: however, as indicated above, they cannot be formed from the same state of $(\text{HCOOH})^+$. It has also been found that the ions $(\text{HCO}_2)^+$ and $(\text{DCO}_2)^+$ can both be generated from DCOOH [11], with appearance potentials of 12.8 eV and 12.4 eV respectively. Calculation of the heat of formation of $(\text{HCO}_2)^+$ with a fixed geometry corresponding to that of $(\text{HCOOH})^+$ minus the hydrogen connected to the oxygen gave the heat of formation of +648 kJ mol⁻¹. This value corresponds to an appearance potential of 12.8

eV, exactly that observed. It was therefore deduced that the ion $(\text{HCO}_2)^+$ was formed in an excited vibrational configuration.

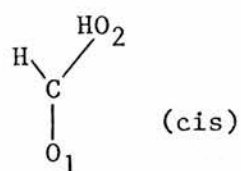
Proton affinities were also calculated from the results of these investigations. The values found were (kJ mol^{-1}): CO, +699; HO, 630; CO_2 , 672: the second proton affinity of CO_2 , corresponding to the protonation of $(\text{COOH})^+$ was -12.6.

Molecule	Point Group	State	ΔH_f^\ominus (kJ mol ⁻¹)
HCOOH _{trans}	C _S	1A'	-371.5
HCOOH _{cis}	C _S	1A'	-357.5
(HCOOH) ⁺ _{trans}	C _S	2A'	+647.8
(HCOOH) ⁺ _{cis}	C _S	2A'	+655.4
(COOH) ⁺	C _S	1A'	+455.2
(HOCO) ²⁺	C _S	1A	+1995.9
CO ₂	D _{∞h}	1Σ _g ⁺	-400.6
(CO ₂) ⁺	D _{∞h}	2Π _g	+824.2
HCO	C _S	2A'	-10.7
(HCO) ⁺	C _{∞v}	1Σ ⁺	+772.3
CO	C _{∞v}	1Σ ⁺	-56.5
(CO) ⁺	C _{∞v}	2Σ ⁺	+985.8
H ₂ O	C _{2v}	1A ₁	-224.3
(H ₂ O) ⁺	C _{2v}	2B ₁	+968.8
HO	C _{∞v}	2Π	+70.6
(HO) ⁺	C _{∞v}	3Σ ⁻	+1308.9
(HO) ⁺	C _{∞v}	1Σ ⁺	+1457.5
(HO) ⁺	C _{∞v}	1Δ	+1531.8

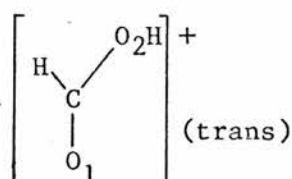
Table 5.1 Molecular Energies for Optimised Geometries



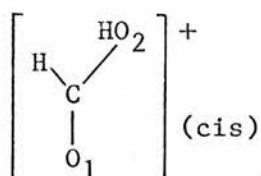
HC, 1.138Å; CO₁, 1.203Å; CO₂, 1.320Å; O₂H, 0.952Å;
 HCO₁, 123.1°; HCO₂, 102.2°; O₁CO₂, 134.7°;
 CO₂H, 118.2°; <(O₁CO₂H), 0.0°



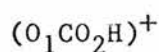
HC, 1.142Å; CO₁, 1.203Å; CO₂, 1.322Å; O₂H, 0.949Å;
 HCO₁, 121.3°; HCO₂, 111.0°; O₁CO₂, 127.7°;
 CO₂H, 116.0°; <(O₁CO₂H), 180.0°



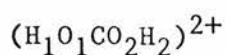
HC, 1.197Å; CO₁, 1.187Å; CO₂, 1.265Å; O₂H, 0.965Å;
 HCO₁, 96.1°; HCO₂, 110.1°; O₁CO₂, 153.8°;
 CO₂H, 119.7°



HC, 1.194Å; CO₁, 1.188Å; CO₂, 1.266Å; O₂H, 0.958Å;
 HCO₁, 95.8°; HCO₂, 119.8°; O₁CO₂, 144.4°;
 CO₂H, 121.6°



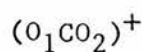
O₁C, 1.145Å; CO₂, 1.238Å; O₂H, 0.960Å; O₁CO₂, 172.9°;
 CO₂H, 122.0°; <(O₁CO₂H), 180.0°



H₁O₁, 0.985Å; O₁C, 1.192Å; CO₂, 1.192Å; O₂H₂, 0.985Å;
 H₁O₁C, 133.5°; O₁CO₂, 169.5°; CO₂H₂, 133.5°;
 <(H₁O₁CO₂), 239.8°; <(O₁CO₂H₂), 239.8°



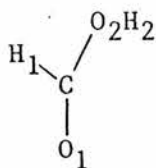
O₁C, 1.180Å; CO₂, 1.180Å; O₁CO₂, 180.0°



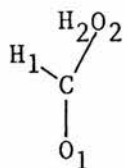
O₁C, 1.182Å; CO₂, 1.182Å; O₁CO₂, 180.0°

HCO	HC, 1.140Å; CO, 1.154Å; HCO, 135.5°
(HCO) ⁺	HC, 1.094Å; CO, 1.115Å; HCO, 180.0°
CO	CO, 1.134Å
(CO) ⁺	CO, 1.101Å
H ₁ OH ₂	H ₁ O, 0.948Å; OH ₂ , 0.948Å; H ₁ OH ₂ , 104.0°
(H ₁ OH ₂) ⁺	H ₁ O, 0.975Å; OH ₂ , 0.975Å; H ₁ OH ₂ , 108.4°
HO	HO, 0.948Å
(HO) ⁺	HO, 0.980Å

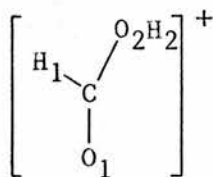
Table 5.2 Molecular Geometries at Equilibrium



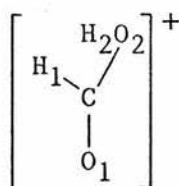
H₁, 1.086; C, 3.143; O₁, 6.541; O₂, 6.500; H₂, 0.730



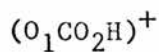
H₁, 1.155; C, 3.126; O₁, 6.503; O₂, 6.487; H₂, 0.729



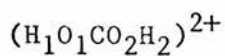
H₁, 0.790; C, 3.096; O₁, 6.165; O₂, 6.328; H₂, 0.621



H₁, 0.841; C, 3.092; O₁, 6.145; O₂, 6.298; H₂, 0.624



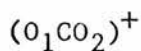
O₁, 6.151; C, 2.954; O₂, 6.302; H, 0.953



H₁, 0.481; O₁, 6.151; C, 2.736; O₂, 6.151; H₂, 0.481



O₁, 6.476; C, 3.048; O₂, 6.476



O₁, 5.980; C, 3.040; O₂, 5.980



H, 1.110; C, 3.568; O, 6.322



H, 0.785; C, 3.219; O, 5.996



C, 3.711; O, 6.289



C, 3.078; O, 5.922

H_1OH_2	$H_1, 0.747; O, 6.506; H_2, 0.747.$
$(H_1OH_2)^+$	$H_1, 0.604; O, 5.792; H_2, 0.604$
HO	$H, 0.749; O, 6.251$
$(HO)^+$	$H, 0.605; O, 5.395$

Table 5.3 Electron Populations at Equilibrium

Molecule		State	Vertical I.E. (eV)	ΔH_f^\ominus (kJ mol ⁻¹)
(HCOOH) ⁺	trans	\tilde{X}^2A'	11.158	+705.2
		\tilde{A}^2A''	12.470	+831.7
		\tilde{B}^2A'	12.501	+834.7
		\tilde{C}^2A''	15.711	+1144.4
		\tilde{D}^2A'	16.178	+1188.5
		\tilde{E}^2A'	16.789	+1247.4
HCOOH		\tilde{X}^1A'	Ground State	-371.5
(HCOOH) ⁺	cis	\tilde{X}^2A'	11.004	+704.3
		\tilde{A}^2A''	12.495	+848.2
		\tilde{B}^2A'	13.296	+925.5
		\tilde{C}^2A'	14.489	+1041.6
		\tilde{D}^2A''	15.761	+1163.3
		\tilde{E}^2A'	18.732	+1450.0
HCOOH		\tilde{X}^1A'	Ground State	-357.5

Table 5.4 Energies and Molecular States of (HCOOH)⁺

	Vertical I.E. (eV)		Adiabatic I.E. (eV)	
	Calc.	Obs. ^a	Calc.	Obs. ^a
HCOOH	11.16	11.51	10.56	11.33
HCO	b	9.88 ^c	8.11	
CO ₂	12.74	13.78	12.69	13.78
CO	10.96	14.01	10.80	14.01
H ₂ O	12.76	12.61	12.47	12.61
OH	b	13.18 ^d	{ 12.83 ^e 14.37 ^f	

^a Ref. 2, unless otherwise indicated.

^b MINDO/3 seriously underestimates the ionisation energies of paramagnetic molecules.

^c Ref. 8.

^d Ref. 9.

^e For ionisation to (CO)⁺(³Σ⁻).

^f For ionisation to (CO)⁺(¹Σ⁺).

Table 5.5 Calculated and Observed Ionisation Energies (eV)

$\angle(\text{O}_1\text{CO}_2\text{H})$ ($^\circ$)	ΔH_f^\ominus (HCOOH) (kJ mol $^{-1}$)	ΔH_f^\ominus (HCOOH) $^+$ (kJ mol $^{-1}$)
0	-371.4	+647.8
45	-357.1	+659.4
90	-340.8	+672.0
135	-348.5	+664.4
180	-357.4	+655.4

Table 5.6 Rotational Barriers in (HCOOH) and (HCOOH) $^+$

Ion	Appearance potential (eV)	
	Calc.	Obs. ^a
(HCOOH) $^+$	10.56	11.16
(COOH) $^+$	10.81 ^b	12.8
(CO ₂) $^+$	12.39	
(CO) $^+$	11.74	
(HCO) $^+$	12.59	12.79
(H ₂ O) $^+$	13.30	
(HO) $^+$ ($^3\Sigma^-$)	17.31	c
($^1\Sigma^+$)	18.85	

^a Ref. 10

^b See text

^c Observed appearance potential of (HO) $^+$ from CH₃COOH is 15.1eV.

Table 5.7 Appearance potentials of ions formed from HCOOH

References

- [1] G.P. Happ and D.W. Stewart, J. Am. Chem. Soc., 74(1952), 4404
- [2] D.W. Turner, C. Baker, A.D. Baker and C.R. Brundle, "Molecular Photoelectron Spectroscopy", Wiley Interscience, London, 1970
- [3] J.M. Tedder and P.H. Vidaud, Chem. Phys. Lett., 64(1979), 81
- [4] J.M. Tedder and P.H. Vidaud, unpublished results
- [5] G. Herzberg, "Spectra of Diatomic Molecules", 2nd edn., Van Nostrand, Princeton, N.J., 1950
- [6] B.N. Taylor, W.H. Parker and D.N. Langenberg, Rev. Mod. Phys., 41(1969), 477
- [7] H. Basch, M.B. Robin and N.A. Kuebler, J. Chem. Phys., 49(1968), 5007
- [8] R.I. Reed and J.C.D. Brand, Trans. Far. Soc., 54(1958), 478
- [9] S.N. Foner and R.L. Hudson, J. Chem. Phys., 25(1956), 602
- [10] H.M. Rosenstock, K. Draxl, B.W. Steiner and J.T. Herron, "Energetics of Gaseous Ions", National Bureau of Standards, Washington, D.C., 1977
- [11] H. Pritchard, J.C.J. Thynne and A.G. Harrison, Can. J. Chem., 46(1968), 2141

CHAPTER 6

MOLECULAR FRAGMENTATION OF FORMAMIDE

Formamide has been previously studied by electron-impact mass spectroscopy [1] and He(I) photoelectron spectroscopy [2]. MINDO/3 was used in this work to study the rearrangements and fragmentations possible for formamide.

Calculations were performed using the version of MINDO/3 described in chapters 2 and 3. Energy optimisation was carried out with respect to all geometrical variables, except when the "reaction coordinate" facility of MINDO/3 was used to study a reaction pathway.

Experimental data for the dissociation energy of H_2 , 36116 cm^{-1} ($432.1 \text{ kJ mol}^{-1}$) [3], and the ionisation energy of the hydrogen atom, $1312.1 \text{ kJ mol}^{-1}$ [4], have been used in conjunction with the computed values.

The energies and geometries of formamide and its fragments are given in tables 6.1, 6.2 and 6.4.

Introduction

The electron-impact mass spectrum of formamide [1] contains the major ions: m/z 45, RI=100% (M^+); m/z 44, RI=27% ($M-H$)⁺; m/z 43, RI=12% ($M-2H$)⁺; m/z 42, RI=2% ($M-3H$)⁺; m/z 29, RI=28% (HCO)⁺; m/z 28, RI=10% (CO)⁺ or (H_2CN)⁺; and m/z 27, RI=12% (HCN)⁺.

The fragmentation pattern for different states of the M^+ ion will differ and the calculations demonstrate the possible fragmentation patterns.

Various possibilities exist for the structure of the M^+ ion and its fragmentation products, and the structures of these isomers and their interconversion have also been studied.

The Formamide Parent Molecule

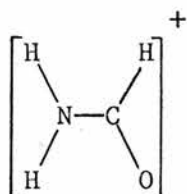
MINDO/3 calculations found the parent neutral molecule to be completely planar. Early microwave studies [5] found the molecule to be planar, but later investigations [6] showed that the sum of the angles at nitrogen was 356.65° , with a barrier to pyramidal inversion at nitrogen of $370 \pm 50 \text{ cm}^{-1}$ (i.e. $4.4 \pm 0.6 \text{ kJ mol}^{-1}$).

Vertical ionisation energies and the corresponding electronic states of (H_2NCHO)⁺ are shown in table 6.6. The ordering of these states was found to be in agreement with ab initio calculations [7], but with energies closer to the experimental values [2]. MINDO/3 is unable to calculate all but

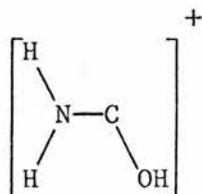
the lowest of the adiabatic ionisation energies.

The Formamide Cation

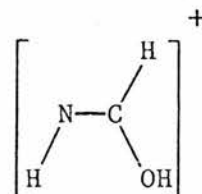
There are seven plausible structures for M^+ :



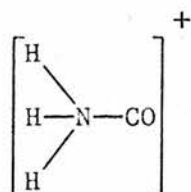
(I)



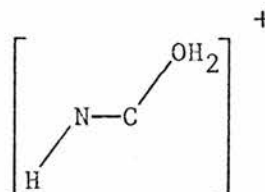
(II)



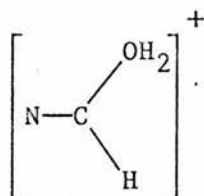
(III)



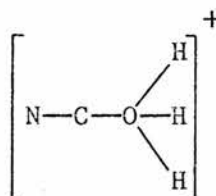
(IV)



(V)



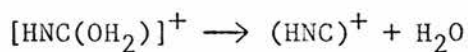
(VI)



(VII)

Of these possibilities, (I) corresponds to the ionisation of the neutral molecule with no subsequent rearrangement; (II), (III) and (IV) would be formed by the migration of one hydrogen atom after ionisation; (V) and (VI) from migration of two hydrogen atoms; and (VII) from migration of all three hydrogens. Optimisations performed with each of geometries (I) to (VII) gave

no bound solution for (I), and (III) converged to (V). The heats of formation of these isomers are shown in table 6.1 with ΔH_f^\ominus in the order (II)<(IV) \approx (V)<(VI)<(VII). The geometries are shown in figure 6.1 and table 6.4. No dihedral angles are quoted for the OH₂ hydrogens in (V) as there was found to be almost free rotation with a barrier <1 kJ mol⁻¹ about the CO bond in this ion. The CO bond was found to be strong as the dissociation



gave a ΔH^\ominus of 296.2 kJ mol⁻¹.

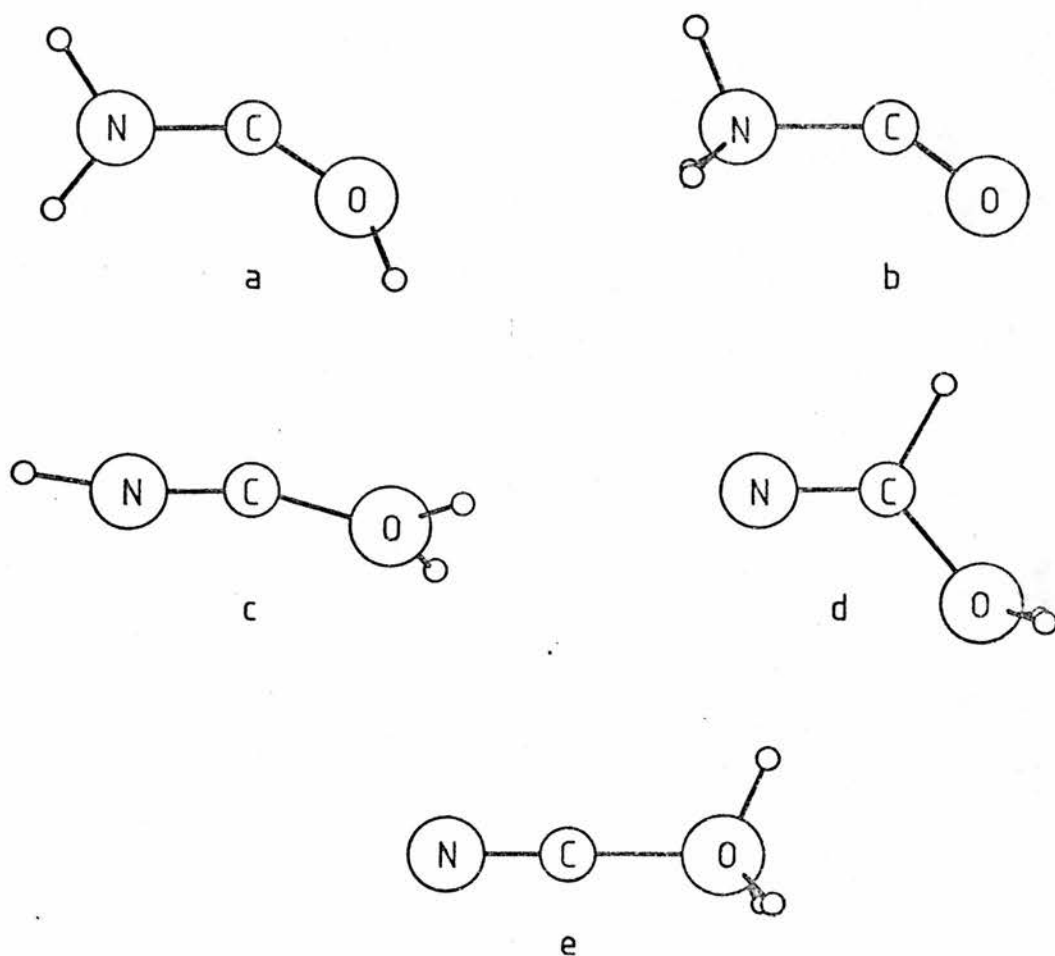


Figure 6.1 Structures of the isomers of M^+

(a) II, (b) IV, (c) V, (d) VI, (e) VII

The doubly charged cation M^{2+} was also investigated and the heat of formation for the optimised geometry is shown in table 6.1. The geometry is given in table 6.4 and is depicted in figure 6.2.

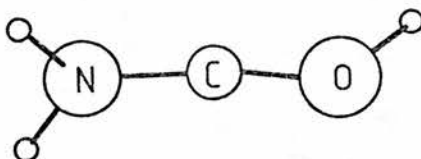


Figure 6.2 Structure of M^{2+}

Isomerization Reactions of the Formamide Cation

Calculations were performed using the "reaction coordinate" facility of MINDO/3 on hydrogen migration within the formamide cation. All other geometrical parameters were fully optimised. The results of these calculations gave the optimised geometries of the transition states in the isomerization which are reproduced in Table 6.4 and depicted in Figure 6.3.

Kinetic A factors were estimated by the method of Benson and O'Neal [8]. The rate constants for the forward (k_1) and backward (k_{-1}) reactions were thus calculated and are given in table 6.3. Thermochemical parameters are given in table 6.2.

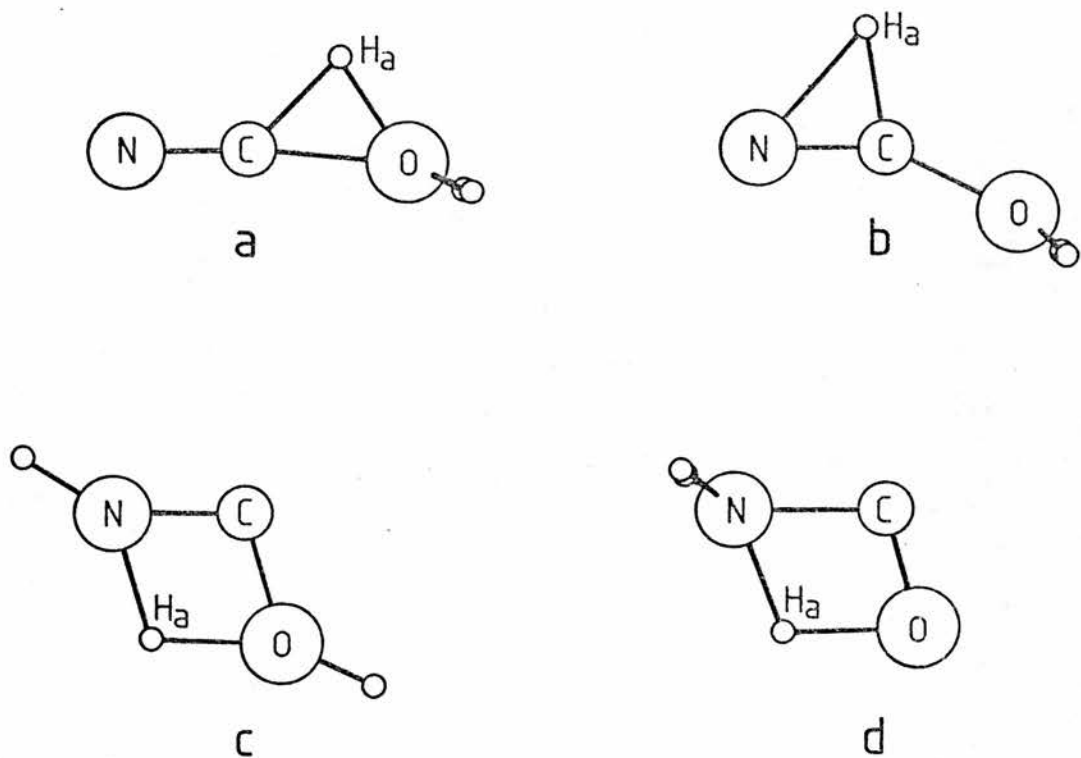


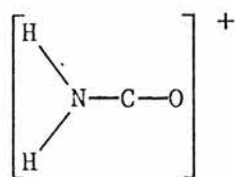
Figure 6.3 Structures of the transition states in the rearrangements of M^+



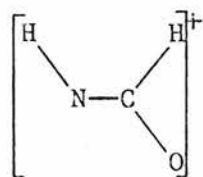
In each instance the migrating hydrogen is designated H_a

Decomposition Products of the Formamide Cation

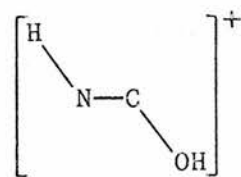
There are five plausible constitutions of the $(M-H)^+$ cation:



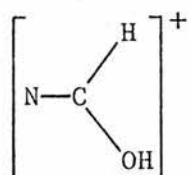
(VIII)



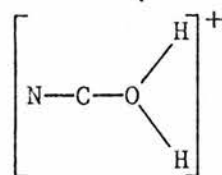
(IX)



(X)



(XI)



(XII)

Optimisations were performed on these possibilities and bound solutions were found for (VIII), (X) and (XII), with ΔH_f^\ominus in the order (VIII)<(X)<(XI). (IX) was found to converge to (VIII), and (XI) to (XII). The optimised structures are depicted in figure 6.4.

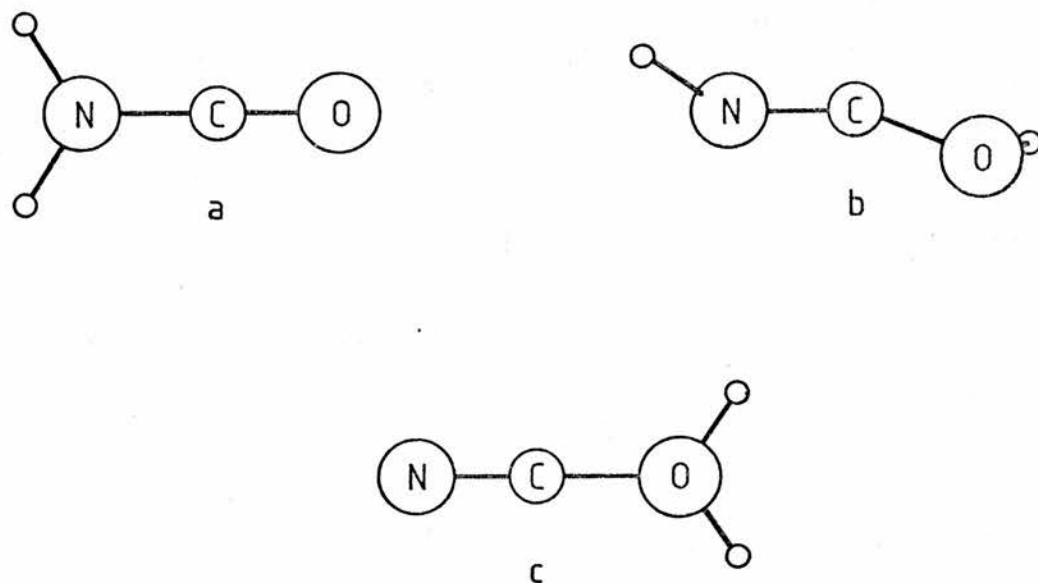


Figure 6.4 Structures of the isomers of $(\text{M-H})^+$

(a) VIII, (b) X, (c) XII

Kinetic parameters for the interconversion of these isomers were calculated as for the formamide cations and are reproduced in table 6.2. The geometries of the transition states are shown in figure 6.5.

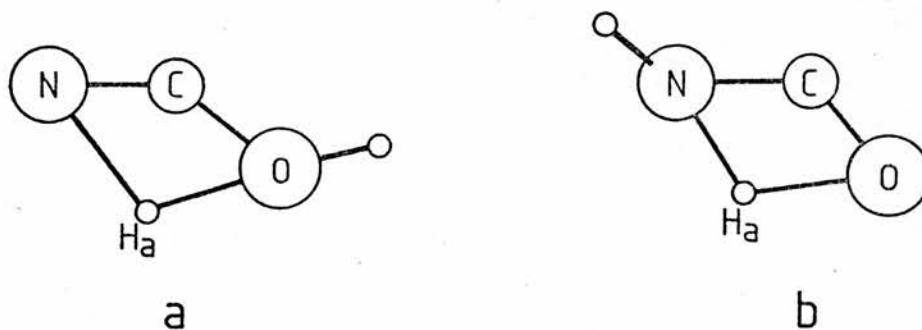
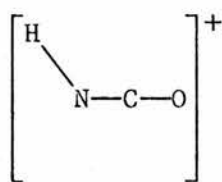


Figure 6.5 Structures of the transition states in the rearrangements of $(M-H)^+$

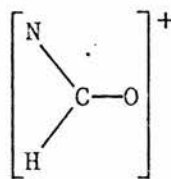


The migrating hydrogen is denoted H_a

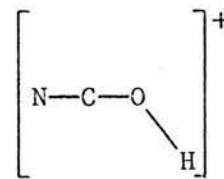
The $(M-2H)^+$ cation (m/z 43) could have three plausible configurations:



(XIII)



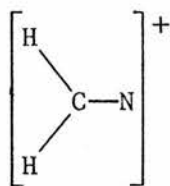
(XIV)



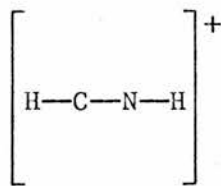
(XV)

Full optimisation of these possibilities gave a bound solution only for (XV).

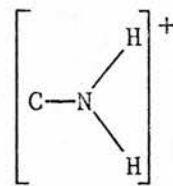
Two compositions other than $(N_2)^+$ are possible for the ion of m/z 28: $(CO)^+$ and $(H_2CN)^+$. For the latter three constitutions are plausible:



(XVI)



(XVII)



(XVIII)

(XVI) was found to converge to (XVII) which is 124 kJ mol^{-1} more stable than (XVIII).

The high resolution mass spectrum of the peak at m/z 28 was studied on a MS-902 mass spectrometer. Accurate mass measurement was not found to be possible, but the accurate mass ratio was found to be 1.000835. Calculated ratios are: $(H_2CN)^+/(N_2)^+$, 1.000499; $(N_2)^+/(CO)^+$, 1.000401; $(H_2CN)^+/(CO)^+$, 1.000850; indicative that the two components at m/z 28 are $(H_2CN)^+$ and $(CO)^+$. There was also a virtual absence of a peak corresponding to m/z 32, indicating that background $(N_2)^+$ was absent as the intensity of background spectra show approximately equal intensities of $(N_2)^+$ and $(O_2)^+$.

The energies of these and the other fragments are given in table 6.1 and the geometries in table 6.4.

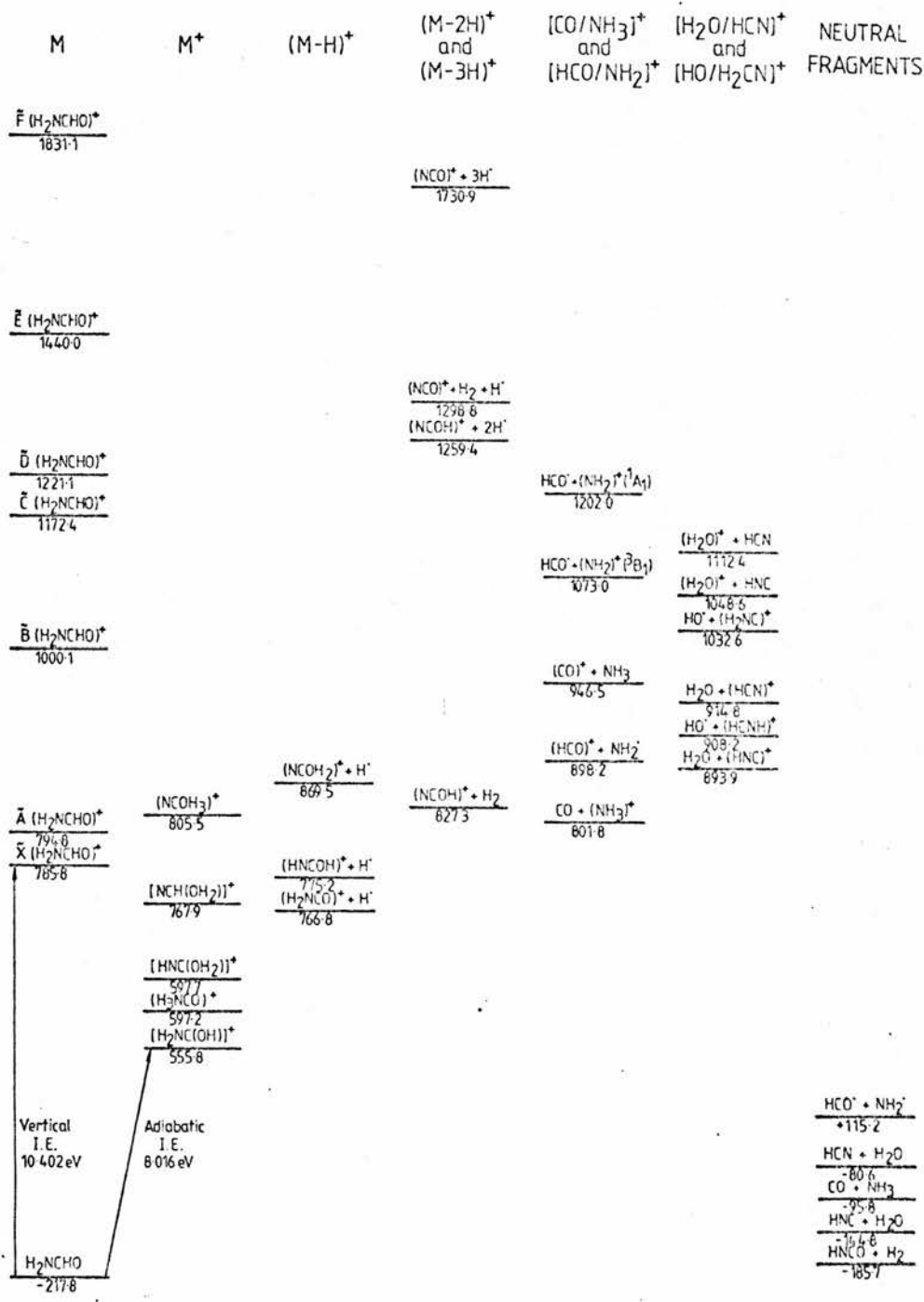


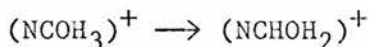
Figure 6.6 Energies of the mass spectral fragment pairs and some neutral fragment pairs

Fragmentation of the Formamide Cation

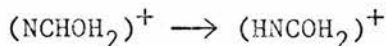
The energies of fragment pairs are shown in figure 6.6 corresponding to all the major ions observed in the mass spectrum together with some neutral fragment pairs. It can be seen from this diagram that four isomers of M^+ ((II), (IV), (V) and (VI)), and two isomers of $(M-H)^+$ ((VIII) and (X)) are accessible from the ground state \tilde{X} (H_2NCHO), but that $(NCOH_3)^+$ and $(NCOH_2)^+$ are accessible from the \tilde{B} and higher states of $(H_2NCHO)^+$. Similarly $(NCOH)^+$, $(HCO)^+$, $(CO)^+$, $(HCNH)^+$ and $(HCN)^+$ are accessible from \tilde{B} or higher states only, $(H_2NC)^+$ from \tilde{C} or higher states only, and $(NCO)^+$ from \tilde{E} or higher states only.

"Reaction coordinate" calculations were performed on the decomposition of M^+ to $(M-H)^+$. Thermodynamic results of these calculations are given in table 6.2 and rate constants in table 6.3. The geometries of the transition states are tabulated in table 6.4 and are depicted in figure 6.7.

The rate constants given in table 6.3 show that the only interconversions which can occur between the isomers of M^+ at a detectable rate are:



and



and that no interconversion between the $(M-H)^+$ is possible.

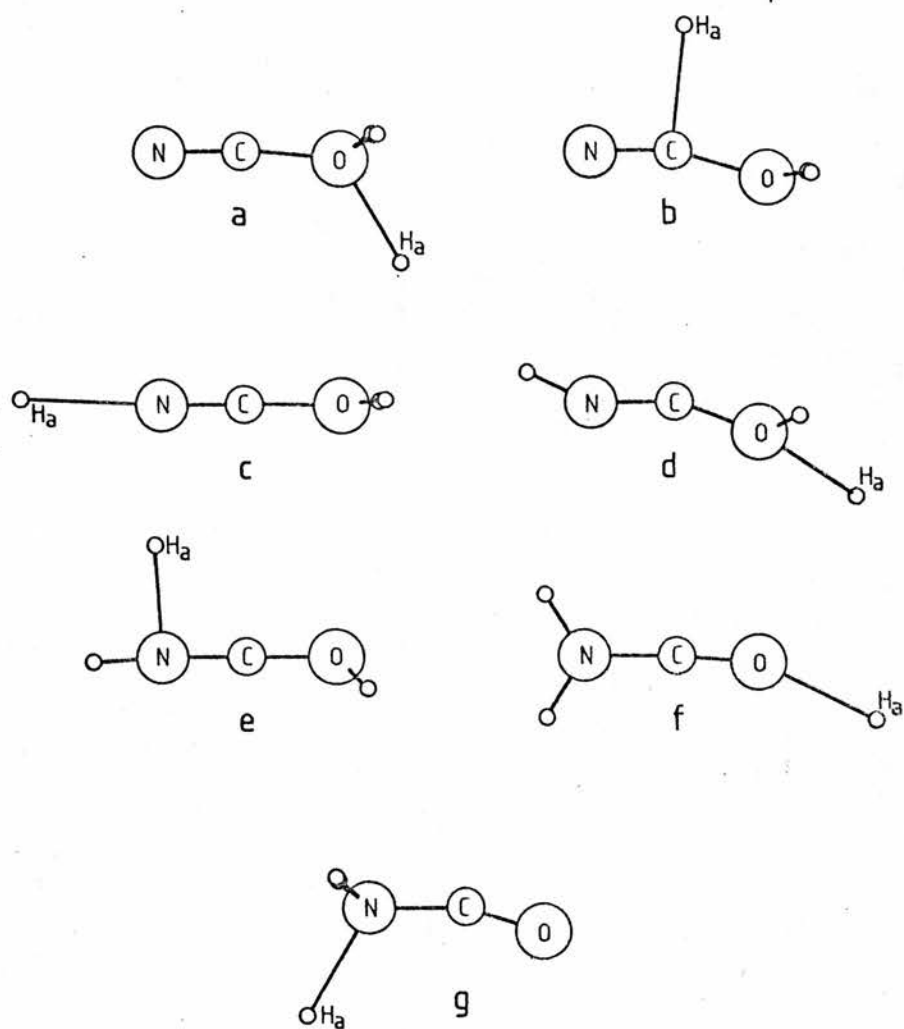
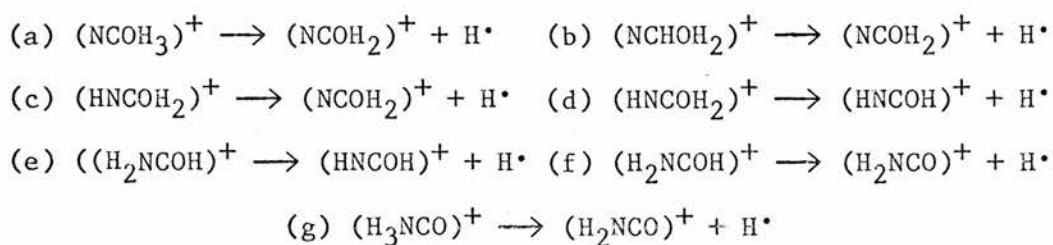


Figure 6.7 Structures of the transition states in the decompositions of M^+ to $(M-H)^+$



In each structure the migrating hydrogen is denoted H_a

Although the thermodynamics of the decompositions of M^+ to $(M-H)^+$ and $H\cdot$ indicates the possibility of most of the decompositions occurring from the first ionisation of H_2NCHO , the kinetic parameters in table 6.3, which indicate extremely slow reactions from the ground state of M^+ , show that these decompositions are much more likely to occur from electronically excited states.

Results of these MINDO/3 computations have also been used to calculate bond dissociation energies as shown in table 6.7, proton affinities shown in table 6.8, and appearance potentials shown in table 6.8. The only experimental appearance potential reported is for m/z 44: 10.24 eV [9], which corresponds to the values calculated of 10.20 eV and 10.29 eV for $(H_2NCO)^+$ and $(HNCOH)^+$.

Molecule	Point Group	State	ΔH_f^\ominus (kJ mol ⁻¹)
H ₂ NCHO	C _s	1A'	-217.8
[H ₂ NC(OH)] ⁺	C ₁	2A	+555.6
(H ₃ NCO) ⁺	C _s	2A'	+597.2
[HNC(OH ₂)] ⁺	C ₁	2A	+597.7
[NCH(OH ₂)] ⁺	C _s	2A'	+767.9
(NCOH ₃) ⁺	C _{3v}	2A ₁	+805.5
(H ₂ NCO) ⁺	C _{2v}	2A ₁	+550.8
(HNCOH) ⁺	C ₁	1A	+559.2
[H ₂ NC(OH)] ²⁺	C ₁	1A	+2013.7
(NCOH ₂) ⁺	C _{2v}	1A ₁	+653.5
HNCO	C _s	1A'	-185.7
HOCN	C _s	1A'	-146.7
(HOCN) ⁺	C _s	2A''	+827.3
(NCO) ⁺	C _{∞v}	1Σ ⁺	+1082.8
(HCNH) ⁺	C _{∞v}	1Σ ⁺	+837.6
(H ₂ NC) ⁺	C _{2v}	1A ₁	+962.0
HNC	C _{∞v}	1Σ ⁺	+79.9
HCN	C _{∞v}	1Σ ⁺	+143.7
(HNC) ⁺	C _s	2A'	+1118.2
(HCN) ⁺	C _s	2A'	+1139.1
NH ₃	C _{3v}	1A ₁	-39.2
(NH ₃) ⁺	D _{3h}	2A ₂ ''	+858.4
NH ₂	C _{2v}	2B ₁	+125.8
(NH ₂) ⁺	C _{2v}	3B ₁	+1083.7
(NH ₂) ⁺	C _{2v}	1A ₁	+1212.7

Table 6.1 Molecular Energies for Optimised Geometries

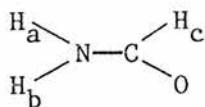
Reaction	Point Group	State	ΔH^\ominus	ΔH^\ddagger
			(kJ mol ⁻¹)	
$(\text{NCOH}_3)^+ \rightarrow (\text{NCHOH}_2)^+$	C_s	$2A'$	-37.6	+73.5
$(\text{NCHOH}_2)^+ \rightarrow (\text{HNCOH}_2)^+$	C_s	$2A'$	-170.2	+49.8
$(\text{HNCOH}_2)^+ \rightarrow (\text{H}_2\text{NCOH})^+$	C_1	$2A$	-42.1	+232.0
$(\text{H}_3\text{NCO})^+ \rightarrow (\text{H}_2\text{NCOH})^+$	C_s	$2A'$	-41.6	+266.5
$(\text{NCOH}_2)^+ \rightarrow (\text{HNCOH})^+$	C_s	$1A'$	-94.3	+295.5
$(\text{HNCOH})^+ \rightarrow (\text{H}_2\text{NCO})^+$	C_1	$1A$	-8.4	+398.4
$(\text{NCOH}_3)^+ \rightarrow (\text{NCOH}_2)^+ + \text{H}\cdot$	C_s	$2A'$	+64.0	+129.1
$(\text{NCHOH}_2)^+ \rightarrow (\text{NCOH}_2)^+ + \text{H}\cdot$	C_s	$2A'$	+101.6	+145.0
$(\text{HNCOH}_2)^+ \rightarrow (\text{NCOH}_2)^+ + \text{H}\cdot$	C_s	$2A'$	+271.8	+325.8
$(\text{HNCOH}_2)^+ \rightarrow (\text{HNCOH})^+ + \text{H}\cdot$	C_1	$2A$	+177.5	+228.9
$(\text{H}_2\text{NCOH})^+ \rightarrow (\text{HNCOH})^+ + \text{H}\cdot$	C_1	$2A$	+219.6	+274.0
$(\text{H}_2\text{NCOH})^+ \rightarrow (\text{H}_2\text{NCO})^+ + \text{H}\cdot$	C_1	$2A$	+211.2	+264.8
$(\text{H}_3\text{NCO})^+ \rightarrow (\text{H}_2\text{NCO})^+ + \text{H}\cdot$	C_s	$2A'$	+169.6	+230.1

Table 6.2

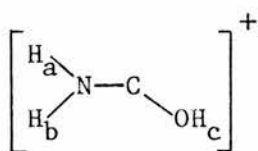
Thermochemical Parameters for Rearrangements and Decompositions

Reaction	k_1 (s^{-1})	k_{-1} (s^{-1})
$(\text{NCOH}_3)^+ \rightarrow (\text{NCHOH}_2)^+$	4.5×10^{-1}	1.1×10^{-7}
$(\text{NCHOH}_2)^+ \rightarrow (\text{HNCOH}_2)^+$	$5.7 \times 10^{+3}$	8.3×10^{-27}
$(\text{HNCOH}_2)^+ \rightarrow (\text{H}_2\text{NCOH})^+$	7.4×10^{-29}	3.1×10^{-36}
$(\text{H}_3\text{NCO})^+ \rightarrow (\text{H}_2\text{NCOH})^+$	6.3×10^{-35}	3.2×10^{-42}
$(\text{NCOH}_2)^+ \rightarrow (\text{HNCOH})^+$	5.6×10^{-40}	1.6×10^{-56}
$(\text{HNCOH})^+ \rightarrow (\text{H}_2\text{NCO})^+$	5.1×10^{-58}	1.7×10^{-59}
$(\text{NCOH}_3)^+ \rightarrow (\text{NCOH}_2)^+ + \text{H}\cdot$	8.0×10^{-11}	
$(\text{NCHOH}_2)^+ \rightarrow (\text{NCOH}_2)^+ + \text{H}\cdot$	1.2×10^{-13}	
$(\text{HNCOH}_2)^+ \rightarrow (\text{NCOH}_2)^+ + \text{H}\cdot$	2.6×10^{-45}	
$(\text{HNCOH}_2)^+ \rightarrow (\text{HNCOH})^+ + \text{H}\cdot$	2.7×10^{-28}	
$(\text{H}_2\text{NCOH})^+ \rightarrow (\text{HNCOH})^+ + \text{H}\cdot$	3.1×10^{-36}	
$(\text{H}_2\text{NCOH})^+ \rightarrow (\text{H}_2\text{NCO})^+ + \text{H}\cdot$	1.3×10^{-34}	
$(\text{H}_3\text{NCO})^+ \rightarrow (\text{H}_2\text{NCO})^+ + \text{H}\cdot$	1.5×10^{-28}	

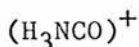
Table 6.3 Rate Constants (298K)



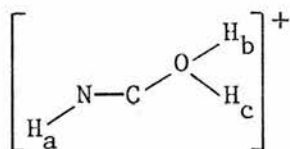
$\text{H}_a\text{N}, 1.016\text{\AA}; \text{H}_b\text{N}, 1.016\text{\AA}; \text{NC}, 1.334\text{\AA}; \text{CH}_c, 1.140\text{\AA};$
 $\text{CO}, 1.207\text{\AA}; \text{H}_a\text{NH}_b, 110.4^\circ; \text{H}_a\text{NC}, 123.9^\circ; \text{H}_b\text{NC},$
 $125.7^\circ; \text{NCH}_c, 110.0^\circ; \text{NCO}, 126.4^\circ; \text{ whole}$
 molecule planar



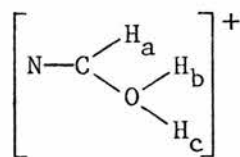
$\text{H}_a\text{N}, 1.020\text{\AA}; \text{H}_b\text{N}, 1.031\text{\AA}; \text{NC}, 1.281\text{\AA}; \text{CO}, 1.209\text{\AA};$
 $\text{OH}_c, 0.958\text{\AA}; \text{H}_a\text{NH}_b, 111.3^\circ; \text{H}_a\text{NC}, 121.9^\circ; \text{H}_b\text{NC},$
 $125.3^\circ; \text{NCO}, 145.4^\circ; \text{COH}_c, 139.4^\circ; \langle (\text{H}_c\text{OCN}),$
 $222.4^\circ; \langle (\text{H}_a\text{NCO}), 182.2^\circ$



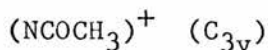
$\text{HN}, 1.046\text{\AA}; \text{NC}, 1.446\text{\AA}; \text{CO}, 1.140\text{\AA}; \text{HNC}, 113.6^\circ;$
 $\text{NCO}, 143.2^\circ; \langle (\text{HNCO}), 60^\circ, 180^\circ, 300^\circ$



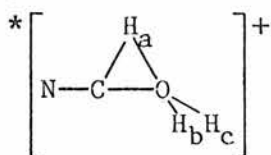
$\text{H}_a\text{N}, 1.004\text{\AA}; \text{NC}, 1.160\text{\AA}; \text{CO}, 1.362\text{\AA}; \text{OH}_b, 0.979\text{\AA};$
 $\text{OH}_c, 0.973\text{\AA}; \text{H}_a\text{NC}, 165.3^\circ; \text{NCO}, 152.9^\circ; \text{COH}_b,$
 $126.5^\circ; \text{COH}_c, 124.7^\circ; \text{H}_b\text{OH}_c, 108.3^\circ; \langle (\text{H}_a\text{NCO}),$
 $179.5^\circ; \text{ see text}$



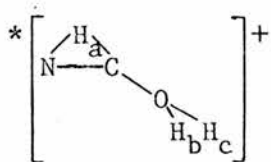
$\text{NC}, 1.206\text{\AA}; \text{CH}_a, 1.140\text{\AA}; \text{CO}, 1.414\text{\AA}; \text{OH}_b = \text{OH}_c,$
 $0.966\text{\AA}; \text{NCH}_a, 118.4^\circ; \text{NCO}, 129.1^\circ; \text{COH}_b = \text{COH}_c,$
 $120.5^\circ; \langle (\text{NCHO}), 180.0^\circ; \langle (\text{H}_b\text{OCN}), 112.5^\circ;$
 $\langle (\text{H}_c\text{OCN}), 247.5^\circ$



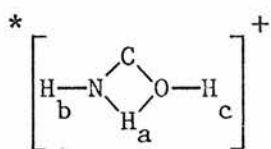
$\text{NC}, 1.139\text{\AA}; \text{CO}, 1.451\text{\AA}; \text{OH}, 1.019\text{\AA}; \text{COH}, 114.3^\circ$



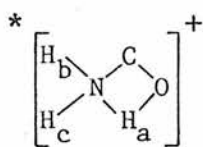
$\text{NC}, 1.140\text{\AA}; \text{CO}, 1.516\text{\AA}; \text{OH}_b = \text{OH}_c, 0.988\text{\AA};$
 $\text{H}_a\text{C}, 1.233\text{\AA}; \text{H}_a\text{O}, 1.208\text{\AA}; \text{NCO}, 174.2^\circ; \text{COH}_b = \text{COH}_c,$
 $125.5^\circ; \text{H}_a\text{CO}, 50.9^\circ; \text{H}_a\text{OC}, 52.4^\circ; \text{H}_b\text{OCN}, 73.5^\circ;$
 $\text{H}_c\text{OCN}, 286.5^\circ; \langle (\text{H}_a\text{NCO}), 180.0^\circ$



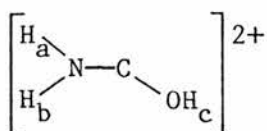
NC, 1.194Å; CO, 1.404Å; OH_b=OH_c, 0.971Å; NH_a, 1.536Å; H_aC, 1.169Å; NCO, 153.1°; COH_b=COH_c, 124.3°; H_aNC, 48.7°; H_aCN, 81.8°; <(H_bOCN), 76.6°; <(H_cOCN), 283.4°; <(H_aNCO), 180.0°



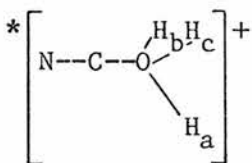
NC, 1.242Å; CO, 1.302Å; H_aN, 1.270Å; H_aO, 1.240Å; NH_b, 1.010Å; OH_c, 0.961Å; NCO, 106.3°; H_aNC, 73.1°; H_aOC, 72.0°; NH_aO, 108.5°; CNH_b, 147.0°; COH_c, 129.5°; <(H_aOCN), 2.3°; <(H_bNCO), 161.7°; <(H_cOCN), 165.6°



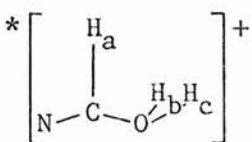
NC, 1.421Å; CO, 1.181Å; NH_b=NH_c, 1.033Å; H_aO, 1.275Å; H_aN, 1.261Å; NCO, 105.8°; H_aNC, 68.2°; H_aOC, 75.8°; NH_aO, 110.2°; CNH_b=CNH_c, 118.3°; <(OCNH_b), 103.9°; <(OCNH_c), 256.1°



H_aN, 1.036Å; H_bN, 1.035Å; NC, 1.254Å; CO, 1.182Å; OH_c, 0.977Å; H_aNH_b, 114.1°; H_aNC, 122.0°; H_bNC, 122.5°; NCO, 175.3°; COH_c, 134.4°; <(H_aNCO), -41.2°; <(H_bNCO), 124.5°; <(H_cOCN), 143.4°

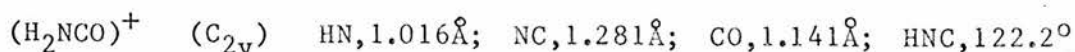
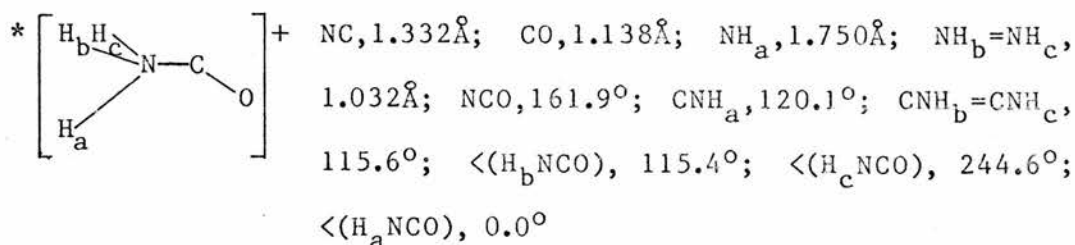
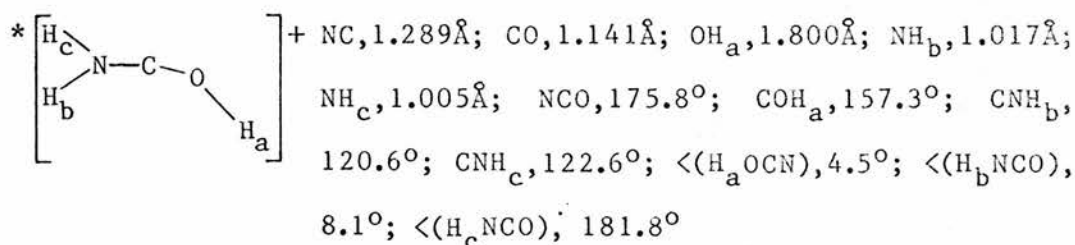
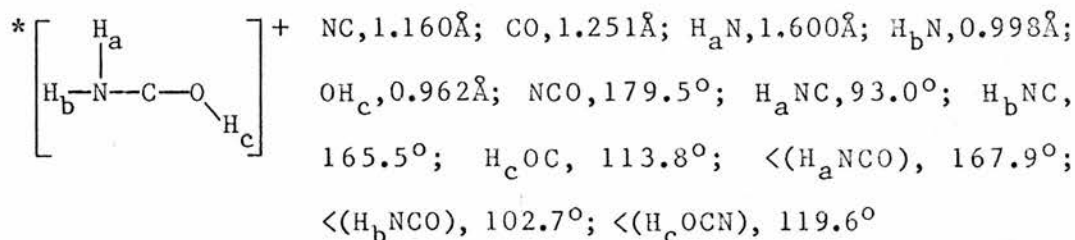
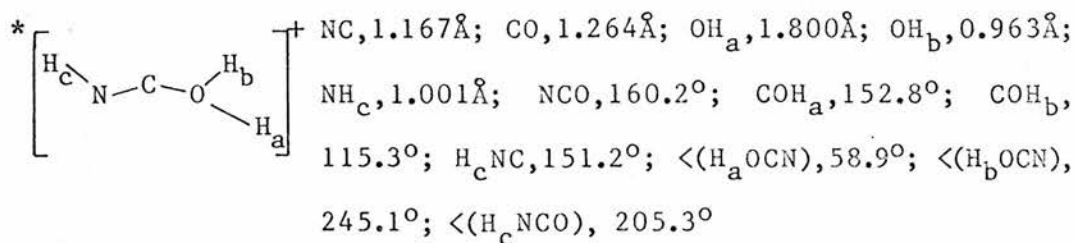
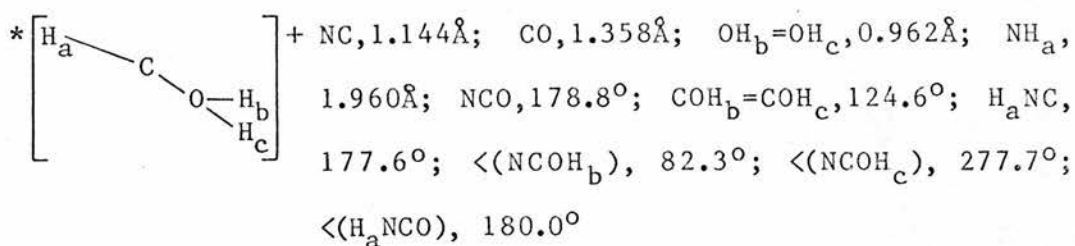


NC, 1.143Å; CO, 1.382Å; OH_b=OH_c, 0.978Å; OH_a, 1.648Å; NCO, 174.9°; COH_a, 124.6°; COH_b=COH_c, 116.3°; <(NCOH_b), 116.3°; <(NCOH_c), 243.7°; <(NCOH_a), 0.0°

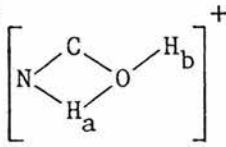


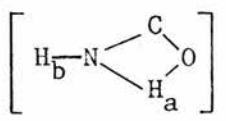
NC, 1.149Å; CO, 1.362Å; OH_b=OH_c, 0.963Å; CH_a, 1.760Å; NCO, 162.9°; COH_b=COH_c, 122.3°; NCH_a,

96.3°; $\langle(\text{NCOH}_b)\rangle$, 106.2°; $\langle(\text{NCOH}_c)\rangle$, 253.8°;
 $\langle(\text{H}_a\text{NCO})\rangle$, 180.0°



$(\text{H}_a\text{NCOH}_b)^+$ $\text{H}_a\text{N}, 1.003\text{\AA}; \text{NC}, 1.173\text{\AA}; \text{CO}, 1.249\text{\AA}; \text{OH}_b, 0.960\text{\AA};$
 $\text{H}_a\text{NC}, 144.5^\circ; \text{NCO}, 158.4^\circ; \text{COH}_b, 116.0^\circ;$
 $\langle(\text{H}_a\text{NCO}), 157.9^\circ$

*  $\text{NC}, 1.189\text{\AA}; \text{CO}, 1.382\text{\AA}; \text{OH}_b, 0.962\text{\AA}; \text{H}_a\text{N}, 1.539\text{\AA};$
 $\text{H}_a\text{O}, 1.324\text{\AA}; \text{NCO}, 141.6^\circ; \text{COH}_b, 127.9^\circ; \text{H}_a\text{NC},$
 $52.4^\circ; \text{H}_a\text{OC}, 57.0^\circ; \text{NH}_a\text{O}, 109.0^\circ; \langle(\text{H}_a\text{NCO}), 0.0^\circ;$
 $\langle(\text{NCOH}_b), 180.0^\circ$

*  $\text{NC}, 1.279\text{\AA}; \text{CO}, 1.172\text{\AA}; \text{H}_b\text{N}, 1.017\text{\AA}; \text{H}_a\text{N}, 1.267\text{\AA};$
 $\text{H}_a\text{O}, 1.410\text{\AA}; \text{NCO}, 128.1^\circ; \text{H}_b\text{NC}, 130.3^\circ; \text{H}_a\text{NC},$
 $60.4^\circ; \text{H}_a\text{OC}, 58.6^\circ; \text{NH}_a\text{O}, 110.8^\circ; \langle(\text{H}_a\text{OCN}),$
 $13.3^\circ; \langle(\text{H}_b\text{NCO}), 221.5^\circ$

$(\text{NCOH}_2)^+ \quad (\text{C}_{2v}) \quad \text{NC}, 1.140\text{\AA}; \text{CO}, 1.347\text{\AA}; \text{OH}, 0.957\text{\AA}; \text{COH}, 124.7^\circ$

$\text{HNCO} \quad \text{HN}, 1.002\text{\AA}; \text{NC}, 1.211\text{\AA}; \text{CO}, 1.182\text{\AA}; \text{HNC}, 134.1^\circ;$
 $\text{NCO}, 162.8^\circ; \langle(\text{HNCO}), 180.0^\circ$

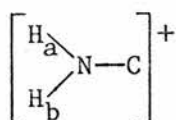
$\text{HOCN} \quad \text{HO}, 0.951\text{\AA}; \text{OC}, 1.293\text{\AA}; \text{CN}, 1.160\text{\AA}; \text{HOC}, 113.6^\circ;$
 $\text{OCN}, 174.8^\circ; \langle(\text{HOCN}), 180.0^\circ$

$(\text{HOCN})^+ \quad \text{HO}, 0.959\text{\AA}; \text{OC}, 1.221\text{\AA}; \text{CN}, 1.215\text{\AA}; \text{HOC}, 125.9^\circ;$
 $\text{OCN}, 172.1^\circ; \langle(\text{HOCN}), 180.0^\circ$

$(\text{OCN})^+ \quad \text{OC}, 1.136\text{\AA}; \text{CN}, 1.312\text{\AA}; \text{OCN}, 180.0^\circ$

$(\text{H}_a\text{CNH}_b)^+ \quad \text{H}_a\text{C}, 1.089\text{\AA}; \text{CN}, 1.138\text{\AA}; \text{NH}_b, 0.997\text{\AA}; \text{H}_a\text{CN},$

180.0°; CNH_b, 180.0°



H_aN, 1.034Å; H_bN, 1.034Å; NC, 1.223Å; H_aNH_b,
106.6°; H_aNC, 126.7°; H_cNC, 126.7°; whole ion
planar

HNC HN, 1.013Å; NC, 1.145Å; HNC, 180.0°

HCN HC, 1.096Å; CN, 1.152Å; HCN, 180.0°

(HNC)⁺ HN, 1.027Å; NC, 1.158Å; HNC, 134.4°

(HCN)⁺ HC, 1.103Å; CN, 1.122Å; HCN, 173.9°

NH₃ (C_{3v}) NH, 1.031Å; HNH, 104.3°

(NH₃)⁺ (D_{3h}) NH, 1.012Å; HNH, 120.0°

NH₂ (C_{2v}) NH, 1.036Å; HNH, 102.2°

(NH₂)⁺ (³B₁) (C_{2v}) NH, 1.000Å; HNH, 140.6°

(NH₂)⁺ (¹A₁) (C_{2v}) NH, 1.036Å; HNH, 106.0°

* Transition State

Table 6.4 Molecular Geometries at Equilibrium

Molecule	Vertical I.E. (eV)	Adiabatic Energy (eV)	Dipole Moment (D) ^a
H ₂ NCHO	10.40	8.02	3.87
HNCO	10.36	b	2.82
HOCN	10.61	10.10	2.62
HCN	10.50	10.32	1.63
HNC	11.27	10.76	2.23
NH ₃	10.06	9.30	1.63

a $D = 3.3356 \times 10^{-30} \text{ C m}$

b No bound state found for (HNCO)⁺

Table 6.5 Calculated Ionisation Energies and Dipole Moments

State	Vertical I.E. (eV)	ΔH_f^\ominus (kJ mol ⁻¹)
\tilde{X}^2A''	10.40	+785.8
\tilde{A}^2A'	10.50	+794.8
\tilde{B}^2A'	12.62	+1000.1
\tilde{C}^2A''	14.41	+1172.4
\tilde{D}^2A'	14.91	+1221.1
\tilde{E}^2A'	17.18	+1440.0
\tilde{F}^2A'	21.24	+1831.1
\tilde{G}^2A'	27.71	+2456.2
\tilde{H}^2A'	32.57	+2924.9
\tilde{X}^1A'	Ground State	-217.8

Table 6.6 Energies and Molecular States of $(H_2NCHO)^+$

D(H ₂ N-CHO)	333.0
D(H ₂ N-CHO) ⁺	342.4
D(H ₃ N-CO) ⁺	204.6
D(HNC-OH ₂) ⁺	296.2
D(NCH-OH ₂) ⁺	146.9
D(H ₂ N-CO) ⁺	475.3

Table 6.7 Bond Dissociation Energies (kJ mol⁻¹)

Molecule	P (kJ mol ⁻¹)	Molecule	P (kJ mol ⁻¹)
HN [*] CO	792	HCN [*]	834
HNCO [*]	783	HN [*] C	646
HO [*] CN	728	HNC [*]	770
HOCN [*]	822	N [*] H ₂	517

Table 6.8 Proton Affinities

Ion	m/z	AP (eV)	Ion	m/z	AP (eV)
$(\text{H}_2\text{NCO})^+$	44	10.20	$(\text{HCNH})^+$	28	11.67
$(\text{HNCOH})^+$	44	10.29	$(\text{H}_2\text{NC})^+$	28	12.96
$(\text{NCOH}_2)^+$	44	11.27	$(\text{HNC})^+$	27	11.52
$(\text{NCOH})^+$	43	10.83	$(\text{HCN})^+$	27	11.74
$(\text{NCO})^+$	42	15.72	$(\text{H}_2\text{O})^+$	18	13.13
$(\text{HCO})^+$	29	11.57	$(\text{NH}_3)^+$	17	10.57
$(\text{CO})^+$	28	12.07	$(\text{NH}_2)^+$	16	13.34

Table 6.9 Appearance Potentials of Fragment Ions

References

- [1] J.A. Gilpin, Anal. Chem., 31(1959), 4404
- [2] D.W. Turner, C. Baker, A.D. Baker and C.R. Brundle, "Molecular Photoelectron Spectroscopy", Wiley-Interscience, London, 1970
- [3] G. Herzberg, "Spectra of Diatomic Molecules", 2nd edn., Van Nostrand, Princeton, N.J., 1950
- [4] B.N. Taylor, W.H. Parker and D.N. Langenberg, Rev. Mod. Phys., 41(1969), 477
- [5] R.J. Kurland and E.B. Wilson, Jr., J. Chem. Phys., 27(1957), 585
- [6] C. Costain and J.M. Dowling, J. Chem. Phys., 32(1960), 158
- [7] H. Basch, M.B. Robin and N.A. Kuebler, J. Chem. Phys., 49 (1968), 5007
- [8] S.W. Benson and H.E. O'Neal, NSRDS-NBS 211, Nat. Bur. Standards, Washington, DC, 1970
- [9] H.M. Rosenstock, K. Draxl, B.W. Steiner and J.T. Herron, "Energetics of Gaseous Ions", National Bureau of Standards, Washington, DC, 1977

CHAPTER 7

MOLECULAR FRAGMENTATION OF ETHYL ACETATE

Ethyl acetate has been previously studied by electron-impact mass spectroscopy [1]. MINDO/3 was used here to study the structures and energies of ethyl acetate, its cation, and its fragmentation products.

Calculations were performed using the version of MINDO/3 described in chapters 2 and 3. Energy optimisation was carried out with respect to all geometrical variables except when explicitly stated otherwise.

Introduction

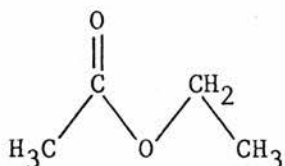
The electron-impact mass spectrum of ethyl acetate [1] contains the major ions: $(C_4H_8O_2)^+$, RI=5.8%; $(C_3H_5O_2)^+$, RI=3.1%; $(C_2H_5O)^+$, RI=12.1%; $(C_2H_3O)^+$, RI=100%; $(C_2H_2O)^+$, RI=5.4%; $(C_2H_5)^+$, RI=14.0%; $(C_2H_4)^+$, RI=3.0%; $(C_2H_3)^+$, RI=9.4%; and $(CH_3)^+$, RI=9.6%. The spectrum also contains the rearrangement ions: $(C_2H_5O_2)^+$, RI=10.5%; $(C_2H_4O_2)^+$, RI=0.57%; $(CH_3O)^+$, RI=1.3%; and $(CHO)^+$, RI=3.1%.

Calculations were performed on the various conformers of ethyl acetate and its cation, and on the fragmentation products of its cation. The calculated energies and molecular states are

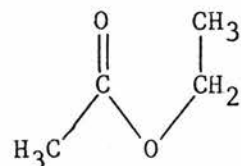
given in table 7.1, and the molecular geometries in table 7.2.

The Ethyl Acetate Parent Molecule

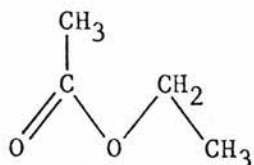
Ethyl acetate was found to have four stable conformations.



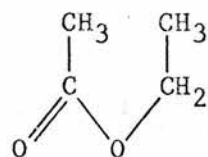
(I)



(II)



(III)



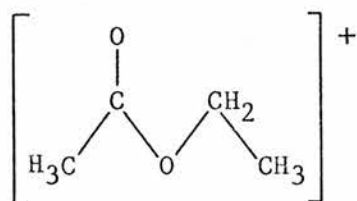
(IV)

The non-hydrogen atoms were found to be co-planar in each of these conformers, with stability decreasing in the order: (I) > (II) = (IV) > (III).

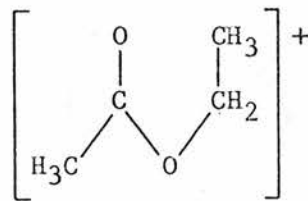
The Ethyl Acetate Molecular Ion

Optimisations were attempted for the ionisation of each of the conformers (I) - (IV). The ionisation of (I) optimised to (V), whose heavy atoms were almost planar but with the $O_2C_3C_4$ bond angle reduced from 110.4° to 95.1° . Conformer (VI), resulting from the ionisation of (II), shows a markedly non-

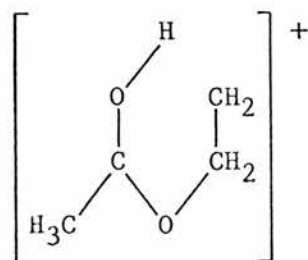
planar framework of non-hydrogen atoms with the $C_3O_2C_2O_1$ dihedral angle increasing from 0.0° to 65.4° . In the neutral molecule (II) the substituents C_3 and O_1 were perfectly eclipsed about the O_2C_2 bond, whereas in the ion (VI) they are markedly staggered. Attempts to optimise geometries of M^+ conformers derived from (III) and (IV) always failed to achieve self-consistence.



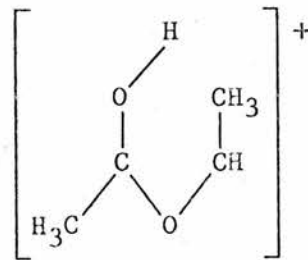
(V)



(VI)



(VII)



(VIII)

Migration of a hydrogen atom from either the CH_2 or CH_3 group of the ethyl fragment to the singly connected oxygen of conformer (IV) yields the plausible isomeric cations (VII) and (VIII). Isomer (VII) has a planar heavy atom skeleton, but isomer (VIII) was found to have C_4 markedly displaced from the plane of the other heavy atoms.

The structures of the isomeric ethyl acetate ions are shown in figure 7.1.

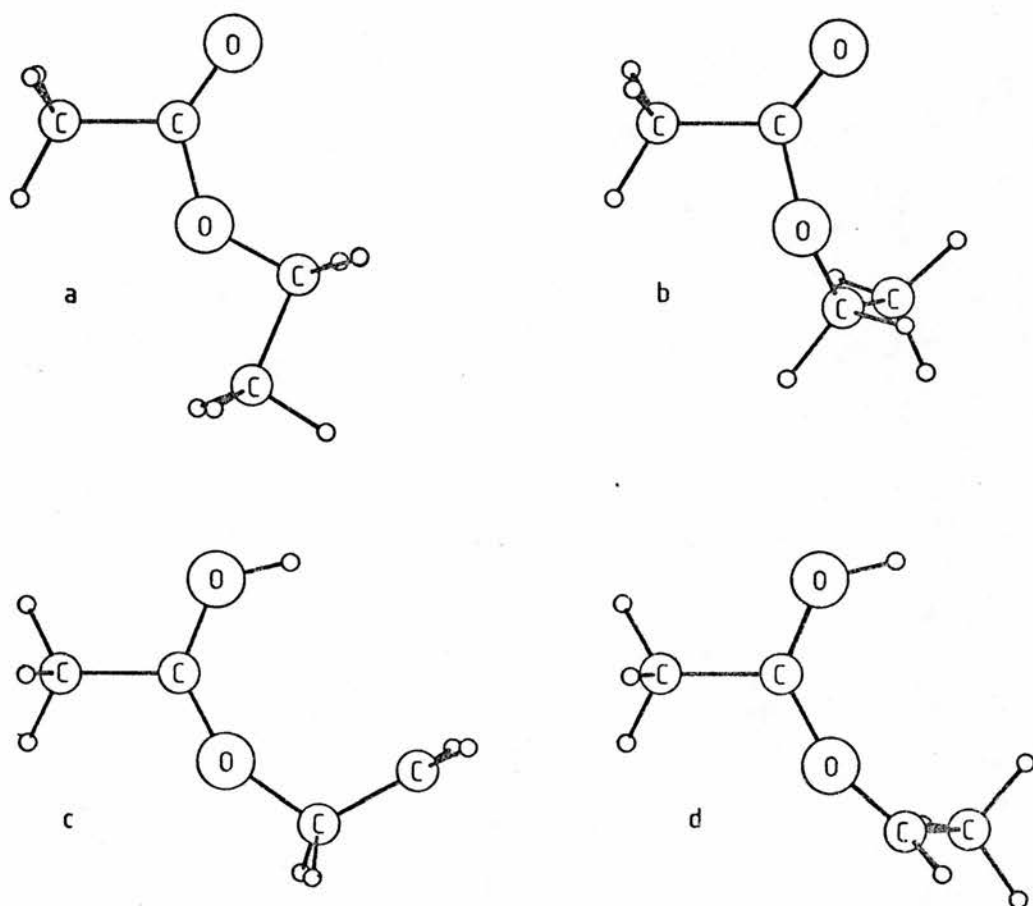
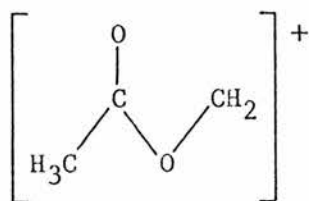


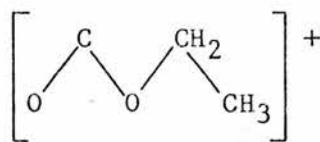
Figure 7.1 The isomers of M^+
 (a) V, (b) VI, (c) VII, (d) VIII

Fragment Ions

The heaviest fragment in the mass spectrum of ethyl acetate corresponds to the loss of CH_3 , yielding two possible isomers: (IX) and (X).

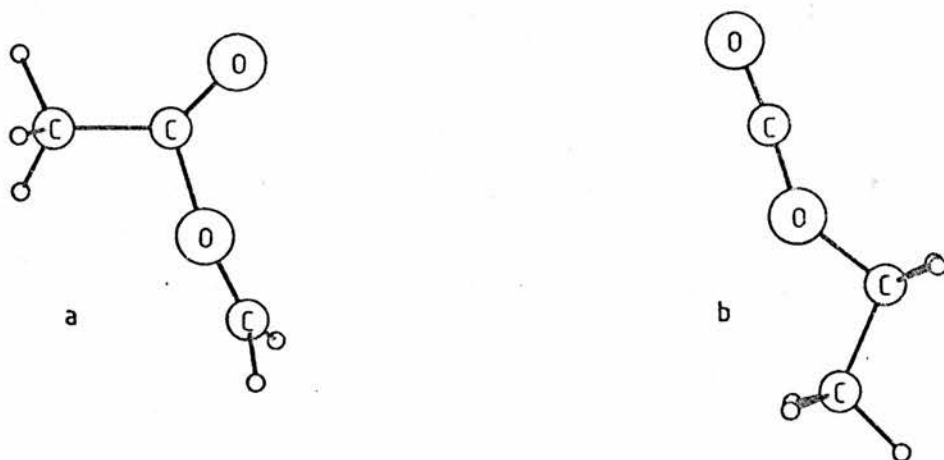


(IX)



(X)

(X), corresponding to the loss of the acetyl methyl group was found to be the more stable by 53 kJ mol^{-1} with coplanar heavy atoms and the OCO fragment almost linear, having an angle of 174.2° . In (IX) the carbon, C_3 , of the CH_2 group is well removed from the plane of the remaining heavy atoms. The structures of these ions are shown in figure 7.2.

Figure 7.2 The isomers of $(\text{M}-\text{CH}_3)^+$

(a) IX, (b) X

Optimisations for the ion $(\text{C}_2\text{H}_5\text{O})^+$ ($m/z=45$), starting at the geometry of the neutral fragment described below, showed dissociation to give $[(\text{CH}_3\text{CO})^+ + \text{H}_2]$. A series of optimisations

were then carried out subject to various constraints. The C-H distances in the CH₂ were fixed at the values found for the neutral fragment CH₃CH₂O[•] and all other geometrical variables were allowed to optimise. This resulted in the geometry given in table 7.2, with the two hydrogen atoms of the CH₂ approaching each other as if to form an H₂ fragment, and gave the enthalpy of formation +855.9 kJ mol⁻¹, compared with H_f=574.1 kJ mol⁻¹ for the dissociation products [(CH₃CO)⁺ + H₂]. A further optimisation was performed with all the geometrical parameters of the CH₂ group fixed at the values found for CH₃CH₂O[•], resulting in a heat of formation of +988.9 kJ mol⁻¹ and exhibiting a shorter CO distance and wider CCO angle compared with its neutral analogue.

Although there was no evidence of rearrangement during the optimisation of (CH₃CH₂O)⁺, calculations were performed on two isomeric forms: O-protonated acetaldehyde, (CH₃CHOH)⁺ [(CH₃CH₂O)⁺ may be considered to be C-protonated acetaldehyde]; and O-protonated oxirane. These were found to have a substantially lower energy than (CH₃CH₂O)⁺ as shown in table 7.1 and figure 7.3.

The ion (CH₃CO)⁺, isoelectronic with CH₃CN optimised to a C_{3v} structure and (CH₂CO)⁺, isoelectronic with CH₂N₂, optimised to a C_{2v} geometry.

Hydrocarbon fragment ions (C₂H₅)⁺, (C₂H₄)⁺, and (C₂H₃)⁺ optimised to give hydrogen-bridged structures for (C₂H₅)⁺ and (C₂H₃)⁺, while (C₂H₄)⁺ retained D_{2h} symmetry but with a longer CC

distance than in its neutral form.

Neutral Fragments

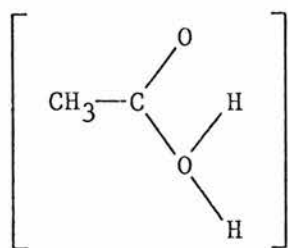
Fragmentations involving a single bond cleavage to give the fragment ions $(M-CH_3)^+$, $(C_2H_5O)^+$, $(CH_3CO)^+$ and $(C_2H_5)^+$ imply the formation of the neutral fragments CH_3^\bullet , CH_3CO^\bullet , $C_2H_5O^\bullet$ and CH_3COO^\bullet . Similarly the rearrangement ions described below, $(C_2H_5O_2)^+$ and $(C_2H_4O_2)^+$, imply the loss of the neutral fragments $C_2H_3^\bullet$ and C_2H_4 . The calculated heats of formation and molecular states of these neutral fragments are given in table 7.1 and the molecular geometries are in table 7.2.

In CH_3COO^\bullet the unpaired electron was found to be in a σ -orbital localised mainly on the two oxygen atoms and on the carbon atom of the methyl group. $C_2H_5O^\bullet$ was calculated to have a staggered molecular configuration with the unpaired electron localised in an oxygen p-orbital perpendicular to the symmetry plane. CH_3CO^\bullet was found to be a σ -radical with the unpaired electron predominantly on the central carbon atom. $C_2H_5^\bullet$ was calculated to be a π -radical with CCH_2 planar and with the unpaired electron localised in a p-orbital perpendicular to the CCH_2 plane, giving a molecular state $^2A'$. The $C_2H_3^\bullet$ fragment was found to be a σ -radical.

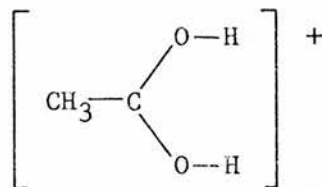
Rearrangement ions

The ions found at the m/z values 61, 60, 31 and 29 correspond to the rearrangement ions with composition $(C_2H_5O_2)^+$, $(C_2H_4O_2)^+$, $(CH_3O)^+$ and $(CHO)^+$.

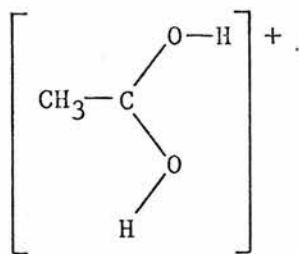
$(C_2H_5O_2)^+$ corresponds to protonated acetic acid and four forms of this ion, (XI) - (XIV), were investigated, each of which occupies a minimum on the overall energy surface.



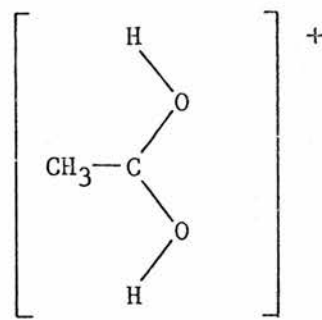
(XI)



(XII)



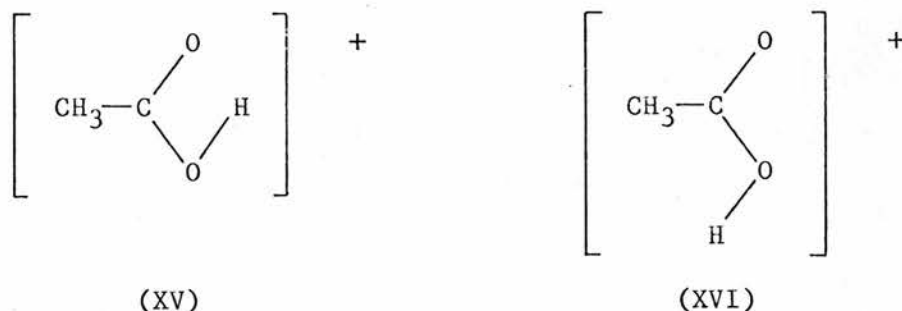
(XIII)



(XIV)

The isomer bearing two hydrogens on a single oxygen atom (XI) was found to be by far the least stable. Of the three conformers (XII) - (XIV), (XII) was found to be the most stable and (XIV) the least stable. All the O-hydrogen atoms in (XI) - (XIV) were found to lie in the plane of the heavy atoms.

The $(\text{C}_2\text{H}_4\text{O}_2)^+$ cation has two possible analogous conformers (XV) and (XVI).



(XV) was found to be more stable than (XVI) and both have the O-hydrogen in the plane of the heavy atoms.

Singlet $(\text{CH}_3\text{O})^+$ rearranged to O-protonated formaldehyde when freely optimised. This may be compared with the $(\text{C}_2\text{H}_5\text{O})^+$ ion, where the O-protonated acetaldehyde was found to be much lower in energy than the C-protonated form, although in that case rearrangement did not occur during optimisation. $(\text{CH}_3\text{O})^+$ would be unable to retain C_{3v} symmetry in its ground electronic state as this would be Jahn-Teller sensitive, with the symmetry of the distorted system no more than C_s . It is thus possible to consider the rearrangement of singlet $(\text{CH}_3\text{O})^+$ to $(\text{H}_2\text{COH})^+$ as an extreme first-order Jahn-Teller distortion. Singlet $(\text{CH}_3\text{CH}_2\text{O})^+$ could not have a symmetry higher than C_s so that no Jahn-Teller distortion would be expected. It has already been observed that MINDO/3 is very efficient at correctly predicting Jahn-Teller distortions [2]. Triplet $(\text{CH}_3\text{O})^+$ optimised to a C_{3v} structure with a much

higher energy.

Miscellaneous Fragments

The neutral fragment $\text{CH}_3\text{CH}_2\text{O}^\bullet$, lost from M^+ to yield $(\text{CH}_3\text{CO})^+$, has an isomeric form $\text{CH}_3\text{CHOH}^\bullet$. This was found to be considerably more stable than $\text{CH}_3\text{CH}_2\text{O}^\bullet$.

A low energy fragment ion which could be formed from (VII) or (VIII) is $(\text{CH}_3\text{COH})^+$. This ion and its isomer $(\text{CH}_3\text{CHO})^+$ could both be precursors of $(\text{CH}_3\text{O})^+$ from (VII) and (VIII).

Molecular Fragmentations

The energies of the various fragment pairs are depicted in figure 7.3 and this may be used to deduce which ions may be produced from a given electronic state of the molecular ion.

The isomeric forms (V) - (VIII) of M^+ , the isomer (X) of $(\text{M}-\text{CH}_3)^+$, the fragment ions $(\text{CH}_3\text{CO})^+$ and $(\text{CH}_3\text{CHOH})^+$, and the rearrangement ion $(\text{CH}_3\text{C}(\text{OH})_2)^+$, may all be produced from the $\tilde{\text{X}}$ state of M^+ . The $\tilde{\text{A}}$ or higher states are required for the production of isomer (IX) of $(\text{M}-\text{CH}_3)^+$, and the $\tilde{\text{C}}$ or higher states are required for the formation of the rearrangement ions $(\text{CH}_3\text{COOH})^+$ and $(\text{C}_2\text{H}_5)^+$.

STATES OF I	M	M ⁺	(M-CH ₃) ⁺	[CH ₃ CO/ C ₂ H ₅ O] ⁺	OTHER [X/M-X] ⁺	NEUTRAL FRAGMENTS
<u>H</u> 4505						
<u>G</u> 6226						<u>CH₃CO + C₂H₅O⁺</u>
<u>F</u> 6681						
<u>E</u> 7022						
<u>D</u> 7454						
<u>C</u> 7226						<u>CH₃COO⁺ + C₂H₅⁺</u> <u>CH₃CHO⁺ + CO</u>
<u>B</u> 5928			<u>CH₃ + CH₃COOCH₃⁺</u> 5722	<u>CH₃CO⁺ + CH₃CO + H₂</u> 5787	<u>CH₃COO⁺ + C₂H₄</u> 6133	
<u>A</u> 5763				<u>CH₃CO⁺ + C₂H₅O</u> 5679		
<u>X</u> 5307			<u>CH₃ + COOC⁺ + H₂</u> 5195	<u>CH₃CO⁺ + COH⁺</u> 5207	<u>CH₃COH⁺ + CO</u> 5024	
		<u>V</u> 4897				<u>CH₃COH⁺ + C₂H₃</u> 4954
		<u>VI</u> 4803				
				<u>CH₃CO⁺ + CH₃CHOH⁺</u> 4735		
				<u>CH₃CO⁺ + CH₃CHOH</u> 4769		
		<u>VII</u> 3461				
		<u>VIII</u> 2765				
						<u>CH₃COO⁺ + Et⁺</u> -917
						<u>CH₃CO⁺ + EtO⁺</u> -990
						<u>CH₃CO + CH₃CHOH⁺</u> -2500
	<u>III</u> -4475					
	<u>II, IV</u> -4642					
<u>I</u> -4731						

Figure 7.3 The energies (ΔH_f^\ominus in kJ mol^{-1}) of the conformers and isomers of M and M⁺, of ionic fragment pairs, and of neutral fragment pairs

It has previously been found [1] that the ion $(\text{CH}_3\text{CO})^+$ is present in a series of mass spectra of alkyl carboxylates. A high abundance of this ion is found in the mass spectra of acetates, but it is also found, in lower abundance, in other simple esters such as formates and propionates. The abundance of the $(\text{CH}_3\text{CO})^+$ ion in these series is substantially higher in ethyl esters than in methyl, n-propyl or n-butyl esters, which supports the above postulate that this ion is formed by the dissociation of the ethoxy cation.

O-protonated oxirane was one of the possible isomers of $(\text{CH}_3\text{CH}_2\text{O})^+$. This may be implicated in the formation of the $(\text{CH}_3\text{O})^+$ ion as a wide range of singly-substituted oxiranes are found to exhibit this ion in their mass spectra [3,4]

Ionisation Energies, Proton Affinities and Bond Dissociation Energies

The data in table 7.1 and figure 7.3 have been used to calculate adiabatic ionisation energies. These are tabulated in table 7.3. Similarly, proton affinities have been calculated and are given in table 7.4, and bond dissociation energies are recorded in table 7.5. The bond energies in table 7.5 show that bond energies in the molecular ion are significantly reduced from those in the parent molecule.

Molecule	Point Group	State	ΔH_f^\ominus
(i) M and M ⁺			
M (I)	C _s	1 _{A'}	-470.6
M (II)	C _s	1 _{A'}	-461.2
M (III)	C _s	1 _{A'}	-447.5
M (IV)	C _s	1 _{A'}	-461.2
M ⁺ (V)	C ₁	2 _A	+483.3
M ⁺ (VI)	C ₁	2 _A	+480.3
M ⁺ (VII)	C _s	2 _{A'}	+346.1
M ⁺ (VIII)	C ₁	2 _A	+276.5
(ii) Fragment Ions			
(CH ₃ COOCH ₂) ⁺ (IX)	C ₁	1 _A	+395.1
(OCOC ₂ H ₅) ⁺ (X)	C _s	1 _{A'}	+342.4
(CH ₃ CH ₂ O) ⁺ a	C _s	1 _{A'}	+988.9
(CH ₃ COH) ⁺ b	C _s	1 _{A'}	+517.7
($\overline{\text{CH}_2\text{CH}_2\text{OH}}$) ⁺ b,c	C _s	1 _{A'}	+614.9
(CH ₃ CO) ⁺	C _{3v}	1 _{A₁}	+572.8
(CH ₂ CO) ⁺	C _{2v}	2 _{B₁}	+758.7
(C ₂ H ₅) ⁺	C _{2v}	1 _{A₁}	+860.8
(C ₂ H ₄) ⁺	D _{2h}	2 _{B_{3u}}	+1032.5
(C ₂ H ₃) ⁺	C _{2v}	1 _{A₁}	+1038.9
(iii) Neutral Fragments			
CH ₃ CH ₂ O•	C _s	2 _{A''}	-4.9
CH ₃ COO•	C _s	2 _{A'}	-185.4
CH ₃ CO•	C _s	2 _{A'}	-94.1
C ₂ H ₅ •	C _s	2 _{A'}	+93.6

C_2H_4	D_{2h}	$1A_{1g}$	+80.4
$C_2H_3^\bullet$	C_s	$2A'$	+280.5
CH_3^\bullet	C_{3v}	$2A_1$	+177.1
(iv) Rearrangement ions			
$(CH_3COOH_2)^+$ (XI)	C_1	$1A$	+321.8
$(CH_3COOH_2)^+$ (XII)	C_s	$1A'$	+214.9
$(CH_3COOH_2)^+$ (XIII)	C_1	$1A$	+233.4
$(CH_3COOH_2)^+$ (XIV)	C_s	$1A'$	+268.8
$(CH_3COOH)^+$ (XV)	C_1	$1A$	+533.0
$(CH_3COOH)^+$ (XVI)	C_1	$2A$	+549.7
$(CH_3O)^+$	C_s	$1A'$	+655.5
$(CH_3O)^+$	C_{3v}	$3A_2$	+1041.4
$(HCO)^+$	$C_{\infty v}$	$1\Sigma^+$	+772.3
(v) Miscellaneous Fragments			
$(CH_3CHO)^+$	C_1	$2A$	+773.6
$(CH_3COH)^+$	C_1	$2A$	+635.1
$\overline{CH_2CH_2O}^d$	C_{2v}	$1A_1$	-111.7
CH_3CHOH^\bullet	C_1	$2A$	-155.9

a Constrained optimisation: all CH_2 parameters fixed at the values found in the radical $CH_3CH_2O^\bullet$; see text.

b Rearrangement ions, isomers of $(CH_3CH_2O)^+$

c O-protonated oxirane

d Oxirane

Table 7.1 Molecular Energies

(i) M and M⁺

M (I)

HC₁, 1.111Å; C₁C₂, 1.497Å; C₂O₁,
1.212Å; C₂O₂, 1.337Å; O₂C₃, 1.359Å;
C₃C₄, 1.493Å; C₃H, 1.131Å; C₄H,
1.111Å; C₁C₂O₁, 123.7°; C₁C₂O₂,
105.9°; O₁C₂O₂, 130.4°; C₂O₂C₃,
133.8°; O₂C₃C₄, 110.4°.

M (II)

HC₁, 1.111Å; C₁C₂, 1.495Å; C₂O₁,
1.213Å; C₂O₂, 1.327Å; O₂C₃, 1.360Å;
C₃C₄, 1.492Å; C₃H, 1.133Å; C₄H,
1.111Å; C₁C₂O₁, 123.6°; C₁C₂O₂,
105.3°; O₁C₂O₂, 131.1°; C₂O₂C₃,
141.0°; O₂C₃C₄, 122.3°.

M (III)

HC₁, 1.111Å; C₁C₂, 1.495Å; C₂O₁,
1.216Å; C₂O₂, 1.332Å; O₂C₃, 1.349Å;
C₃C₄, 1.493Å; C₃H, 1.134Å; C₄H,
1.112Å; C₁C₂O₁, 121.8°; C₁C₂O₂,
117.7°; O₁C₂O₂, 120.5°; C₂O₂C₃,
142.6°; O₂C₃C₄, 110.7°.

M (IV)

HC₁, 1.111Å; C₁C₂, 1.499Å; C₂O₁,
1.213Å; C₂O₂, 1.328Å; O₂C₃, 1.359Å;
C₃C₄, 1.491Å; C₃H, 1.133Å; C₄H,
1.111Å; C₁C₂O₁, 123.8°; C₁C₂O₂,
105.5°; O₁C₂O₂, 130.9°; C₂O₂O₃,
140.3°; O₂C₃C₄, 122.2°.

M⁺ (V)

HC₁, 1.109Å; C₁C₂, 1.507Å; C₂O₁,
1.188Å; C₂O₂, 1.360Å; O₂C₃, 1.351Å;
C₃C₄, 1.510Å; C₃H, 1.122Å; C₄H,
1.111Å; C₁C₂O₁, 116.6°; C₁C₂O₂,

113.0°; $O_1C_2O_2$, 130.4°; $C_2O_2C_3$,
133.1°; $O_2C_3C_4$, 95.1°; $C_4C_3O_2C_2$,
184.2°.

M^+ (VI)

HC_1 , 1.110Å; C_1C_2 , 1.510Å; C_2O_1 ,
1.188Å; C_2O_2 , 1.347Å; O_2C_3 , 1.330Å;
 C_3C_4 , 1.474Å; C_3H , 1.142Å; C_4H ,
1.109Å; $C_1C_2O_1$, 127.4°; $C_1C_2O_2$,
102.2°; $O_1C_2O_2$, 130.3°; $C_2O_2C_3$,
148.8°; $O_2C_3C_4$, 124.3°; $C_1C_2O_1O_2$,
184.5°; $C_3O_2C_2O_1$, 65.4°; $C_4C_3O_2C_2$,
-0.9°.

M^+ (VII)

HC_1 , 1.109Å; C_1C_2 , 1.490Å; C_2O_1 ,
1.288Å; O_1H_1 , 0.950Å; C_2O_2 , 1.264Å;
 O_2C_3 , 1.413Å; C_3C_4 , 1.420Å; C_3H ,
1.125Å; C_4H , 1.099Å; $C_1C_2O_1$,
111.9°; $C_1C_2O_2$, 117.2°; $O_1C_2O_2$,
130.9°; C_2O_1H , 125.7°; $C_2O_2C_3$,
151.8°; $O_2C_3C_4$, 117.6°; O_2C_3H ,
102.7°; C_3C_4H , 123.9°; HC_3OC_2 ,
 $\pm 124.4^\circ$; $HC_4C_3O_2$, $\pm 89.7^\circ$; $H...C_4$,
3.123Å.

M^+ (VIII)

HC_1 , 1.110Å; C_1C_2 , 1.491Å; C_2O_1 ,
1.283Å; O_1H , 0.949Å; C_2O_2 , 1.320Å;
 O_2C_3 , 1.285Å; C_3C_4 , 1.456Å; C_3H ,
1.123Å; C_4H , 1.108Å; $C_1C_2O_1$,
112.3°; $C_1C_2O_2$, 112.3°; $O_1C_2O_2$,
130.1°; $C_2O_2C_3$, 158.0°; $O_2C_3C_4$,
126.8°; C_2O_1H , 126.3°; O_2C_3H ,

113.2°; HC₃O₂C₂, 246.0°; C₄C₃O₂C₂,
45.2°; HC₄C₃O₂, 50.7°, 171.3°,
289.9°.

(ii) Fragment Ions

(CH₃COOCH₂)⁺ (IX)

HC₁, 1.109Å; C₁C₂, 1.476Å; C₂O₁,
1.178Å; C₂O₂, 1.444Å; O₂C₃, 1.212Å;
C₃H, 1.113Å; HC₁C₂, 112.2°; C₁C₂O₁,
134.8°; C₁C₂O₂, 106.5°; O₁C₂O₂,
118.7°; C₂O₂C₃, 165.3°; O₂C₃H,
1220.°; C₁C₂O₁O₂, 180.0°; C₁C₂O₂C₃,
227.9°; HC₁C₂O₁, 95.7°, 216.8°,
336.6°; HC₃O₂C₂, 27.2°, 205.3°.

(OCOC₂H₅)⁺ (X)

O₁C₁, 1.153Å; C₁O₂, 1.220Å; O₂C₂,
1.407Å; C₂C₃, 1.482Å; C₂H, 1.123Å;
C₃H, 1.109Å; O₁C₁O₂, 174.2°;
C₁O₂C₂, 145.3°; O₂C₂C₃, 105.8°;
O₂C₂H, 107.1°; C₂C₃H, 112.2°;
HC₂O₂C₁, +56.1°.

(CH₃CH₂O)⁺ a

C₁C₂, 1.486Å; C₂O, 1.230Å; HC₁,
1.108Å; HC₁C₂, 111.7°; C₁C₂O,
130.3°.

(CH₃COH)⁺ b

HC₁, 1.110Å; C₁C₂, 1.457Å; C₂O,
1.242Å; C₂H, 1.120Å; OH, 0.957Å;
HC₁C₂, 111.7°; C₁C₂O, 120.4; C₁C₂H,
119.0°; HC₂O, 120.5°; C₂OH, 122.9°.

(CH₂CH₂OH)⁺ b,c

CC, 1.455Å; CO, 1.433Å; HC, 1.111Å;
OH, 0.961Å; COC, 61.0°; COH,
118.2°; H_{eno}CO, 110.2°; H_{endo}CO,

	116.4°.
(CH ₃ CO) ⁺	HC ₁ , 1.110Å; C ₁ C ₂ , 1.424Å; C ₂ O, 1.127Å; HC ₁ C ₂ , 110.5°.
(CH ₂ CO) ⁺	HC ₁ , 1.100Å; C ₁ C ₂ , 1.379Å; C ₂ O, 1.134Å; HC ₁ C ₂ , 121.3°
(C ₂ H ₅) ⁺	H _t C, 1.103Å; H _b C, 1.291Å; CC, 1.381Å; CH _b C, 57.7°; H _t CC, 177.4°.
(C ₂ H ₄) ⁺	HC, 1.100Å; CC, 1.403Å; HCC, 123.0°.
(C ₂ H ₃) ⁺	H _t C, 1.083Å; H _b C, 1.280Å; CC, 1.240Å; CH _b C, 57.1°; H _t CC, 177.4°.

(iii) Neutral Fragments

CH ₃ CH ₂ O [•]	HC ₁ , 1.112Å; C ₁ C ₂ , 1.491Å; C ₂ H, 1.150Å; C ₂ O, 1.269Å; HC ₁ C ₂ , 114.1°; HC ₂ C ₁ , 112.7°; C ₁ C ₂ O, 119.7°; HC ₂ C ₁ H, ±51.4°; HC ₁ C ₂ O, 180.0°, 60.1°, 300.1°.
CH ₃ COO [•]	HC ₁ , 1.109Å; C ₁ C ₂ , 1.585Å; C ₂ O, 1.220Å; HC ₁ C ₂ , 112.5°; C ₁ C ₂ O, 106.8°; OCO, 146.4°; HC ₁ C ₂ O, 90.4°, 210.2°, 330.4°.
CH ₃ CO [•]	HC ₁ , 1.114Å; C ₁ C ₂ , 1.457Å; C ₂ O, 1.167Å; HC ₁ C ₂ , 112.7°; C ₁ C ₂ O, 140.7°; HC ₁ C ₂ O, 61.2°, 179.8°, 298.3°.
C ₂ H ₅ [•]	HC ₁ , 1.117Å(x3); C ₁ C ₂ , 1.416Å; C ₂ H, 1.096Å(x2); HC ₁ C ₂ , 113.7°; C ₁ C ₂ H,

	123.5°; HC ₂ C ₁ H, 89.2°, 207.8°, 332.2°.
C ₂ H ₄	HC, 1.100Å; CC, 1.314Å; HCC, 124.6°.
C ₂ H ₃ •	H ₁ C ₁ , 1.107Å; H ₂ C ₁ , 1.092Å; C ₁ C ₂ , 1.283Å; C ₂ H ₃ , 1.087Å; H ₁ C ₁ C ₂ , 122.4°; H ₂ C ₁ C ₂ , 126.0°; C ₁ C ₂ H ₃ , 144.0°.
CH ₃ •	HC, 1.094Å; HCH, 116.6°.

(iv) Rearrangement ions

(CH ₃ COOH ₂) ⁺ (XI)	H ₁ C ₁ , 1.109Å; C ₁ C ₂ , 1.471Å; C ₂ O ₁ , 1.173Å; C ₂ O ₂ , 1.493Å; O ₂ H ₂ , 0.964Å; O ₂ H ₃ , 0.960Å; HC ₁ C ₂ , 112.2°; C ₁ C ₂ O ₁ , 136.5°; C ₁ C ₂ O ₂ , 107.1°; O ₁ C ₂ O ₂ , 116.4°; H ₂ O ₂ C ₂ , 123.4°; H ₃ O ₂ C ₂ , 130.4°; H ₃ O ₂ C ₂ O ₁ , 180.6°; H ₂ O ₂ C ₂ O ₁ , 0.4°.
(CH ₃ COOH ₂) ⁺ (XII)	HC ₁ , 1.110Å; C ₁ C ₂ , 1.483Å; C ₂ O, 1.278Å; OH, 0.955Å; HC ₁ C ₂ , 112.1°; C ₁ C ₂ O, 114.9°; C ₂ OH, 126.2°; HC ₁ C ₂ O, 90.0°, 210.0°, 330.0°.
(CH ₃ COOH ₂) ⁺ (XIII)	HC ₁ , 1.111Å; C ₁ C ₂ , 1.479Å; C ₂ O ₁ , 1.279Å; C ₂ O ₂ , 1.287Å; O ₁ H ₂ , 0.958Å; O ₂ H ₃ , 0.952Å; HC ₁ C ₂ , 112.4°; C ₁ C ₂ O ₁ , 114.3°; C ₁ C ₂ O ₂ , 124.8°; C ₂ O ₁ H ₂ , 123.8°; C ₂ O ₂ H ₃ , 122.0°; O ₂ C ₂ O ₁ H ₂ , 0.1°; O ₁ C ₂ O ₂ H ₃ , 180.2°; H ₁ C ₁ C ₂ O ₁ , 90.3°, 210.1°, 330.2°.

$(\text{CH}_3\text{COOH}_2)^+$ (XIV)	HC_1 , 1.110Å; C_1C_2 , 1.478Å; C_2O , 1.290Å; OH , 0.953Å; HC_1C_2 , 112.8°; $\text{C}_1\text{C}_2\text{O}$, 123.4°; C_2OH , 119.2°; $\text{HC}_1\text{C}_2\text{O}$, 90.1°, 210.1°, 330.0°.
$(\text{CH}_3\text{COOH})^+$ (XV)	HC_1 , 1.112Å; C_1C_2 , 1.545Å; C_2O_1 , 1.198Å; C_2O_2 , 1.290Å; O_2H , 0.963Å; HC_1C_2 , 109.9°; $\text{C}_1\text{C}_2\text{O}_1$, 107.1°; $\text{C}_1\text{C}_2\text{O}_2$, 109.5°; $\text{O}_1\text{C}_2\text{O}_2$, 143.4°; $\text{C}_2\text{O}_2\text{H}$, 117.6°; $\text{O}_1\text{C}_2\text{O}_2\text{H}$, 0.0°; $\text{HC}_1\text{C}_2\text{O}_1$, 89.7°, 212.6°, 330.2°.
$(\text{CH}_3\text{COOH})^+$ (XVI)	HC_1 , 1.111Å; C_1C_2 , 1.556Å; C_2O_1 , 1.198Å; C_2O_2 , 1.283Å; O_2H , 0.955Å; HC_1C_2 , 109.6°; $\text{C}_1\text{C}_2\text{O}_1$, 106.0°; $\text{C}_1\text{C}_2\text{O}_2$, 120.6°; $\text{O}_1\text{C}_2\text{O}_2$, 133.4°; $\text{C}_2\text{O}_2\text{H}$, 123.7°; $\text{O}_1\text{C}_2\text{O}_2\text{H}$, 180.0°; $\text{HC}_1\text{C}_2\text{O}_1$, 93.1°, 214.9°, 333.0°.
$(\text{CH}_3\text{O})^+$ ($^1\text{A}'$)	H_1C , 1.110Å; H_2C , 1.111Å; CO , 1.223Å; OH_3 , 0.960Å; H_1CO , 125.7°; H_2CO ; 115.1°; COH_3 , 124.1°.
$(\text{CH}_3\text{O})^+$ ($^3\text{A}_2$)	HC , 1.152Å; CO , 1.201Å; HCO , 114.8°.
$(\text{HCO})^+$	HC , 1.094Å; CO , 1.115Å; HCO , 180.0°.

(v) Miscellaneous Fragments

$(\text{CH}_3\text{CHO})^+$	HC_1 , 1.110Å; C_1C_2 , 1.483Å; C_2H , 1.164Å; C_2O , 1.161Å; HC_1C_2 , 109.6°; $\text{C}_1\text{C}_2\text{O}$, 140.5°; $\text{C}_1\text{C}_2\text{H}$, 116.1°; HC_2O ,
-----------------------------	--

	103.4°; HC ₁ C ₂ O, 86.8°, 208.8°, 328.3°.
(CH ₃ COH) ⁺	HC ₁ , 1.111Å; C ₁ C ₂ , 1.438Å; C ₂ O, 1.204Å; OH, 0.949Å; HC ₁ C ₂ , 110.7°; C ₁ C ₂ O, 131.6°; C ₂ OH, 132.7°; HC ₁ C ₂ O, 61.1°, 179.7°, 298.4°; C ₁ C ₂ OH, 180.0°.
$\overline{\text{CH}_2\text{CH}_2\text{O}^{\text{d}}}$	CO, 1.389Å; CH, 1.114Å; HCO, 117.5°; COC, 62.8°.
CH ₃ CHOH•	HC ₁ , 1.116Å; C ₁ C ₂ , 1.451Å; C ₂ H, 1.122Å; C ₂ O, 1.301Å; OH, 0.951Å; HC ₁ C ₂ , 112.9°; C ₁ C ₂ O, 118.9°; C ₁ C ₂ H, 117.8°; HC ₂ O, 118.3°; C ₂ OH, 114.1°; HC ₁ C ₂ O, 59.5°, 177.9°, 298.4°; C ₁ C ₂ OH, 148.1°.

a,b,c,d See footnotes to Table 7.1

Table 7.2 Molecular Geometries

$\text{CH}_3\text{COOC}_2\text{H}_5$ (I)	\longrightarrow	{ (V)	9.91
		{ (VI)	9.88
		{ (VII)	8.49
		{ (VIII)	7.77
$\text{CH}_3\text{CH}_2\text{O}$	\longrightarrow	{ $(\text{CH}_3\text{CH}_2\text{O})^+$	10.30
		{ $(\overline{\text{CH}_2\text{CH}_2\text{OH}})^+$	6.42
		{ $(\text{CH}_3\text{CHOH})^+$	5.42
CH_3CHOH	\longrightarrow	$(\text{CH}_3\text{CHOH})^+$	6.98
CH_3CO	\longrightarrow	$(\text{CH}_3\text{CO})^+$	6.91
C_2H_5	\longrightarrow	$(\text{C}_2\text{H}_5)^+$	8.05
C_2H_4	\longrightarrow	$(\text{C}_2\text{H}_4)^+$	9.86
C_2H_3	\longrightarrow	$(\text{C}_2\text{H}_3)^+$	7.86
CH_3O	\longrightarrow	{ $(\text{H}_2\text{COH})^+$ ($^1\text{A}'$)	6.29
		{ $(\text{H}_3\text{CO})^+$ ($^3\text{A}_2$)	10.30

Table 7.3 Adiabatic Ionisation Energies (eV)

$\text{CH}_3\text{CO}\cdot$	799	$\text{CH}_3\text{COO}\cdot$	810
$\text{CH}_3\text{CO}\cdot$	660	C_2H_4	564
$\overline{\text{CH}_2\text{CH}_2\text{O}}$	803	C_2H_3	536

Table 7.4 Proton Affinities (kJ mol^{-1})

$\text{CH}_3\text{CO-OC}_2\text{H}_5$	346.1	$\text{CH}_3\text{COO-C}_2\text{H}_5$	381.4
$\text{CH}_3\text{CO}^+-\text{OC}_2\text{H}_5$	87.7	$\text{CH}_3\text{COO-C}_2\text{H}_5^+$	192.1
$\text{CH}_3\text{CO-OCH}_2\text{CH}_3^+$	414.4	$\text{CH}_3\text{-COOC}_2\text{H}_5$	36.2
$\text{CH}_3\text{CO-(HO)CHCH}_3^+$	-66.4	$\text{CH}_3\text{COOCH}_2^+-\text{CH}_3$	88.9

Table 7.5 Bond Dissociation Energies (kJ mol^{-1})

References

- [1] J.H. Beynon, R.A. Saunders and A.E. Williams, *Anal. Chem.*, 33 (1961), 22

- [2] J.R. Bews and C. Glidewell, *J. Mol. Struct.*, 64 (1980), 87

- [3] E.J. Gallegos and R.W. Kiser, *J. Am. Chem. Soc.*, 83 (1961), 773

- [4] Y. Wada and R.W. Kiser, *J. Phys. chem.*, 66 (1962), 1652

CHAPTER 8

MOLECULAR FRAGMENTATION OF CARBON TETRACHLORIDE

Carbon tetrachloride has been previously studied by electron-impact mass spectrometry [1], charge-exchange mass spectrometry [2], and photoelectron spectrometry [3-6]. The parent ion $(\text{CCl}_4)^+$ has not been observed by mass spectrometry and MINDO/3 has been utilised here for a theoretical study of carbon tetrachloride and its fragmentation.

Calculations were performed using the version of MINDO/3 described in chapters 2 and 3. Full geometry optimisations were performed except where explicitly stated otherwise. "Reaction coordinate" calculations were performed with optimisation of all geometrical variables except the one under study.

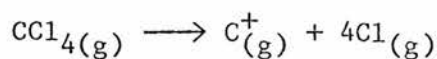
Introduction

The electron-impact mass spectrum of carbon tetrachloride [1] contains the major ions: $(\text{CCl}_3)^+$, RI=100%; $(\text{CCl}_2)^+$, RI=22%; $(\text{CCl})^+$, RI=22.5%; and Cl^+ , RI=26.9%. The doubly charged ions $(\text{CCl}_3)^{2+}$, RI=2.6% and $(\text{CCl}_2)^{2+}$, RI=0.6% are also present, but the ion $(\text{CCl}_4)^+$ is absent from both electron-impact and charge-exchange mass spectra.

Molecular Energies

Table 8.1 contains the point groups, molecular states, enthalpies of formation and optimised geometries. The calculated energies of the electronic states of $(\text{CCl}_4)^+$ arising from the vertical ionisation of CCl_4 are given in table 8.2. The ordering of the first three molecular orbitals in CCl_4 calculated in this work were found to be, in order of increasing binding energy, $t_2 < t_1 < e$. This is in agreement with CNDO/2 calculations [5], although the order $t_1 < t_2 < e$ has been suggested on the basis of spin-orbit couplings [4,8]. The corresponding calculated ionisation energies, 11.3, 11.5 and 13.5 eV, are in reasonable agreement with the first three bands observed in the photoelectron spectrum [4].

The calculated enthalpy of formation of CCl_4 was found to be $-102.8 \text{ kJ mol}^{-1}$, very close to the experimental value of $-105.9 \text{ kJ mol}^{-1}$ [9]. This value, combined with the atomisation enthalpies of carbon and chlorine and the ionisation energy of carbon, shows that the enthalpy for the atomisation of the molecule with a single concurrent ionisation:



is $2386.4 \text{ kJ mol}^{-1}$, i.e. 24.73 eV. Ionisation of the deep valence electrons giving either the $\tilde{\text{E}}$ or $\tilde{\text{F}}$ states of $(\text{CCl}_4)^+$ would provide sufficient energy to completely disrupt the molecule.

Molecular Structures

Table 8.1 shows the equilibrium geometries. Neutral CCl_4 has T_d symmetry as expected. Ionisation to either of the states \tilde{X} (2T_2) or \tilde{A} (2T_1) will give rise to a Jahn-Teller distortion either along one of the t_2 vibrations ν_3 or ν_4 giving C_{2v} or C_{3v} symmetry, or along the e vibration ν_2 which has two components, one of which lowers the symmetry to D_2 (and in the limit to D_{4h}), and the other lowers the symmetry to D_{2d} (again with D_{4h} as the limit). The \tilde{B} (2E) state of $(\text{CCl}_4)^+$ would also be expected to lead to a Jahn-Teller distortion along the e vibration ν_2 .

Geometry optimisation for $(\text{CCl}_4)^+$ without any constraints gave a structure of exact C_{2v} symmetry as expected for a distortion along a t_2 vibration. Constrained optimisations were carried out for the other point group, C_{3v} , expected from a t_2 distortion, for those (D_2 , D_{2d} , and D_{4h}) expected as possible products of distortion along ν_2 , and for T_d . The C_{3v} structure was found to have the nearest energy to the ground state C_{2v} . For the possible symmetries arising from distortions along ν_2 the energies were found to decrease in the order $D_{4h} > D_{2d} > D_2$ as the number of constraints decreases. The T_d form gave an energy very close to that of the \tilde{X} (2T_2) state arising from vertical ionisation, with the structure differing only slightly in carbon-chlorine distance. This geometry is Jahn-Teller sensitive as is the D_{4h} form, which has an 2E_g ground state. This implies a Jahn-Teller distortion along either the b_{1g} vibration ν_3 , or the b_{2g} vibration ν_4 . The b_{1g} vibration lowers the symmetry to D_{2h} , with

two different carbon-chlorine distances, but with all bond angles still 90° , whereas the b_{2g} vibration also lowers the symmetry to D_{2h} , but with all the bond lengths equal and non-orthogonal bonds. Optimisations were carried out subject to these constraints, when the b_{1g} distortion converged back to the D_{4h} structure, but the b_{2g} distortion converged to a structure of almost, but not exact, D_{4h} symmetry some 17 kJ mol^{-1} more stable. The overall energy sequence of the $(\text{CCl}_4)^+$ geometries investigated was $D_{4h} > D_{2h} > D_{2d} > T_d > D_2 > C_{3v} > C_{2v}$. All but the D_{4h} and D_{2h} forms are accessible from the $\tilde{X} (^2T_2)$ state arising from the first vertical ionisation of neutral CCl_4 .

The $(\text{CCl}_3)^+$ cation has exact D_{3h} symmetry in its ground electronic state, but the first excited singlet and triplet are both non-planar. In each of the excited states one of the bond angles is less than 90° , with the sum of the angles at carbon 336.4° for the $^1A''$ state, and 347.2° for the $^3A''$ state. The doubly charged ion $(\text{CCl}_3)^{2+}$ also has one bond angle below 90° but the ion is planar overall. In the doubly charged ion and the two excited states of $(\text{CCl}_3)^+$ the unique carbon-chlorine distance is substantially shorter than the two which enclose the small inter-bond angle. The CCl_3 radical is almost planar with C_{3v} symmetry.

The fragment CCl_2 can exist both as a singlet and as a triplet. The bond angle is much larger in the triplet as found in CH_2 [10,11], but unlike CH_2 the singlet was found to have lower energy. $(\text{CCl}_2)^{2+}$ was found to be linear.

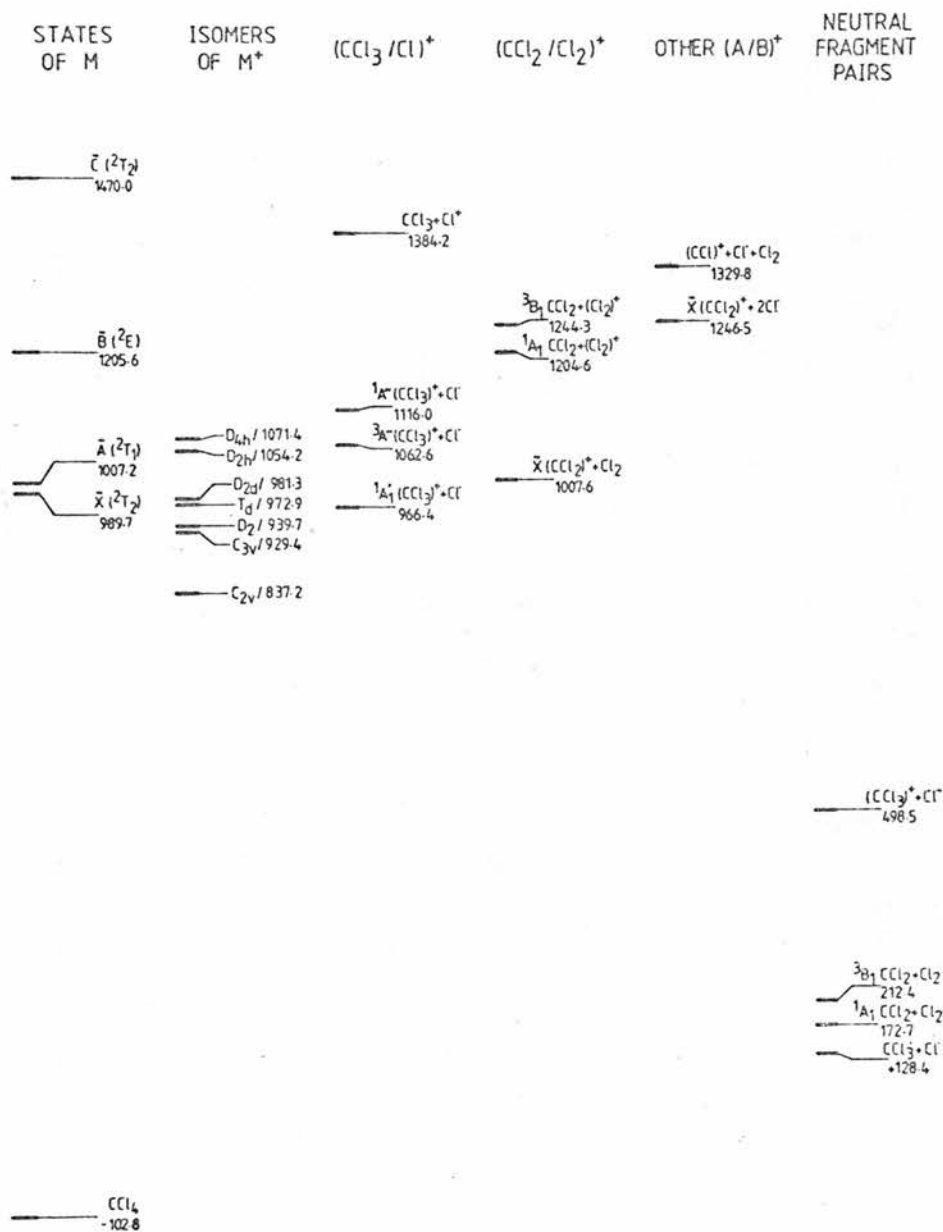
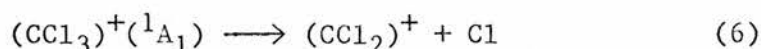
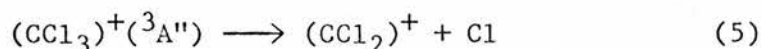
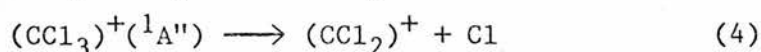
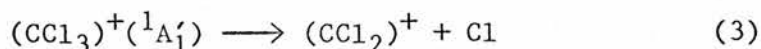
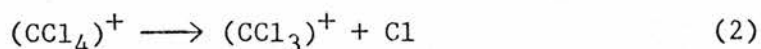
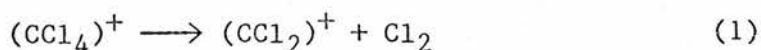


Figure 8.1 The energies (ΔH_f^\ominus in kJ mol⁻¹) of the fragments

Molecular Fragmentations

The following molecular fragmentations, (1) - (6), were investigated using the "reaction coordinate" facility of MINDO/3. Energies of the fragment pairs are depicted in figure 8.1.



All of the fragmentations except (3) involve no change in the number of unpaired electrons and were investigated using single configuration wave functions. Fragmentation (3), involving conversion of a ground state singlet with no unpaired electrons, was investigated using both single and double configuration wavefunctions.

Fragmentation (1), involving the loss of neutral Cl_2 from $(\text{CCl}_4)^+$, was studied using the distance $d(\text{C-X})$ as the reaction coordinate, where X was constrained to be the mid-point of the departing Cl-Cl fragment. No other constraints were applied. Throughout the reaction path the point X always stayed in the plane of the bonded $(\text{ClCCl})^+$ fragment, but the departing Cl_2 fragment, initially perpendicular to CCl_2 , twisted to give a dihedral angle of 4.5° when $d(\text{C-X})$ reached 4\AA . An energy maximum was reached at a C-X distance of 3\AA where ΔH_f^\ominus was found to be

+1009.2 kJ mol⁻¹. The final enthalpy of formation at a C-X distance of 4Å was +1007.6 kJ mol⁻¹. The enthalpy of the fragmentation (1) is +170.4 kJ mol⁻¹.

Fragmentation (2) represents the loss of a single chlorine atom from (CCl₄)⁺ to yield the ion (CCl₃)⁺. The reaction coordinate was taken as a carbon-chlorine distance and was followed without constraint from its equilibrium value of 1.800Å in (CCl₄)⁺ (C_{2v}) to 6Å. The structure of the decomposing (CCl₄)⁺ fragment, viewed along a direction normal to the plane of the three chlorine atoms and passing through their centre of mass, is shown in figure 8.2. The energy profile for the reaction is shown in figure 8.3. There is an initial maximum for C-Cl of 2.8Å, 97.1 kJ mol⁻¹ above the equilibrium energy, with a structure similar to that shown for a C-Cl length of 3.0Å in figure 8.2d. An intermediate equilibrium is seen at a carbon-chlorine distance of 3.656Å where the geometry, shown in figure 8.2f, has the departing chlorine ca. 2.0Å from one of the chlorine atoms in the CCl₃ fragment. This chlorine-chlorine distance is the same as that found in an isolated chlorine molecule and is smaller than the 2.215Å chlorine-chlorine distance found in (CCl₄)⁺, suggesting that the reaction pathway would involve the loss of a chlorine molecule. However as the reaction coordinate is increased only the single chlorine atom departed from the parent ion to show a second energy maximum for C-Cl at 4.5Å with an energy 108.6 kJ mol⁻¹ above that of the intermediate, 158.5 kJ mol⁻¹ above that of (CCl₄)⁺, and 29.3 kJ mol⁻¹ above the final

products $(\text{CCl}_3)^+ + \text{Cl}$. The residual CCl_3 fragment was found to be planar by the time the reaction coordinate had reached 2.5\AA , and by 3.5\AA the whole system was planar.

Fragmentation (3) was initially investigated using single configuration wavefunctions taking a C-Cl distance as the reaction coordinate. The energy increased very steeply as shown in figure 8.4, and at values of the reaction coordinate greater than 3\AA the calculations failed to achieve self-consistence. The use of configuration interaction, involving only the first doubly excited configuration, showed the reaction profile also depicted in figure 8.4. A smooth increase in energy to the reaction products $\tilde{\text{X}}(\text{CCl}_2)^+ + \text{Cl}^\bullet$ was shown with no activation enthalpy in excess of the enthalpy of reaction.

In fragmentation (4) the first excited singlet of $(\text{CCl}_3)^+$ gave $\tilde{\text{A}}(\text{CCl}_2)^+ + \text{Cl}^\bullet$ as the reaction products with an energy maximum at the reaction coordinate value of 2.75\AA , 9.3 kJ mol^{-1} above the energy of the products, as shown in figure 8.4.

Fragmentation (5), involving the first triplet state of $(\text{CCl}_3)^+$, gave rise to $\tilde{\text{X}}(\text{CCl}_2)^+$ with an energy maximum at a carbon-chlorine distance of 3.5\AA , 4.3 kJ mol^{-1} above the energy of the products, as is also shown in figure 8.4.

In fragmentation (6) no activation barrier was found above the enthalpy of reaction.

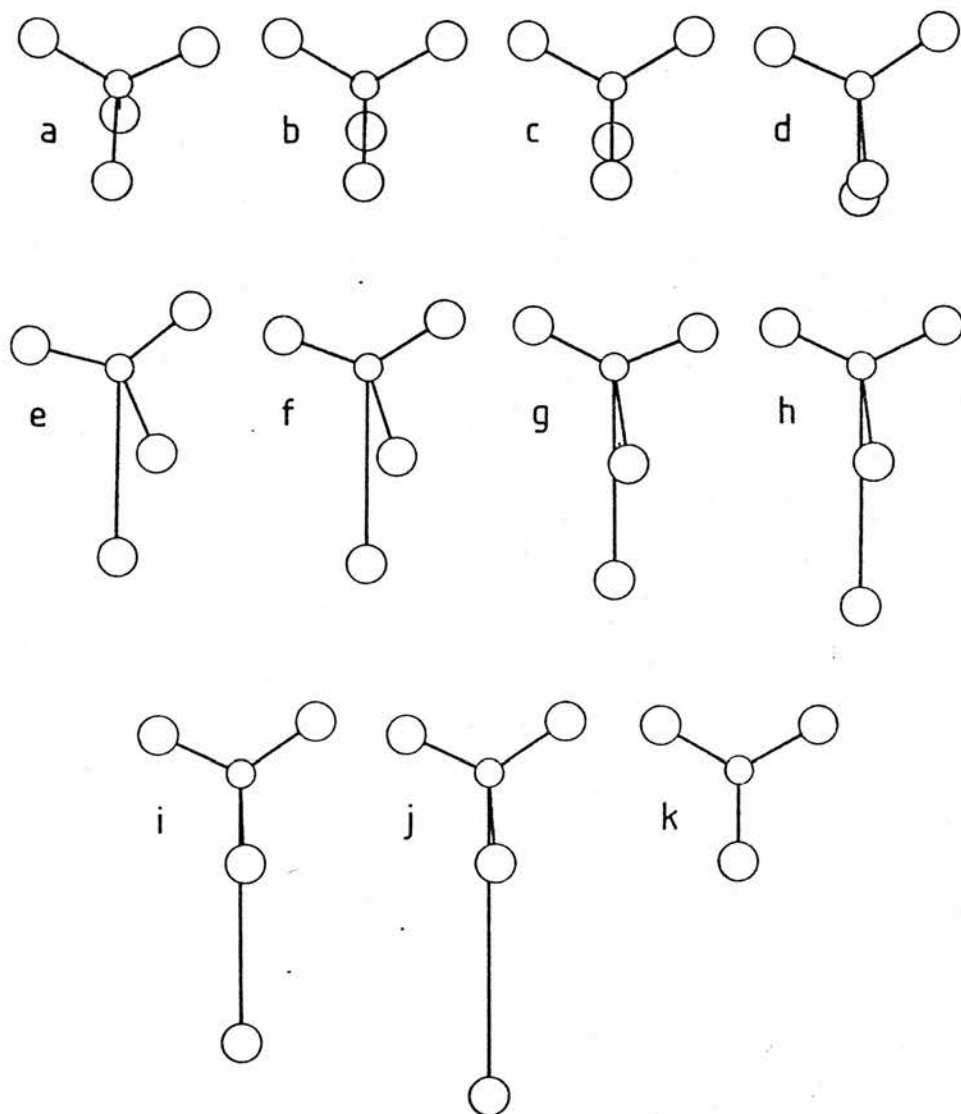


Figure 8.2 Structures of the fragment $(\text{CCl}_3^+-\text{Cl})$ at values of the reaction coordinate (\AA):

(a) 1.800	(b) 2.000	(c) 2.500	(d) 3.000
(e) 3.500	(f) 3.656	(g) 4.000	(h) 4.500
(i) 5.000	(j) 6.000	(k)	

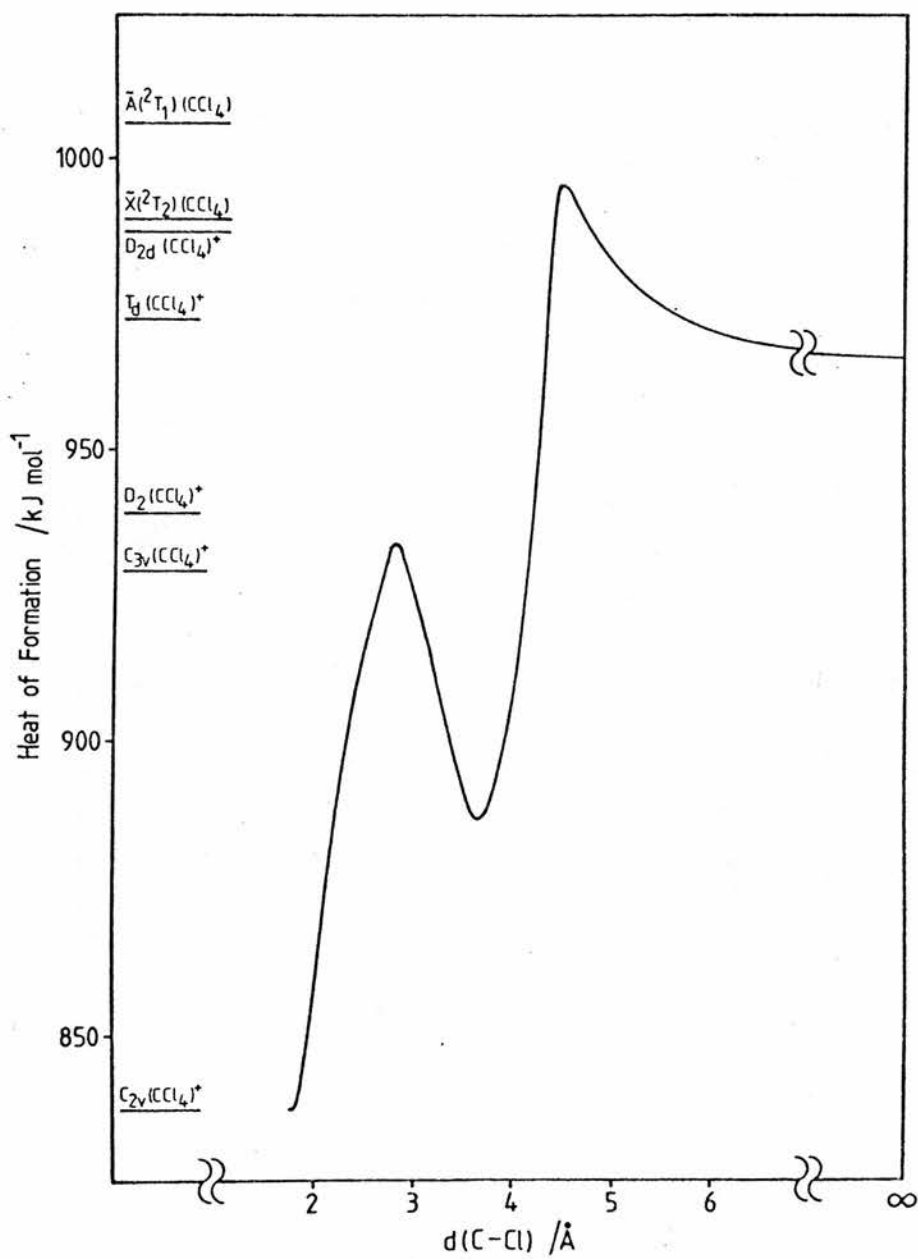


Figure 8.3 Energy profile for the reaction
 $(\text{CCl}_4)^+ \rightarrow (\text{CCl}_3)^+ + \text{Cl}\cdot$

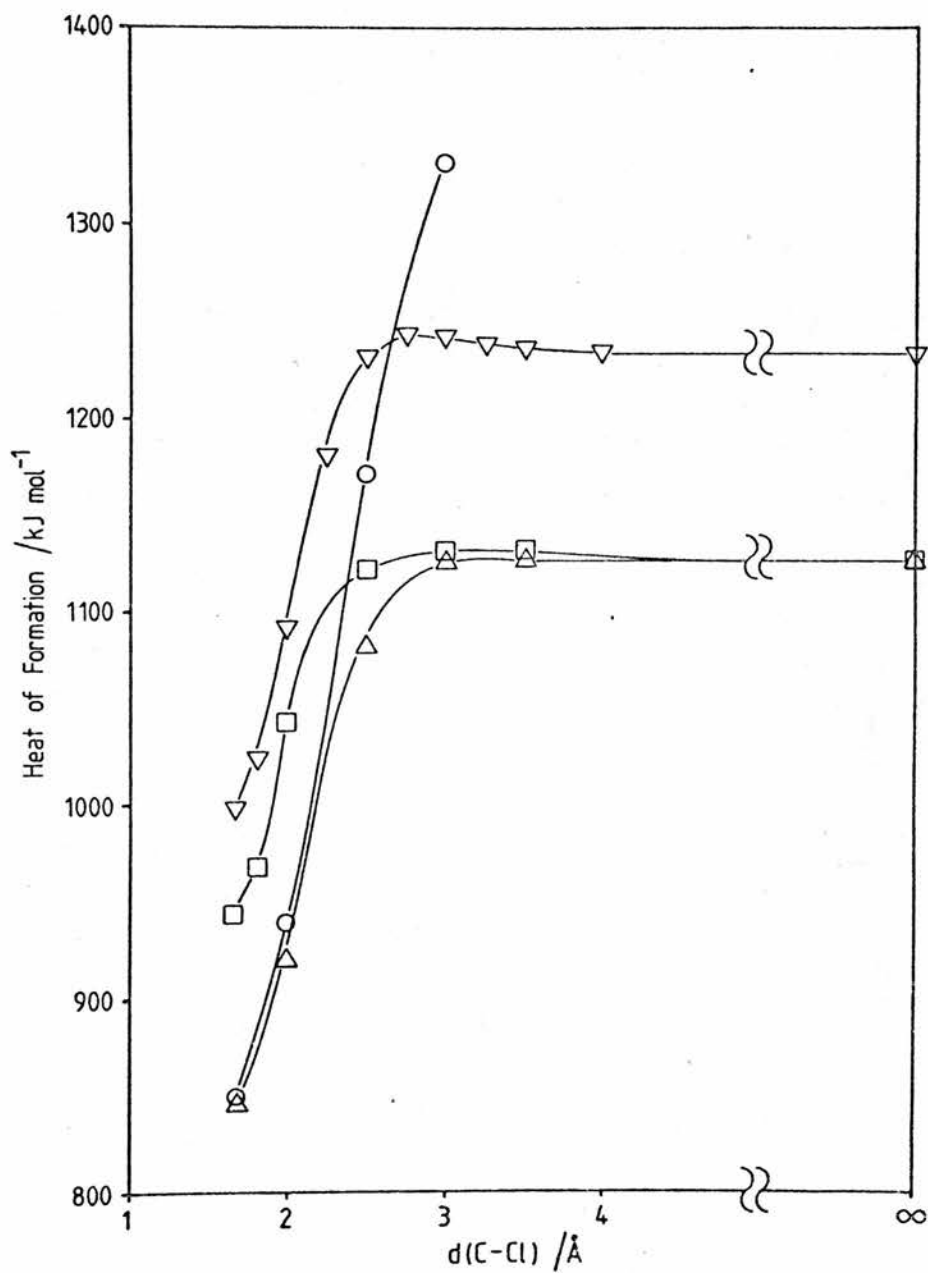
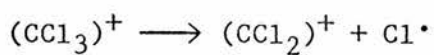


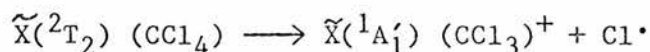
Figure 8.4 Energy profiles for the fragmentations



- $(^1\text{A}') (\text{CCl}_3)^+ \longrightarrow \tilde{\text{X}} (\text{CCl}_2)^+ + \text{Cl}\cdot$, single configuration
- △ $(^1\text{A}') (\text{CCl}_3)^+ \longrightarrow \tilde{\text{X}} (\text{CCl}_2)^+ + \text{Cl}\cdot$, double configuration
- $(^3\text{A}'') (\text{CCl}_3)^+ \longrightarrow \tilde{\text{X}} (\text{CCl}_2)^+ + \text{Cl}\cdot$
- ▽ $(^1\text{A}'') (\text{CCl}_3)^+ \longrightarrow \tilde{\text{A}} (\text{CCl}_2)^+ + \text{Cl}\cdot$

The Absence of $(\text{CCl}_4)^+$ from the Mass Spectrum

Five of the seven isomers of $(\text{CCl}_4)^+$ studied here, namely D_{2d} , T_d , D_2 , C_{3v} and C_{2v} , were calculated to have energies lower than that of the first vertical ionisation of CCl_4 to the $\tilde{X} (^2T_2)$ state. Of these, three are of lower energy than $\tilde{X} (\text{CCl}_3)^+ + \text{Cl}\cdot$ as shown in figure 8.1. However, $\tilde{X} (\text{CCl}_3)^+ + \text{Cl}\cdot$ is of lower energy than the $\tilde{X} (^2T_2)$ state of vertically ionised CCl_4 , so that no matter which distortion of vertically ionised CCl_4 occurs, the initial ionisation provides sufficient energy for the dissociation to $(\text{CCl}_3)^+ + \text{Cl}\cdot$. Although the investigation of fragmentation pathways showed that the dissociation of $(\text{CCl}_4)^+$ to $(\text{CCl}_3)^+ + \text{Cl}\cdot$ has an activation enthalpy of 29.3 kJ mol^{-1} above the final products, this energy is only 6.0 kJ mol^{-1} above the vertical ionisation energy of CCl_4 . Thus the fragmentation



is exothermic by 23.3 kJ mol^{-1} with an activation energy of only 6.0 kJ mol^{-1} .

It has previously been suggested [7] that $(\text{CCl}_4)^+$ is not observed because excitation of CCl_4 occurs at the lowest observed photoelectron absorption at 11.5 eV to give a repulsive excited state of neutral CCl_4 which dissociates to $\text{CCl}_3 + \text{Cl}$, the major ion CCl_3 being produced by the subsequent ionisation of CCl_3 . The low potential barrier found in this work between the vertically ionised CCl_4 and the $(\text{CCl}_3)^+$ cation suggests that this postulate is unnecessary to explain the absence of $(\text{CCl}_4)^+$ from

the mass spectrum of CCl_4 .

Ionisation Energies, Appearance Potentials and Bond Energies

Observed and calculated ionisation energies and appearance potentials are shown in table 8.3, exhibiting good agreement between experimental values and the results of MINDO/3 calculations. Bond energies are recorded in table 8.4, showing increasing bond energies for loss of chlorine from CCl_n as n decreases, and with lower bond energies for the cations. Loss of Cl^+ from the ions $(\text{CCl}_n)^+$ requires much greater energies because of the high ionisation energy of the chlorine atom.

Molecule	Point Group	State	ΔH_f^\ominus kJ mol ⁻¹	Geometry
CCl ₄	T _d	¹ A ₁	-102.8	CCl, 1.751Å
(CCl ₄) ⁺ a,b	C _{2v}	² B ₁	+837.2	CCl _a , 1.715Å (x2); CCl _b , 1.800Å (x2); Cl _a CCl _a , 116.0°; Cl _b CCl _b , 75.9°; Cl _a CCl _b , 114.6° (x4)
(CCl ₄) ⁺	C _{3v}	² A ₁	+929.4	CCl _a , 1.707Å (x3); CCl _b , 1.860Å (x1); Cl _a CCl _a , 117.7° (x3); Cl _a CCl _b , 98.9° (x3)
(CCl ₄) ⁺	D ₂	² B ₁	+939.7	CCl, 1.738Å; ClCCl, 122.6° (x2), 115.3° (x2), 92.0° (x2)
(CCl ₄) ⁺	T _d	² T ₂	+972.9	CCl, 1.740Å
(CCl ₄) ⁺	D _{2d}	² A ₂	+981.3	CCl, 1.729Å; ClCCl, 129.4° (x2), 100.5° (x4)
(CCl ₄) ⁺	D _{2h}	² B _{1g}	+1054.2	CCl, 1.758Å; ClCCl, 89.9°
(CCl ₄) ⁺	D _{4h}	² E _g	+1071.4	CCl, 1.730Å

CCl_3^\bullet	C_{3v}	$^2\text{A}_1$	+8.9	CCl , 1.716Å; ClCCl , 119.3°
$(\text{CCl}_3)^+{}^c$	D_{3h}	$^1\text{A}'_1$	+847.0	CCl , 1.673Å
$(\text{CCl}_3)^+$	C_s	$^3\text{A}''$	+943.2	CCl_a , 1.646Å (x1); CCl_b , 1.751Å (x2); Cl_aCCl_b , 133.5° (x2); Cl_bCCl_b , 80.2° (x1)
$(\text{CCl}_3)^+$	C_s	$^1\text{A}''$	+996.5	CCl_a , 1.672Å (x1); CCl_b , 1.743Å (x2); Cl_aCCl_b , 129.0° (x2); Cl_bCCl_b , 78.4° (x1)
$(\text{CCl}_3)^{2+}$	C_{2v}	$^2\text{B}_2$	+2419.5	CCl_a , 1.627Å (x1); CCl_b , 1.711Å (x2); Cl_aCCl_b , 137.9° (x2); Cl_bCCl_b , 84.2° (x1)
CCl_2	C_{2v}	$^1\text{A}_1$	+173.2	CCl , 1.679Å; ClCCl , 119.4°
CCl_2	C_{2v}	$^3\text{B}_1$	+213.0	CCl , 1.663Å; ClCCl , 149.1°
$\text{X}(\text{CCl}_2)^+$	C_{2v}	$^2\text{B}_2$	+1007.6	CCl , 1.610Å; ClCCl , 149.8°
$\text{A}(\text{CCl}_2)^+$	C_{2v}	$^2\text{B}_2$	+1113.3	CCl , 1.718Å; ClCCl , 81.2°

$(\text{CCl}_2)^{2+}$	$D_{\infty h}$	$1\Sigma_g^+$	+2523.1	CCl, 1.574Å
Cl_2	$D_{\infty h}$	$1\Sigma_g^+$	-0.5	ClCl, 2.037Å
$(\text{Cl}_2)^+$	$D_{\infty h}$	$2\Pi_g$	+1031.4	ClCl, 1.924Å
CCl	$C_{\infty v}$	$2\Sigma^+$	+418.2	CCl, 1.640Å
$(\text{CCl})^+$	$C_{\infty v}$	$1\Sigma^+$	+1210.8	CCl, 1.555Å

a Free optimisation of $(\text{CCl}_4)^+$ always gives C_{2v} geometry: all other geometries result from optimisations constrained to particular point group symmetries

b Subscripts a and b on chlorine atoms indicate atoms of differing type within the particular point group

c With configuration interaction, ΔH_f^\ominus is +845.3 kJ mol⁻¹ and $d(\text{C-Cl})$ is 1.670Å

Table 8.1 Molecular Properties at Equilibrium

State	Vertical I. E. (eV)	ΔH_f^\ominus kJ mol ⁻¹
\tilde{F} (2A_1)	30.448	+2835.0
\tilde{E} (2T_2)	24.747	+2285.0
\tilde{D} (2A_1)	22.841	+2101.1
\tilde{C} (2T_2)	16.291	1470.0
\tilde{B} (2E)	13.560	+1205.4
\tilde{A} (2T_1)	11.505	+1007.2
\tilde{X} (2T_2)	11.323	+989.7
\tilde{X} (1A_1)	Ground state of neutral molecule	-102.8

Table 8.2 Electronic States of $(CCl_4)^+$

M	Ionisation Energy of M (eV)		Appearance Potentials of M ⁺ (eV)	
	Vertical	Adiabatic	Calculated	Observed
CCl ₄	11.32 \tilde{X} (² T ₂)	9.74 (C _{2v})	9.74	b
	11.51 \tilde{A} (² T ₁)	10.70 (C _{3v})	10.70	
		10.80 (D ₂)	10.80	
		10.15 (T _d)	11.15	
		11.23 (D _{2d})	11.23	
		11.99 (D _{2h})	11.99	
	13.56 \tilde{B} (² E)	11.99 (D _{2h})	11.99	
	12.17 (D _{4h})	12.17		
CCl ₃	c	8.69 (D _{3h})	11.08	11.67
		9.69 (C _s , ³ A'')		
		10.24 (C _s , ¹ A'')		
(CCl ₃) ⁺	17.65	16.30	27.38	d
CCl ₂ (¹ A ₁)	9.29	8.65		
CCl ₂ (³ B ₁)	c	8.24	11.51	15.4
(CCl ₂) ⁺	c	15.71	27.21	d
CCl	c	8.21	14.85	19.35
Cl ₂	10.82	10.69	13.55	11.48

a H.M. Rosenstock, K. Draxl, B.W. Steiner, and J. Herron, "Energetics of Gaseous Ions", NBS, Washington (1977).

b (CCl₄)⁺ not observed.

c MINDO seriously underestimates the vertical ionisation energies of paramagnetic species.

d Not recorded.

Table 8.3 Ionisation Energies and Appearance Potentials

D(CCl ₃ -Cl)	231.2
D(CCl ₂ -Cl)	283.7
D(CCl-Cl)	464.4
D(CCl ₃ ⁺ -Cl)	129.2
D(CCl ₂ ⁺ -Cl)	280.0
D(CCl ⁺ -Cl)	322.6
D(CCl ₃ -Cl ⁺)	547.0
D(CCl ₂ -Cl ⁺)	701.5
D(CCl-Cl ⁺)	775.9

Table 8.4 Bond Dissociation Energies (kJ mol⁻¹)

References

- [1] R.B. Bernstein, G.P. Semeluk and C.B. Arends, *Anal. Chem.* 25 (1959), 139
- [2] J.M. Tedder and P.H. VIDAUD, *J. Chem. Soc. Faraday Trans. 2*, 75 (1979), 1648
- [3] A.W. Potts, H.J. Lempka, D.G. Streets and W.C. Price, *Phil. Trans. R. Soc. London, Ser. A*, 268 (1976), 59
- [4] J.C. Green, M.L.H. Green, P.J. Joachim, A.F. Orchard and D.W. Turner, *Phil. Trans. R. Soc. London, Ser. A*, 268 (1970), 111
- [5] S. Katsumata and K. Kimura, *Bull. Chem. Soc. Japan*, 46 (1973), 1342
- [6] A.S. Werner, B.P. Tsai and T. Baer, *J. Chem. Phys.*, 60 (1974), 3650
- [7] J.J. Kaufman, E. Kerman and W.S. Koski, *Int. J. Quantum Chem., Symp.*, 4 (1971), 391
- [8] R.N. Dixon, J.N. Murrell and B. Narayan, *Mol. Phys.*, 20 (1971), 611
- [9] E. Steinmetz and H. Roth, *J. Less-Common Met.*, 16 (1968), 295
- [10] G. Herzberg and J.W.C. Johns, *Proc. R. Soc. London, Ser. A*, 295 (1966), 107

[11] G. Herzberg and J.W.C. Johns, J. Chem. Phys., 54 (1971),

2276

CHAPTER 9

MASS SPECTRAL FRAGMENTATION OF BORON HALIDES

The boron halides BCl_3 , B_2Cl_4 and B_4Cl_4 have been previously studied by mass spectrometry [1,3,4]. MNDO has been used here for a theoretical study of the boron halides, the singly and doubly charged ions present in their mass spectra, and the corresponding neutral fragments.

Calculations were performed using the version of MNDO described in chapters 2 and 3. Full optimisation was carried out with respect to all geometrical parameters.

Introduction

The photoionisation mass spectrum of boron trichloride, at 21.23 eV, contains the ions: $(\text{BCl}_3)^+$, RI=59%; $(\text{BCl}_2)^+$, RI=100%; BCl^+ , RI=7.2%; and B^+ , RI=0.1% [1,2]. Electron impact mass spectrometry showed the same unipositive ions with relative intensities 36, 100, 7.6 and 2.9% and the doubly charged ions: $(\text{BCl}_3)^{2+}$, RI=1.1%; and $(\text{BCl}_2)^{2+}$, RI=3.7% [3]. The ion BCl^{2+} was not observed, unlike the presence of the corresponding BX^{2+} ions in the mass spectra of BBr_3 and BI_3 .

Photoionisation mass spectrometry of diboron tetrachloride, also at 21.23 eV, gave the ions: $(\text{B}_2\text{Cl}_4)^+$, RI=34%; $(\text{B}_2\text{Cl}_3)^+$, RI=

57%; $(B_2Cl_2)^+$, RI=14%; $(BCl_2)^+$, RI=100%; BCl^+ , RI=5.4%; and the rearrangement ion $(BCl_3)^+$ in low abundance [1].

Both of the above boron halides have mass spectra where $(BCl_2)^+$ is the most intense peak, and the molecular ion is of modest intensity, typical of open-chain compounds which can give rise to stable fragments.

In contrast the electron impact mass spectrum of tetraboron tetrachloride [4], whose structure is based on a B_4 tetrahedron [5], has the molecular ion as the most intense peak and other ions: $(B_4Cl_3)^+$, RI=91%; $(B_3Cl_3)^+$, RI=82%; $(B_3Cl_2)^+$, RI=32%; $(B_2Cl_2)^+$, RI=46%; $(B_2Cl)^+$, RI=10%; and BCl^+ , RI=16%. The ions $(B_4Cl_2)^+$ and $(B_3Cl)^+$, and the doubly charged ion $(B_4Cl_3)^{2+}$ are also present in low abundance [6].

MOLECULAR STRUCTURES

M and M^+

BCl_3 optimised to a D_{3h} structure as found experimentally [11], with bond lengths within 1% of the experimental value. Ionisation to BCl_3^+ gives a relaxation to planar C_{2v} geometry, in which two of the chlorine atoms close to 2.465Å, a possible indication of incipient fragmentation.

B_2Cl_4 when freely optimised gave a structure of exact D_{2d}

symmetry, with BCl bond lengths somewhat longer than the BB bond length, as was found experimentally. Constraint to D_{2h} symmetry gave an increase in ΔH_f^\ominus from $-488.4 \text{ kJ mol}^{-1}$ to $-462.2 \text{ kJ mol}^{-1}$, the BB distance increased from 1.646\AA to 1.682\AA , the BCl distance was unchanged, and the BBCl angle increased slightly from 120.6° to 121.3° . The calculated barrier of 22.2 kJ mol^{-1} is rather higher than the 7.8 kJ mol^{-1} found experimentally [13], but is nevertheless small. The structural difference between the D_{2d} symmetry of the fluid phase and the D_{2h} symmetry of the crystalline state may be partly attributed to the small rotational barrier [14]. On ionisation to $B_2Cl_4^+$ the symmetry remained unchanged, but the BB distance increased to 1.805\AA , and the BCl distance decreased to 1.707\AA . The rotational barrier was found to be 43.2 kJ mol^{-1} , almost twice that of the neutral parent. Constrained to D_{2h} symmetry, the BB distance increased to 1.918\AA , the BCl distance showed a marginal increase to 1.709\AA , and the BBCl angle increased slightly from 112.4° to 114.3° .

B_4Cl_4 optimised to a structure of exact T_d symmetry in which the BB distance is very slightly shorter than the BCl distance; experimentally [5] these distances have been found to be essentially identical. Ionisation caused a lowering of symmetry to exactly D_{2d} , in which the B_4 cage took the form of a flattened tetrahedron with four short and two long BB distances. A slight reduction in BCl distance was found to occur, similar to that for the ionisation of B_2Cl_4 . The calculated structures of B_4Cl_4 and $B_4Cl_4^+$ are depicted in figure 9.1.

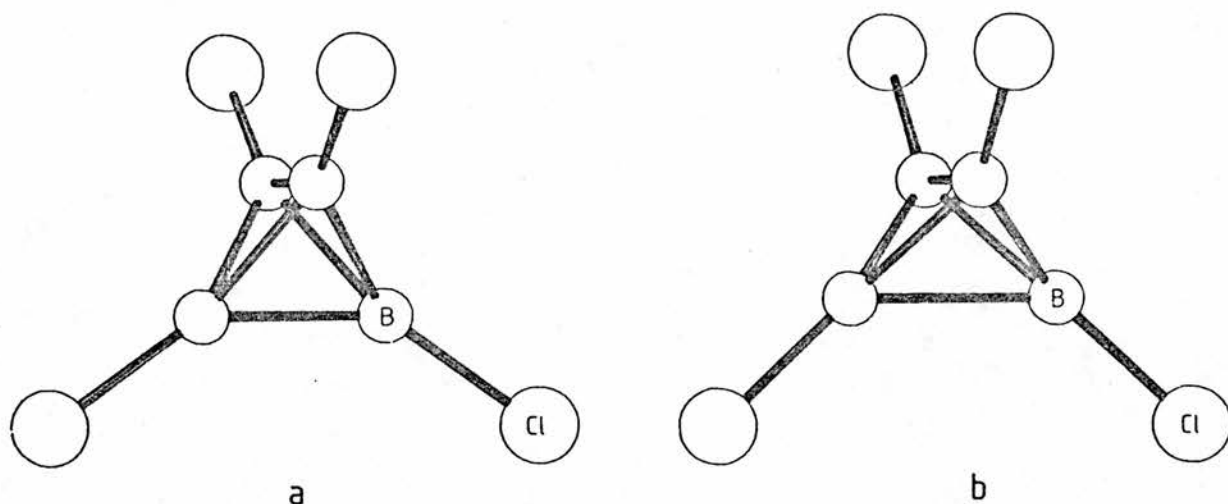


Figure 9.1 The structures of (a) B_4Cl_4 and (b) $B_4Cl_4^+$

Fragment Ions

The triatomic fragment ions B_2Cl^+ and BCl_2^+ have 12 and 16 valence electrons respectively, and were found to be linear as expected [15].

Loss of two chlorine atoms or a chlorine molecule from $B_2Cl_4^+$ could arise in two ways: loss of one chlorine from each boron will yield the ion $ClBBCl^+$, and loss of both chlorine atoms will give a Cl_2BB^+ ion. Optimisations of both possible isomers were performed; the $ClBBCl^+$ gave a structure of exact C_{2h} symmetry, while the ion Cl_2BB^+ gave a planar structure of C_{2v} symmetry, some 90 kJ mol^{-1} less stable.

The loss of a single chlorine atom from $B_2Cl_4^+$ gave the ion

Cl_2BBCl^+ with C_{2v} symmetry and a linear BBCl fragment. A chlorine-bridged cation was also found which is ca. 50 kJ mol^{-1} less stable. The calculations showed this ion to have a quasi-aromatic B_2Cl ring system of π orbitals normal to the plane of the ion, occupied by two π electrons.

The most abundant fragment ion derived from B_4Cl_4^+ is formed by the loss of a single chlorine atom to give B_4Cl_3^+ . This ion was found to have exact C_{3v} symmetry with a trigonal pyramidal B_4 cage, much shallower than the tetrahedral cage of B_4Cl_4 . Its doubly charged analogue $\text{B}_4\text{Cl}_3^{2+}$ was found to have such a shallow B_4 pyramid that it attained exact D_{3h} symmetry, and this ion is shown in figure 9.2.

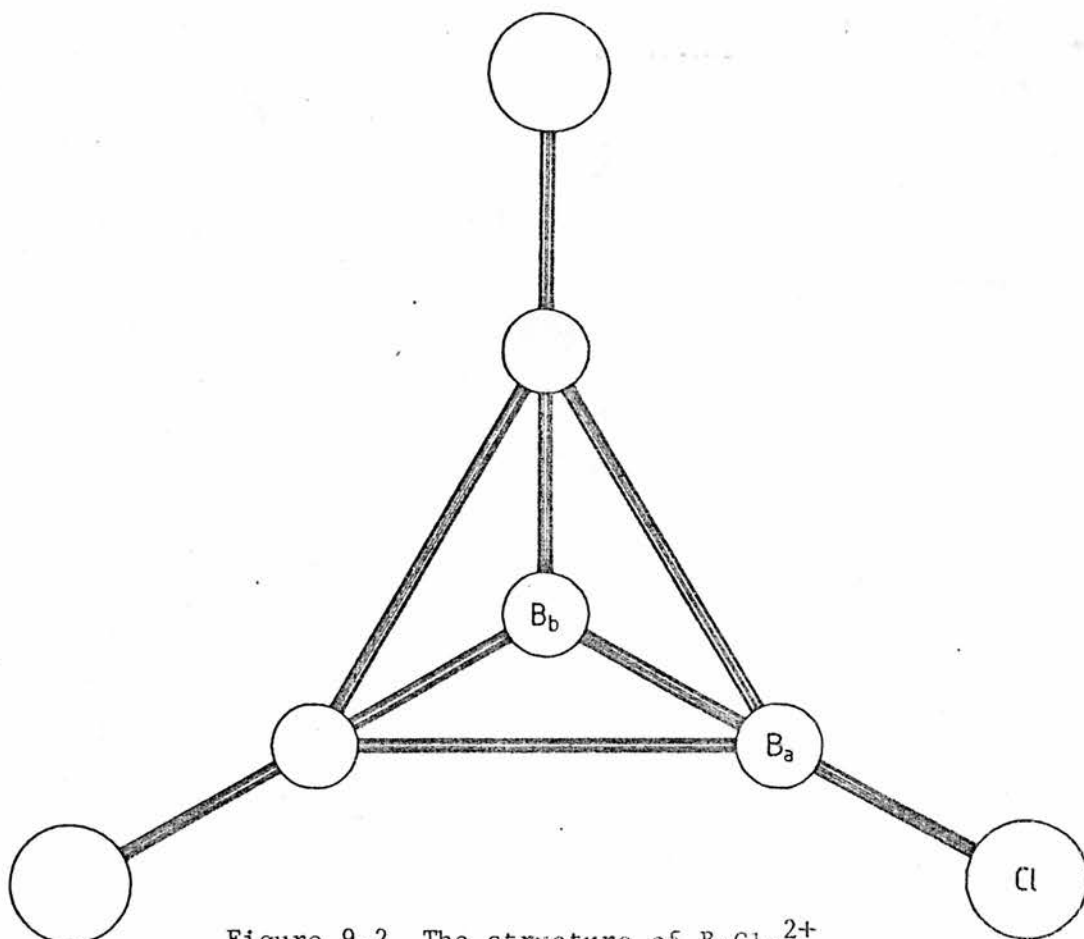


Figure 9.2 The structure of $\text{B}_4\text{Cl}_3^{2+}$

Optimisations for the ion $B_2Cl_2^+$ were performed from three distinct starting configurations. Starting the optimisation from a tetrahedral B_4 cage gave a structure of only C_2 symmetry, which may be regarded as the initial flattening of the cage along one of the C_2 axes, followed by a twisting in which the two pairs of boron atoms mutually related by the C_2 axis are rotated about that axis in opposite senses. The structure of this ion is depicted in figure 9.3a. Optimisations were also performed with a square planar B_4 framework and the two chlorines either trans or cis to each other. These converged to structures of D_{2h} and C_{2v} symmetry respectively, as shown in figures 9.3b and 9.3c.

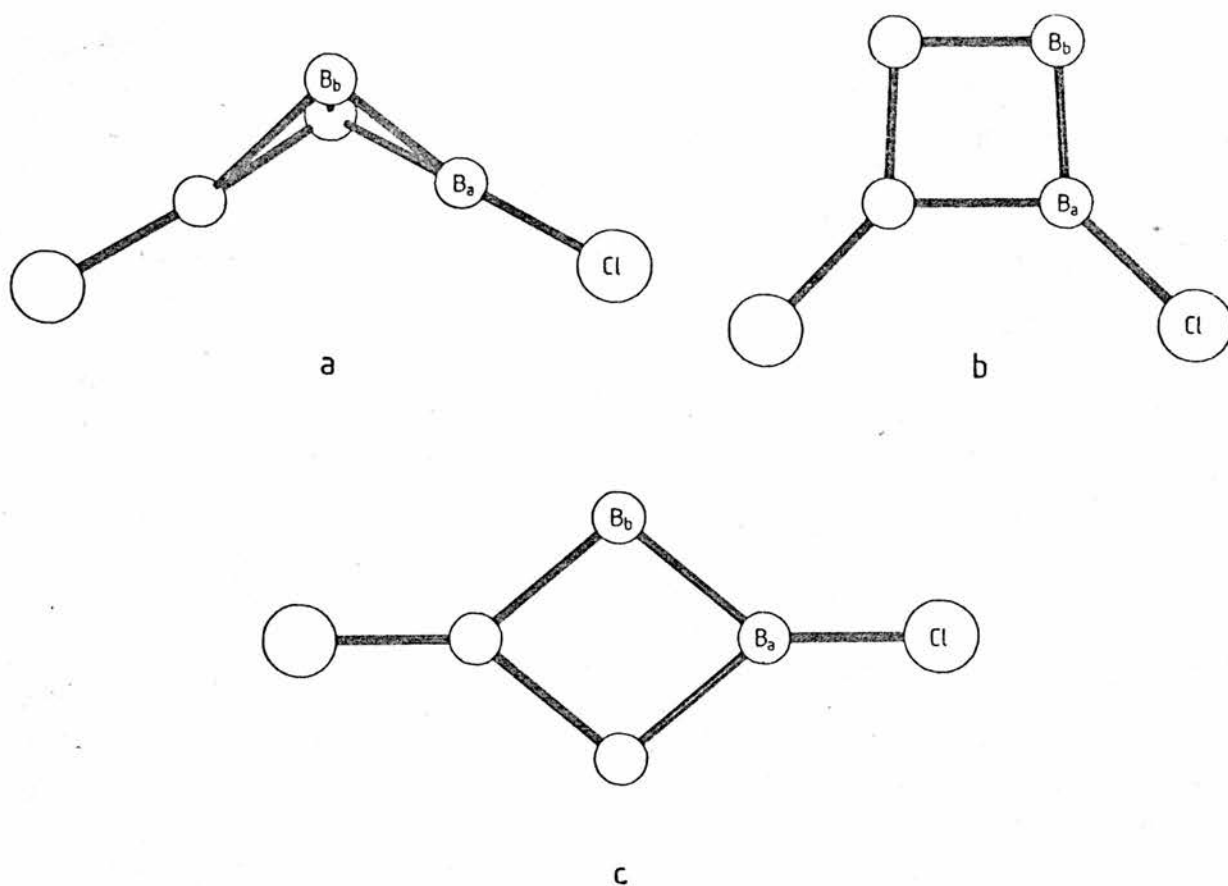


Figure 9.3 The structures of the isomeric $B_4Cl_2^+$ ions.

(a) C_2

(b) C_{2v}

(c) D_{2h}

The ion $B_3Cl_3^+$ optimised to yield only C_{2v} symmetry, based on a flattened isosceles triangle of boron atoms, as shown in figure 9.4a. $B_3Cl_2^+$ gave a similar C_{2v} symmetry, with a slightly less flattened B_3 group as shown in figure 9.4b. B_3Cl^+ was also found to have C_{2v} symmetry, based on a slightly elongated B_3 triangle. An optimisation was also performed starting from a C_{3v} cage configuration with approximately tetrahedral symmetry. This optimisation yielded a planar configuration of exact D_{3h} symmetry with the chlorine atom coordinated by the three boron atoms: this unexpected arrangement has ΔH_f^\ominus some 260 kJ mol^{-1} above the C_{2v} isomer, and has a BCl distance of 1.969 \AA , 0.2 \AA longer than any other molecule or ion studied in this work.

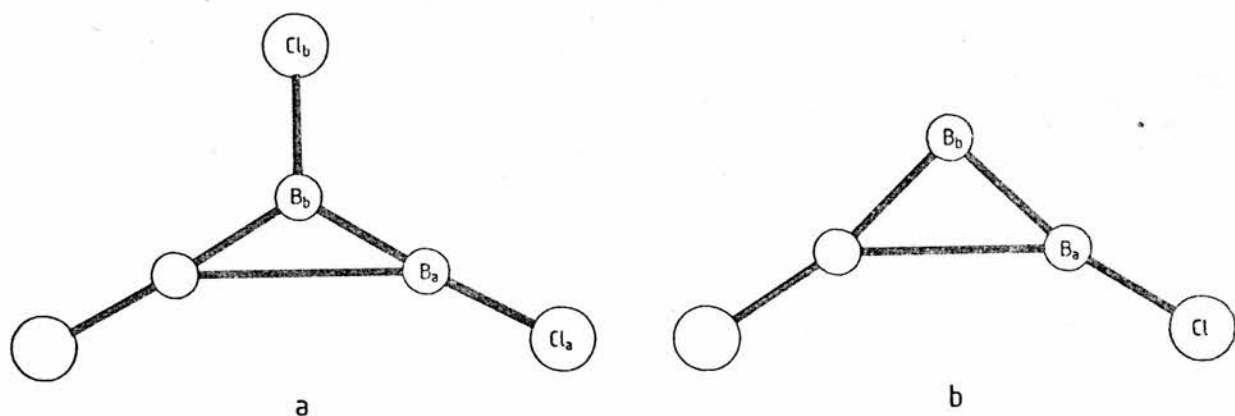


Figure 9.4 The structures of (a) $B_3Cl_3^+$ and (b) $B_3Cl_2^+$

Neutral Fragments

B_3Cl_3 was found to have the maximum possible symmetry, D_{3h} . B_2Cl_2 was found to have only C_{2h} symmetry, with the same minimum being found for a variety of starting geometries. As for $B_2Cl_3^+$,

B_2Cl_3 was found to have two distinct minima with the unbridged isomer having lower energy. The bridged neutral isomer, unlike Cl_2BBCl^+ , has only C_s symmetry. Of the three states of BCl investigated, $^1\Sigma^+$ was the lowest in energy, followed by $^3\Pi$ and then $^1\Pi$, as expected.

Rearranged Fragments

Because of the observation [1] of the rearrangement ion BCl_3 in the spectrum of B_2Cl_4 , neutral and cationic Cl_3BBCl species were investigated. The neutral species, which has been suggested as an intermediate in the preparation of B_2Cl_4 from BCl_3 [16], optimised to exact C_{3v} symmetry as shown in figure 9.5a. It had an energy below that of $BCl_3 + BCl$ and above B_2Cl_4 , indicating that it is a plausible intermediate in the formation of B_2Cl_4 . Optimisation of the cation, starting at the C_{3v} geometry of the neutral species, yielded a dibridged cation, which is completely planar, but of C_{2v} rather than D_{2h} symmetry, as shown in figure 9.5b. Attempts to optimise the geometry, starting at a D_{2h} symmetry using the mean values of the geometrical variables derived from the C_{2v} geometry, reverted back to exactly the same energy minimum and C_{2v} geometry. This ion cannot be regarded as a loose complex as its H_f value is substantially lower ($597.2 \text{ kJ mol}^{-1}$) than those of the pairs BCl_3^+/BCl ($844.2 \text{ kJ mol}^{-1}$) and BCl_3/BCl^+ ($783.8 \text{ kJ mol}^{-1}$). It was also noted that the charge distribution indicates complete delocalisation of the +1 charge, as no atom carries a local charge greater than +0.2. The geometry

obtained for the bridged cation was also used in an attempt to optimise a similar neutral structure. However this was found to dissociate into $\text{BCl}_3 + \text{BCl}$, in spite of the energy of the C_{3v} species Cl_3BBCl being more stable than $\text{Cl}_3\text{B} + \text{BCl}$ by ca. 34 kJ mol^{-1} . It is apparent that the complete potential surfaces of B_2Cl_4 and B_2Cl_4^+ are extremely complex.

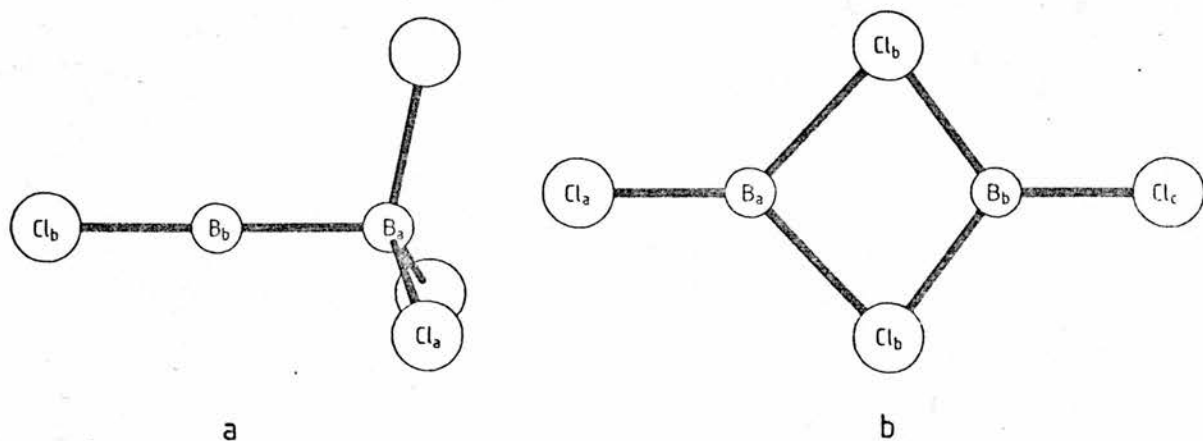


Figure 9.5 The structures of (a) Cl_3BBCl and (b) $\text{ClBCl}_2\text{BCl}^+$

ELECTRONIC STRUCTURES

Several studies have been made of the electronic structure of BCl_3 by photoelectron spectroscopy. These differ slightly in their assignments, particularly of the first band. Bassett and Lloyd [17] assign the lowest state of BCl_3^+ as A_2' as calculated in this work, but Boyd and Frost [18] assign the same state as E' . In general the symmetries calculated here are in good agreement with the assignments of Bassett and Lloyd as shown in table 9.2, although all the calculated levels are deeper than the experimental values. The assignments of the photoelectron bands

in B_4Cl_4 [19] are also virtually identical with the order calculated in this work, but again the calculated levels are rather too deep as is also shown in table 9.2. B_4Cl_4 has also been the subject of an extensive ab initio study [20].

Jahn-Teller Effect

The table 9.1 contains a number of pairs, consisting of a diamagnetic fragment, either neutral or cationic, and the corresponding fragment, uni- or di-positive, containing one fewer electron. These pairs may be considered with respect to the first-order Jahn-Teller effect. Table 9.3 lists, for the diamagnetic fragments M, their point groups, the symmetry of their HOMOs, the distortions which are possible on ionisation, and the observed point groups of the ions M^+ . For $M = B_4Cl_4$, B_3Cl_3 , B_2Cl_4 , B_2Cl_2 , and BCl_2^+ the predictions of the Jahn-Teller theorem are fulfilled without ambiguity. The ionisation of $B_4Cl_3^+$ to $B_4Cl_3^{2+}$ shows a change of point group where none is predicted, but the change from C_{3v} to D_{3h} is to a supergroup of C_{3v} , and, no element of symmetry being lost, the change to the point group D_{3h} is permissible.

The sole exception to the predictions of the Jahn-Teller theorem in table 9.3 is the ionisation of BCl_3 . This molecule has as its HOMO a molecular orbital of A'_2 symmetry, localised entirely on the chlorine atoms in the molecular plane. Vertical ionisation from this orbital will lead to a non-degenerate cation

which is not expected to distort on relaxing to its adiabatic energy minimum. However, the optimised geometry of BCl_3^+ has only C_{2v} symmetry, and corresponds to a distortion along one of the E' in-plane coordinates in which bending and stretching are coupled together. At equilibrium BCl_3 is calculated and observed [17] to have a doubly degenerate level, either E' as calculated here, or E'' [17], very close below A'_2 . The alternative assignment [18] reverses the order of E' and A'_2 . At the equilibrium configuration the energy gap between A'_2 and E' is only 0.155 eV. Although this varies somewhat with the boron to chlorine distance, the gap decreasing as the bond length increases, for all vibrationally plausible changes in distance the energy order is unchanged. Nevertheless the relaxation of BCl_3^+ is along an E' vibration just as if ionisation had occurred from the E' level rather than from A'_2 . Vertical ionisation, as judged from the eigenvectors for BCl_3^+ constrained to the optimised geometry of BCl_3 , was always found to occur from A'_2 , this being unaltered by small variations in the bond length. The reason for this anomalous behaviour is not clear.

In B_3Cl_3 the HOMO has E' symmetry, being located in the molecular plane, and is primarily a boron-chlorine interaction n to the B-Cl bond, and tangential to the B_3 ring. On ionisation there are two possible modes consistent with the Jahn-Teller requirements. The A'_2 mode is effectively a contra-rotation of the B_3 and Cl_3 triangles, which reduces the symmetry from D_{3h} to C_{3h} but does not remove the electronic degeneracy. Only the E' modes can remove the electronic degeneracy, and it is one of these

modes which is the coordinate which transforms B_3Cl_3 to $B_3Cl_3^+$.

B_2Cl_2 optimised to a non-linear geometry of C_{2h} symmetry, with four of the five highest occupied molecular orbitals clustered between 13.2 and 13.9 eV and primarily localised on the chlorine atoms. The HOMO, at 9.92 eV, is of B_u symmetry and is localised primarily on the two boron atoms in the plane of the molecule.

MASS SPECTRAL FRAGMENTATION

Molecular Energies

Figure 9.6 shows an energy diagram constructed from the data contained in tables 9.1 and 9.2. From this diagram it may be seen that in the mass spectrum of BCl_3 , both BCl_3^+ and BCl_2^+ can arise after excitation to the \tilde{X} state of the molecular ion. BCl^+ could arise from the \tilde{D} state of the molecular ion if concerted loss of the two chlorine atoms was involved, but the appearance potentials described below indicate that sequential loss of the chlorine atoms is involved, which requires excitation to the \tilde{E} state of the molecular ion. The formation of the doubly charged ions BCl^{2+} and BCl_2^{2+} cannot arise from the ionisation of a valence electron of BCl_3 as the deepest valence level corresponds to a state of BCl_3^+ with $\Delta H_f^\ominus = 2332 \text{ kJ mol}^{-1}$, whereas the ΔH_f^\ominus values for the fragment pairs $(BCl_2^{2+} + Cl)$ and $(BCl^{2+} + 2Cl)$ are $2794.9 \text{ kJ mol}^{-1}$ and $3334.6 \text{ kJ mol}^{-1}$ respectively. Consequently

ionisation of one of the deep levels, B (1s) or Cl (1s, 2s or 2p) must occur. Complete disruption with simultaneous ionisation to yield $(B^+ + 3Cl)$ requires an input of only 2100 kJ mol^{-1} and may be readily achieved.

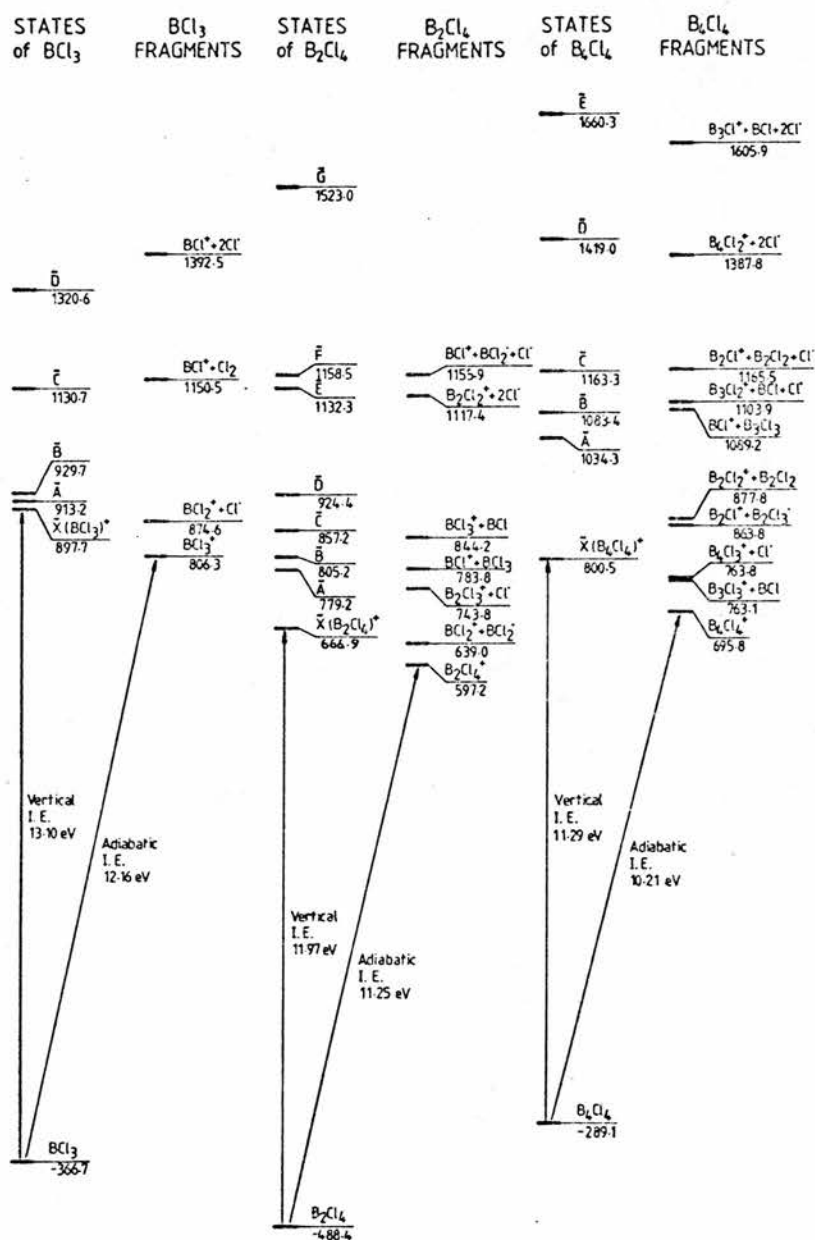


Figure 9.6 Energies of the states of BCl_3 , B_2Cl_4 and B_4Cl_4 and of their mass spectral fragments

In the mass spectrum of B_2Cl_4 , both $B_2Cl_4^+$ and BCl_2^+ can arise by excitation to the \tilde{X} state of the molecular ion. BCl_2^+ is the most abundant ion in the spectra of both BCl_3 and B_2Cl_4 , being formed from the \tilde{X} state of each molecular ion with only a small change in energy. Formation of $B_2Cl_3^+$, BCl^+ and BCl_3^+ require excitation to the \tilde{A} , \tilde{B} and \tilde{C} states respectively. Similarly $B_2Cl_2^+$ and BCl^+ require excitation to the \tilde{E} and \tilde{F} states respectively. Formation of BCl^+ from the \tilde{B} or \tilde{F} states involves the neutral fragments BCl_3 and $(BCl_2 + Cl)$ respectively, and it might be considered, by comparison with the formation of BCl^+ from BCl_3 , that the latter may be the process involved. However, the appearance potential of the BCl^+ ion formed from B_2Cl_4 as shown below indicates that the fragmentation involving the loss of the BCl_3 fragment is the process involved.

The ions $B_4Cl_4^+$, $B_4Cl_3^+$ and $B_3Cl_3^+$ can all be attained by excitation to the \tilde{X} state of $B_4Cl_4^+$, these being the most abundant ions in the mass spectrum of $B_4Cl_4^+$. Both B_2Cl^+ and $B_2Cl_2^+$ can be reached from the \tilde{X} state of $B_4Cl_4^+$, while excitation to \tilde{C} is necessary for the formation of BCl^+ , B_2Cl^+ and $B_3Cl_2^+$. The low abundance ions $B_4Cl_2^+$ and B_3Cl^+ require excitation to the \tilde{D} and \tilde{E} states of the molecular ion, and the doubly charged ion $B_4Cl_3^{2+}$ requires excitation to the \tilde{F} state.

Appearance Potentials

The energies of the ions and their conjugate neutral fragments have been used to calculate the appearance potentials for those ions which have been experimentally determined and these values are given in table 9.4.

As was noted above the comparison of the calculated and experimental appearance potentials may be used to distinguish which of the possible fragmentation routes is followed for the production of BCl^+ from BCl_3^+ and B_2Cl_4^+ . The formation of BCl^+ from B_2Cl_4^+ with loss of the BCl_3 neutral fragment, rather than the loss of a chlorine atom from BCl_2^+ with the BCl_2 neutral fragment, and the formation of the fragment pair ($\text{BCl}_3^+ + \text{BCl}$), suggests a common intermediate in the two fragmentation processes. This is a further indication of the earlier observation that the potential surface of B_2Cl_4^+ is complex.

For the formation of B_2Cl_2^+ from B_2Cl_4 , the experimental appearance potential, when compared with the calculated values, suggests stepwise loss of chlorine atoms rather than loss of molecular chlorine. Although the C_{2h} isomer is some 90 kJ mol^{-1} more stable than the C_{2v} isomer the appearance potential, which are generally calculated somewhat high, suggests that the C_{2v} isomer is the one formed.

The stepwise loss of atomic chlorine may be extended to the fragmentation of B_4Cl_4^+ , yielding B_4Cl_3^+ and then B_4Cl_2^+ . Loss of

BCl from the latter ion could then give B_3Cl^+ . The loss of BCl from the parent ion yields $B_3Cl_3^+$, which may then undergo stepwise loss of chlorine to give $B_3Cl_2^+$ and B_3Cl^+ . Of the two routes to B_3Cl^+ the latter seems the more plausible. The molecular ion is a very flattened tetrahedron in its ground state as shown in figure 9.1, although excited states may be different; either a flattened or elongated tetrahedron allow cleavage of B_4 into $2B_2$ more readily than cleavage of a regular tetrahedron, and this allows the formation of $B_2Cl_2^+ + B_2Cl_2$.

Bond Dissociation Energies and Bond Energy Terms

The individual bond energies for stepwise loss of chlorine atoms from neutral BCl_3 are calculated to be 373.1, 273.5 and 654.2 kJ mol^{-1} , giving a mean value $D(\text{B-Cl})$ in BCl_3 of 433.6 kJ mol^{-1} , close to the experimental value of 443.9 kJ mol^{-1} . The very large value for the dissociation of BCl is explained by the high bond order of BCl, and the fact that BCl is formally isoelectronic with species such as N_2 and CO. Transfer of the mean value from BCl_3 to B_2Cl_4 yields a bond energy term $E(\text{B-B})$ in B_2Cl_4 of 380.2 kJ mol^{-1} , whereas the dissociation energy $D(\text{Cl}_2\text{B-BCl}_2)$ is only 259.2 kJ mol^{-1} . Alternatively if $D(\text{Cl}_2\text{B-BCl}_2)$ is transferred as the $E'(\text{B-B})$ in B_2Cl_4 , then the bond energy term $E(\text{B-Cl})$ in B_2Cl_4 becomes 463.8 kJ mol^{-1} , equal to the mean of the second and third dissociation energies in BCl_3 .

These wide variations in bond energy terms show the

difficulty in assessing the cohesive energy of the B_4 cage in B_4Cl_4 . Excluding the very high bond energy in BCl which does not refer to a "single" bond, the range of available $E(B-Cl)$ values is from 273.5 to 463.8 kJ mol^{-1} , implying a range of $E(B-B)$ values for B_4Cl_4 of 327 kJ mol^{-1} down to 200 kJ mol^{-1} .

Apart from bond energy terms simple dissociation energies have been calculated and are given in table 9.5. It can be seen from this table that dissociations of ions which form Cl^+ are strongly disfavoured. In general bond dissociation energies were found to be smaller in ionic species than in the corresponding neutral species, except where BCl is formed, distorting the overall pattern with its high dissociation energy. Exceptions to the overall pattern are exhibited by the doubly charged ions BCl_2^{2+} and BCl^{2+} which are unstable with respect to $(BCl^+ + Cl^+)$ and $(B^+ + Cl^+)$ respectively.

Symmetry Constraints on Fragmentation

The energetic constraints on the formation of fragment ions are such that the excitation of the parent ion must be to a state of higher energy than the combined energies of the fragment ion and the corresponding neutral species, as described previously and shown in figure 9.6. For particular transition state point groups there are also symmetry constraints on the formation of fragment ions as is shown in table 9.6.

The highest symmetry possible for the transition state in

the fragmentation of BCl_3^+ is C_{2v} . In C_{2v} symmetry the pair $(\text{BCl}_2^+ + \text{Cl}^\bullet)$ is accessible from all the states of BCl_3^+ , but the pair $(\text{BCl}^+ + \text{Cl}_2)$ is accessible only from $\tilde{\text{A}}, \tilde{\text{D}}, \tilde{\text{E}}, \tilde{\text{F}}$ and $\tilde{\text{G}}$, of which $\tilde{\text{A}}$ is ruled out on energetic grounds. The only states which can relax to the adiabatic ground state of BCl_3^+ are $\tilde{\text{X}}, \tilde{\text{A}}, \tilde{\text{D}}, \tilde{\text{F}}$ and $\tilde{\text{G}}$.

Fragmentation of B_2Cl_4^+ could be envisaged as occurring via a transition state of C_{2v} symmetry when forming both $(\text{BCl}_2^+ + \text{BCl}_2^\bullet)$ and $(\text{Cl}_2\text{BB}^+ + \text{Cl}_2)$. The $\tilde{\text{A}}, \tilde{\text{B}}, \tilde{\text{D}}, \tilde{\text{F}}$ and $\tilde{\text{I}}$ states are forbidden precursors in this point group. The highest alternative symmetry for these fragmentations is C_2 or C_s both of which permit, on symmetry grounds, the formation of these fragment pairs from all states of B_2Cl_4^+ . In the remaining fragmentations of B_2Cl_4^+ the highest possible symmetry is C_s , which imposes no symmetry constraints on the fragmentation processes.

The pair $(\text{B}_4\text{Cl}_3^+ + \text{Cl}^\bullet)$ is accessible from all the states of B_4Cl_4^+ via a transition state of C_{3v} symmetry, but the pair $(\text{BCl}^+ + \text{B}_3\text{Cl}_3)$ is accessible in the same symmetry only from the $\tilde{\text{X}}, \tilde{\text{C}}, \tilde{\text{D}}, \tilde{\text{E}}, \tilde{\text{F}}, \tilde{\text{G}}$ and $\tilde{\text{H}}$ states. The highest possible symmetry of the transition state giving rise to the fragment pair $(\text{BCl}_2^+ + \text{B}_2\text{Cl}_2)$ is D_2 , which is permitted by symmetry from the $\tilde{\text{X}}, \tilde{\text{A}}, \tilde{\text{C}}, \tilde{\text{E}}$ and $\tilde{\text{G}}$ states. The fragment pair $(\text{B}_3\text{Cl}_3^+ + \text{BCl})$ is accessible from a transition state of C_s symmetry which imposes no symmetry constraints.

	Point Group	Molecular State	$\Delta H_f^\ominus / \text{kJ mol}^{-1}$	
(i) M and M ⁺				
BCl ₃	D _{3h}	1A ₁ '	-366.7	(-402.9) ^a
BCl ₃ ⁺	C _{2v}	2B ₂	+806.3	(+718) ^b
B ₂ Cl ₄	D _{2d}	1A ₁	-488.4	(-488.7) ^c
B ₂ Cl ₄ ⁺	D _{2d}	2A ₁	+597.1	(+506.0) ^b
B ₄ Cl ₄	T _d	1A ₁	-289.1	
B ₄ Cl ₄ ⁺	D _{2d}	2B ₂	+695.8	
(ii) Fragment Ions				
BCl ⁺	C _{∞v}	2Σ ⁺	+1150.5	(+1130) ^b
BCl ₂ ⁺	D _{∞h}	1Σ _g ⁺	+753.6	(+664) ^b
B ₂ Cl ⁺	C _{∞h}	1Σ ⁺	+1042.2	
B ₂ Cl ₂ ⁺	$\left\{ \begin{array}{l} C_{2h} \\ C_{2v} \end{array} \right.$	2B _u	+875.4	(934) ^b
		2A ₁	+965.6	
B ₂ Cl ₃ ⁺	$\left\{ \begin{array}{l} \text{bridged } C_{2v} \\ \text{unbridged } C_{2v} \end{array} \right.$	1A ₁	+674.2	(502) ^b
		1A ₁	+622.8	
B ₃ Cl ⁺	$\left\{ \begin{array}{l} D_{3h} \\ C_{2v} \end{array} \right.$	2A ₁ '	+1588.2	
		2B ₁	+1326.0	
B ₃ Cl ₂ ⁺	C _{2v}	1A ₁	+945.0	
B ₃ Cl ₃ ⁺	C _{2v}	2A ₁	+725.2	
B ₄ Cl ₂ ⁺	$\left\{ \begin{array}{l} C_2 \\ C_{2v} \\ D_{2h} \end{array} \right.$	2A	+1145.8	
		2B ₁	+1235.7	
		2B _{2g}	+1186.9	
B ₄ Cl ₃ ⁺	C _{3v}	1A ₁	+642.8	

(iii) Doubly Charged Ions

BCl^{2+}	$C_{\infty v}$	$1\Sigma^+$	+3092.6
BCl_2^{2+}	$D_{\infty h}$	$2\Pi_g$	+2673.9
BCl_3^{2+}	Dissociates to BCl^+ and Cl_2^+		
$\text{B}_4\text{Cl}_3^{2+}$	D_{3h}	$2A_2''$	+1976.9

(iv) Neutral Fragments

BCl	$C_{\infty v}$	$\left\{ \begin{array}{l} 1\Sigma^+ \\ 1\Pi \\ 3\Pi \end{array} \right.$	+37.9 ^c
			+669.1
			+493.1 ^d
BCl_2	C_{2v}	$2A_1$	-114.6
B_2Cl_3	$\left\{ \begin{array}{l} \text{bridged } C_{2v} \\ \text{unbridged } C_s \end{array} \right.$	$2B_2$	-154.3
		$2A'$	-178.6
B_3Cl_3	D_{3h}	$1A_1'$	-61.3

(v) Rearrangement Fragments

Cl_3BBCl	C_{3v}	$1A_1$	-362.6
$\text{ClBCl}_2\text{BCl}^+$	C_{2v}	$2A_1$	+597.2

a Ref. 7

b Ref. 1

c Ref. 8

d Experimental values range from +141.4 kJ mol⁻¹ [Ref. 9] to +261.9 kJ mol⁻¹ [Ref. 10]

Table 9.1 Point Groups and Molecular Energies

-I /eV	Symmetry	Other Assignments	
(a) BCl_3^a			
-13.105	$\tilde{X} A'_2$	A'_2	E'
-13.265	$\tilde{A} E'$	E''	A'_2
-13.437	$\tilde{B} E''$	E'	E''
-15.520	$\tilde{C} A''_2$	A''_2	A''_2
-17.488	$\tilde{D} E'$	$E' \left. \vphantom{\begin{matrix} E' \\ E' \end{matrix}} \right\}$	E'
-22.493	$\tilde{E} A'_1$		
-26.502	$\tilde{F} E'$	A'_1	A'_1
-27.972	$\tilde{G} A'_1$		
(b) B_2Cl_4			
-11.90	$\tilde{X} A_1$		
-13.138	$\tilde{A} E$		
-13.407	$\tilde{B} E$		
-13.947	$\tilde{C} B_2$		
-14.643	$\tilde{D} E$		
-16.797	$\tilde{E} A_1$		
-17.069	$\tilde{F} E$		
-20.847	$\tilde{G} B_2$		
-23.957	$\tilde{H} A_1$		
-26.414	$\tilde{I} E$		
-27.112	$\tilde{J} B_2$		
-28.296	$\tilde{K} A_1$		

(c) B_4Cl_4 ^b

-11.293	$\tilde{X} T_2$	T_2	T_2
-13.716	$\tilde{A} T_1$	T_1	T_1
-14.225	$\tilde{B} E$	E	E
-15.053	$\tilde{C} T_2$	T_2	T_2
-17.703	$\tilde{D} A_1$	T_2	A_1
-20.204	$\tilde{E} T_2$	A_1	T_2
-26.314	$\tilde{F} A_1$	A_1	A_1
-26.671	$\tilde{G} T_2$		T_2
-31.924	$\tilde{H} A_1$		A_1

a Other assignments from Ref. 17 (left hand column) and Ref. 18 (right hand column).

b Other assignments from Ref. 19 (left hand column) and Ref. 20 (right hand column).

Table 9.2 Energy Levels in BCl_3 , B_2Cl_2 , and B_4Cl_4

M	Point Group of M	HOMO of M	Possible Distortions in M ⁺	Observed Point Group of M ⁺
B ₄ Cl ₄	T _d	T ₂	$\left\{ \begin{array}{l} E \rightarrow D_{2d} \\ T_1 \rightarrow C_3, S_4, C_s \\ T_2 \rightarrow C_{3v}, C_{2v} \end{array} \right.$	D _{2d}
B ₄ Cl ₃ ⁺	C _{3v}	A ₁	None	D _{3h}
B ₃ Cl ₃	D _{3h}	E'	$\left\{ \begin{array}{l} A'_2 \rightarrow C_{3h} \\ E' \rightarrow C_{2v} \end{array} \right.$	C _{2v}
B ₂ Cl ₄	D _{2d}	A ₁	None	D _{2d}
B ₂ Cl ₂	C _{2h}	B _u	None	C _{2h}
BCl ₃	D _{3h}	A' ₂	None	C _{2v} (see text)
BCl ₂ ⁺	D _{∞h}	Π _g	None	D _{∞h}

Table 9.3 Jahn-Teller Effect

Ion	Source	Other Products	Appearance Potential	
			Calculated /eV	Observed ^a /eV
BCl^+	$\left\{ \begin{array}{l} \text{BCl}_3 \\ \text{B}_2\text{Cl}_4 \end{array} \right.$	$\left\{ \begin{array}{l} 2\text{Cl}\cdot \\ \text{Cl}_2 \end{array} \right.$	18.23	18.37
		$\left\{ \begin{array}{l} \text{BCl}_3 \\ \text{BCl}_2\cdot + \text{Cl}\cdot \end{array} \right.$	15.72	
	$\left\{ \begin{array}{l} \text{BCl}_3 \\ \text{B}_2\text{Cl}_4 \end{array} \right.$	$\left\{ \begin{array}{l} \text{BCl}_3 \\ \text{BCl}_2\cdot + \text{Cl}\cdot \end{array} \right.$	13.18	13.71
		$\left\{ \begin{array}{l} \text{BCl}_3 \\ \text{BCl}_2\cdot + \text{Cl}\cdot \end{array} \right.$	17.14	
BCl_2^+	$\left\{ \begin{array}{l} \text{BCl}_3 \\ \text{B}_2\text{Cl}_4 \end{array} \right.$	$\left\{ \begin{array}{l} \text{Cl}\cdot \\ \text{BCl}_2\cdot \end{array} \right.$	12.86	12.30
		$\left\{ \begin{array}{l} \text{BCl}_3 \\ \text{BCl}_2\cdot \end{array} \right.$	11.68	11.32
BCl_3^+	$\left\{ \begin{array}{l} \text{BCl}_3 \\ \text{B}_2\text{Cl}_4 \end{array} \right.$	$\left\{ \begin{array}{l} - \\ \text{BCl} \end{array} \right.$	12.16	11.60
		$\left\{ \begin{array}{l} \text{BCl}_3 \\ \text{BCl} \end{array} \right.$	13.81	-
B_2Cl_2^+ ($\text{C}_{2\text{h}}$)	B_2Cl_4	$\left\{ \begin{array}{l} 2\text{Cl}\cdot \\ \text{Cl}_2 \end{array} \right.$	16.64	17.24
		$\left\{ \begin{array}{l} 2\text{Cl}\cdot \\ \text{Cl}_2 \end{array} \right.$	14.13	
B_2Cl_2^+ ($\text{C}_{2\text{v}}$)	B_2Cl_4	$2\text{Cl}\cdot$	17.58	17.24
B_2Cl_3^+	B_2Cl_4	$\text{Cl}\cdot$	12.77	11.52
B_2Cl_4^+	B_2Cl_4	-	11.25	10.32
BCl_2^{2+}	BCl_3	$\text{Cl}\cdot$	32.76	33.77 ^b

^a Experimental values from Ref. 1, unless otherwise stated

^b Ref. 21

Table 9.4 Appearance Potentials

$D(\text{Cl}_2\text{B}-\text{Cl})$	373.1	$D(\text{Cl}_2\text{B}-\text{BCl}_2)$	259.2
$D(\text{Cl}_2\text{B}^+-\text{Cl})$	68.3	$D(\text{Cl}_2\text{B}^+-\text{BCl}_2)$	41.9
$D(\text{Cl}_2\text{B}-\text{Cl}^+)$	456.0		
		$D(\text{Cl}_2\text{B}-\text{BCl})$	101.9
$D(\text{ClB}-\text{Cl})$	173.5	$D(\text{Cl}_2\text{B}^+-\text{BCl})$	168.7
$D(\text{ClB}^+-\text{Cl})$	517.9	$D(\text{Cl}_2\text{B}-\text{BCl}^+)$	413.1
$D(\text{ClB}-\text{Cl}^+)$	661.2		
		$D(\text{ClBBCl}-\text{Cl})$	302.0
$D(\text{Cl}_2\text{BBCl}-\text{Cl})$	430.8	$D(\text{ClBBCl}^+-\text{Cl})$	373.6
$D(\text{Cl}_2\text{BBCl}^+-\text{Cl})$	146.7	$D(\text{ClBBCl}-\text{Cl}^+)$	756.5
$D(\text{Cl}_2\text{BBCl}-\text{Cl}^+)$	601.2		
		$D(\text{ClB}-\text{BCl})$	73.4
$D(\text{ClB}^{2+}-\text{Cl})$	539.7	$D(\text{ClB}^+-\text{BCl})$	313.0
$D(\text{ClB}^+-\text{Cl}^+)$	-146.5		
$D(\text{B}^+-\text{Cl}^+)$	-344.6		

Table 9.5 Bond Dissociation Energies (kJ mol^{-1})

Fragment	Symmetry of Transition State	Available States of M ⁺
(a) BCl ₃		
BCl ₃ ⁺	C _{2v}	\tilde{X} , \tilde{A} , \tilde{D} , \tilde{F}
BCl ₂ ⁺ + Cl [•]	C _{2v}	all
BCl ⁺ + Cl ₂	C _{2v}	\tilde{A} , \tilde{D} , \tilde{E} , \tilde{F} , \tilde{G}
(b) B ₂ Cl ₄		
B ₂ Cl ₄ ⁺	D _{2d}	\tilde{X} , \tilde{E} , \tilde{H} , \tilde{K}
BCl ₂ ⁺ + BCl [•]	C _{2v}	\tilde{X} , \tilde{C} , \tilde{E} , \tilde{G} , \tilde{H} , \tilde{J} , \tilde{K}
Cl ₂ BB ⁺ + Cl ₂	C _{2v}	\tilde{X} , \tilde{C} , \tilde{E} , \tilde{G} , \tilde{H} , \tilde{J} , \tilde{K}
(c) B ₄ Cl ₄		
B ₄ Cl ₄ ⁺	D _{2d}	\tilde{X} , \tilde{C} , \tilde{E} , \tilde{G}
B ₄ Cl ₃ ⁺ + Cl [•]	C _{3v}	all
B ₃ Cl ₃ ⁺ + BCl	C _s	all
B ₂ Cl ₂ ⁺ + B ₂ Cl ₂	D ₂	\tilde{X} , \tilde{A} , \tilde{C} , \tilde{E} , \tilde{G}
BCl ⁺ + B ₃ Cl ₃	C _{3v}	\tilde{X} , \tilde{C} , \tilde{D} , \tilde{E} , \tilde{F} , \tilde{G} , \tilde{H}

Table 9.6 Symmetry Constraints on Fragmentations

References

- [1] V.H. Dibeler and J.A. Walker, *Inorg. Chem.*, 8 (1969), 50.
- [2] Relative intensities of ions in the spectra of BCl_3 and B_2Cl_4 are all calculated on an anisotropic basis [1,3].
- [3] W.S. Koski, J.J. Kaufman and C.F. Pachuki, *J. Am. Chem. Soc.*, 81 (1959), 1326.
- [4] A.G. Massey, D.S. Urch and A.K. Holliday, *J. Inorg. Nucl. Chem.*, 28 (1966), 365.
- [5] M. Atoji and W.N. Lipscomb, *Acta Cryst.*, 6 (1953), 547.
- [6] Relative intensities of ions in the spectrum of B_4Cl_4 are quoted for $^{11}\text{B}_x^{35}\text{Cl}_y$ [4].
- [7] D.R. Stull (Ed.), "JANAF Thermochemical Tables", Dow Chemical Company, Midland, Michigan, 1965.
- [8] S.R. Gunn, L.G. Green and A.I. Von Egidy, *J. Phys. Chem.*, 63 (1957), 1787.
- [9] R.F. Barrow, *Trans. Faraday Soc.*, 56 (1960), 952.
- [10] G. Herzberg and W. Hushley, *Can. J. Res.*, A19 (1941), 127.
- [11] S. Konaka, Y. Murata, K. Kuchitsu and Y. Morino, *Bull. Chem. Soc. Japan*, 39 (1966), 1134.
- [12] D.D. Danielson and K. Hedberg, *J. Am. Chem. Soc.*, 101 (1979), 3199.

- [13] K. Hedberg and R.R. Ryan, *J. Chem. Phys.*, 50 (1969), 4986.
- [14] M. Atoji, P.J. Wheatley and W.N. Lipscomb, *J. Chem. Phys.*, 27 (1957), 196.
- [15] A.D. Walsh, *J. Chem. Soc.*, (1953), 2266.
- [16] A.G. Briggs, M.S. Reason and A.G. Massey, *J. Inorg. Nucl. Chem.*, 37 (1975), 313.
- [17] B.J. Bassett and D.R. Lloyd, *J. Chem. Soc. A*, (1971), 1551.
- [18] R.J. Boyd and D.C. Frost, *Chem. Phys. Lett.*, 1 (1968), 649.
- [19] D.R. Lloyd and N. Lynaugh, *Chem. Commun.*, (1971), 627.
- [20] J.H. Hall, Jr., and W.N. Lipscomb, *Inorg. Chem.*, 13 (1974), 710.
- [21] J. Marriott and J.D. Craggs, *J. Electron. Control*, 3 (1957), 194.

APPENDIX A

PUBLICATIONS

- [1] "MINDO/3 study of first-row triatomic hydrides, HMH, and of their cations and anions"; J.R. Bews and C. Glidewell, *Inorg. Chim. Acta*, 39 (1980), 217-225.
- [2] "Molecular Fragmentations Part I. Structures and energies of molecular fragments derived from formic acid"; J.R. Bews, C. Glidewell and P.H. Vidaud, *J. Mol. Struct.*, 64 (1980), 75-85.
- [3] "Jahn-Teller effects in the MINDO approximation: Structures of the molecular cations of methane and the chloromethanes"; J.R. Bews and C. Glidewell, *J. Mol. Struct.*, 64 (1980), 87-92.
- [4] "Molecular Fragmentations Part II. Structures and energies of molecular fragments derived from formamide and its molecular cation"; J. Bews and C. Glidewell, *J. Mol. Struct.*, 67 (1980), 141-150.
- [5] "Molecular Fragmentations Part III. Structures and energies of the transition states in the rearrangement and decomposition of formamide molecular cations"; J.R. Bews and C. Glidewell, *J. Mol. Struct.*, 67 (1980), 151-157.

- [6] "Molecular Fragmentations Part IV. The mass spectral fragmentation of carbon tetrachloride"; J. Bews and C. Glidewell, *J. Mol. Struct.* 71 (1981), 287-296.
- [7] "Molecular Fragmentations Part V. Structures and energies of mass spectral fragments derived from ethyl acetate"; J.R. Bews and C. Glidewell, *J. Mol. Struct.*, 71 (1981), 297-310.
- [8] "Novel beryllium derivatives of $(CH)_n$ carbocycles: An MNDO study"; J.R. Bews and C. Glidewell, *J. Organometall. Chem.*, 219 (1981), 279-293.
- [9] "Molecular Fragmentations Part VI. Structures and energies of the valence isomers of benzene, and their molecular cations"; J.R. Bews and C. Glidewell, *J. Mol. Struct.*, 86 (1982), 197-204.
- [10] "Molecular Fragmentations Part VII. Structures and energies of mass spectral fragments derived from benzene"; J.R. Bews and C. Glidewell, *J. Mol. Struct.*, 86 (1982), 205-215.
- [11] "Molecular Fragmentations Part VIII. Structures and energies of mass spectral fragments derived from tetraphosphorus trisulphide"; J.R. Bews and C. Glidewell, *J. Mol. Struct.*, 86 (1982), 217-230.

- [12] "Molecular Fragmentations Part IX. Structures and energies of mass spectral fragments derived from xanthan hydride, 5-amino-1,2,4-dithiazolin-3-thione"; J.R. Bews and C. Glidewell, *J. Mol. Struct.*, 86 (1982), 377-385.
- [13] "Molecular Fragmentations Part X. Mass spectral fragmentation of boron trichloride, diboron tetrachloride and tetraboron tetrachloride"; J.R. Bews and C. Glidewell, *J. Mol. Struct.*, 89 (1982), 333-347.
- [14] "Homolytic ring fission reactions of cycloalkylmethyl and bicycloalkyl radicals"; J.R. Bews, C. Glidewell and J.C. Walton, *J. Chem. Soc. Perkin Trans. II*, (1982), 1447-1453.
- [15] "Molecular Fragmentations Part XI. Mass spectral fragmentation of dimethylberyllium, trimethylboron and trimethyl aluminium"; J.R. Bews and C. Glidewell, *J. Mol. Struct.*, 90 (1982), 151-163.
- [16] "Molecular Fragmentations Part XII. Mass spectral fragmentation of pyridine"; J.R. Bews and C. Glidewell, *J. Mol. Struct.*, 91 (1983), 353-371.
- [17] "Molecular Fragmentations Part XIII. The structure and energies of mass spectral fragments derived from phosphine-3, diphosphine-4, diphosphine-2, and triphosphine-5"; J.R. Bews and C. Glidewell, *J. Mol. Struct.*, 94 (1983), 305-318.

APPENDIX B

ESR SPECTRUM SIMULATION

A program written by Dr. M.F. Chiu [1] for the simulation of exchange broadened Electron Spin Resonance spectra was obtained from the Chemistry Department of York University. This program incorporates an exchange routine involving the solution of modified Bloch equations [2] by the method of Gutowsky and Holm [3]. It had been modified by C. Gaze at York University to handle up to ten radicals, each having up to ten groups, with a maximum of twenty arrangements per group and a total of

5000

number of radicals

lines per radical. The Fortran source code for the program is contained in the file [CHSJB.PLOT]XESR.FOR.

The program was modified to suit (a) interactive use and (b) the local plotting procedures, in a similar manner to that described for PLUTO in chapter 3. Graphical output was scaled so that hard copy plots generated on the Tektronix T4662 plotter might be directly compared with ESR spectra produced on the Bruker ER200D spectrometer. Initially the program was modified to prompt for input as required, but this was later altered to allow the option of accepting the majority of input from a file, as this was found to be an easier method. Changes to the input being

performed by editing the input file, rather than having to re-enter all the data. Following extensive use it was also found that large systems required execution times greater than that available at a terminal and so a further modification was carried out to enable the program to be run via the QUEUE command described in chapter 3.

The QUEUE command operates via the RUNQCPE command file as described above. This command file creates a temporary file containing the time limit for the batch queue being used, the name of the restart file, and the file name stripped of the file type. The temporary file is assigned to Fortran unit 15 and XESR attempts to read from Fortran unit 15. Should this input be successful a logical flag is set in the program that the program is running in the batch environment, and the name of the gridfile, which is used in exactly the same manner as for PLUTO described in chapter 3, is generated as <filename>.GRD. The Fortran source code was compiled to generate the object file [CHSJB.PLOT]XESR.OBJ and this object file was then linked to form two separate forms of the executable program. Two different forms were required because the interactive version of the program generates the graphics output directly and then gives the option to save the output in a gridfile for subsequent hard copy generation exactly as previously described for PLUTO. This was performed, within the subdirectory [CHSJB.PLOT], by the command

```
LINK XESR,GHOST/LIB,GRIDT4010/LIB
```

creating the executable file [CHSJB.PLOT]XESR.EXE, which is accessible to any user of the VAX computers by the command

```
RUN [CHSJB.PLOT]XESR
```

with copies of the executable program being maintained on both VAX systems at St. Andrews.

The version for batch use must not produce graphics output directly and so the object file was linked by the command

```
LINK/EXEC=XESRB XESR,GHOST/LIB,GRID/LIB
```

which produced a version, [CHSJB.PLOT]XESRB.EXE which generates grid files automatically. These may then be processed to generate hard copy output as described previously for PLUTO and, as for all grid files, may be viewed on a graphics terminal by the command

```
T4010
```

which prompts for the name of the grid file and processes it to generate a video graphics output on a Tektronix or compatible terminal.

Input via the terminal requires no explanation because all input is requested by prompting, except that for termination of input for a given radical, for which the <RETURN> key is pressed in response to the request for input. Input from a file is in exactly the same format as would be entered from the terminal, although some differences exist between the amount of data

required for interactive and batch file input. The file for interactive input would contain the lines:

```
Line 1:  Title of the spectrum
Line 2:  xxx.x,nnn (spectrum width in gauss, number of points)
Line 3:  xx.x      (height of largest peak, -height for -ve phase)
Line 4:  xx.x      (spectrum centre in gauss)
Line 5:  xx.x,yy.y (line width, mole fraction of radical 1)
Line 6:  x.xxxx    (G value for radical 1 <default=2.0023>)
Line 7:  nn,x.x,yy.yy (number of equivalent nuclei,spin,hfs)
Line 8:  .
Line 6+a:  .      (a sets of equivalent nuclei for rad. 1)
Line 6+a+1 (blank line terminates radical 1)
.
.      (set of data for radical 2)
.      (blank line terminates radical 2)
.
.
.      (blank line terminates radical n)
Line 6+n*(a+1): (blank line terminates radical input)
```

Running the XESR program prompts for the name of the input file which could be the file generated as above. After the data has been input the program prompts from the terminal for the number of exchange processes if more than one radical has been input, and then, if only one exchange rate has been specified, prompts for that exchange rate. If more than one exchange rate is to be specified, these are input last. The derivative order is then input as required by the prompt, followed by an instruction as to whether second order shifts are required. Multiple exchange rates will then be input if required. Following generation of the spectrum an opportunity is given to save the gridfile for subsequent hard copy plotting.

The input file for the batch system is exactly as described above, followed by the commands which would normally be input

from the terminal. No command is necessary for saving the gridfile as this is done automatically. Submission to the QUEUE command described earlier is performed by specifying XESR as the job name. The QUEUE command file recognises this as a valid job name and, on entering the execution phase of the job the file [CHSJB.PLOT]XESRB.EXE is used.

Input for equivalent nuclei is given to the current version of the program as

number of nuclei, spin, splitting

unlike the original program which required expansion of the spin quantum numbers, with the relative weights: for example the input for a single equivalent nucleus of spin 0.5 and splitting of 2.1 gauss would require the input in the present version

1,0.5,2.1

but would have required for the previous version an input statement of the form

```
      2.1  2
-0.5 0.5
  1.0 1.0
```

with a corresponding increase in complexity as the number of equivalent nuclei increased, and as the spin quantum number increased. A subroutine was therefore written which accepts the simple input as shown above and expands it into the long form for internal use. This subroutine is reproduced below, where the parameters passed are:

numat: number of equivalent nuclei
 spin: spin quantum number
 iii: iiith radical
 jjj: jjjth set of equivalent nuclei

The arrays into which the results are copied are contained in the COMMON areas.

```

subroutine quant(numat,spin,iii,jjj)
common/groups/a(10,10),na(10,10),nk(20)
common /qnbwt/ qn(10,10,20),pwt(10,10,20)
dimension wt(20,20)
i2=ifix(spin*2.0)
i2l=i2+1
naij=(numat-1)*i2+i2l
if(naij.gt.20) stop 'Too many nuclei or too high a spin'
do 100 i=1,i2l
100 wt(1,i)=1.0
lelem=1
do 300 irow=2,numat
lrow=irow-1
lelem=lelem+i2
nelem=lelem+i2
do 200 i=1,nelem
200 wt(irow,i)=0.0
do 300 ielem=1,lelem
do 300 i=ielem,ielem+i2
300 wt(irow,i)=wt(irow,i)+wt(lrow,ielem)
do 400 k=1,naij
pwt(iii,jjj,k)=wt(numat,k)
400 qn(iii,jjj,k)=(-spin*numat+k-1)
na(iii,jjj)=naij
return
end
  
```

This subroutine expands weights in a similar manner to the Pascal triangle which is headed by $(2*\text{spin})+1$ weights of 1.0, for example for spin 0.5 the weights are:

1 equivalent nucleus		1.0	1.0	
2 equivalent nuclei		1.0	2.0	1.0
3 equivalent nuclei	1.0	3.0	3.0	1.0
				etc.

and these are related to the spin quantum numbers:

1 equivalent nucleus		-0.5	0.5	
2 equivalent nuclei		-1.0	0.0	1.0
3 equivalent nuclei	-1.5	-0.5	0.5	1.5
				etc.

References

- [1] B.C. Gilbert, R.O.C. Norman and M. Trenwith, J. Chem. Soc. Perkin II, (1974), 1033.

- [2] A. Carrington and A.D. McLachlan, "Introduction to Magnetic Resonance", Harper and Row, New York, 1967.

- [3] H.S. Gutowsky and C.H. Holm, J. Chem. Phys., 25 (1965), 1228.